SENSITIVITY OF TERRAIN ATTRIBUTES, WATERSHED ATTRIBUTES, AND SWAT DERIVED HYDROLOGICAL OUTPUTS TO LIDAR DERIVED DEM UNCERTAINTY

by

Tristan Goulden

Submitted in partial fulfilment of the requirements
for the degree of Doctor of Philosophy

at

Dalhousie University
Halifax, Nova Scotia
September 2013

Table of Contents

LIST OF TABLES

LIST OF FIGURES

ABSTRACT

This research analyzes the sensitivity of watershed attributes, and hydrological outputs to LiDAR derived DEM uncertainty introduced through spatial resolution, and LiDAR measurement errors. Sensitivity of watershed attributes to spatial resolution was determined through a scaling analysis at three sites; Mosquito Creek, Scotty Creek and Thomas Brook, with DEMs ranging from 1 to 50 m. Results at Scotty Creek showed the highest sensitivity of watershed area to spatial resolution, due to subtle changes in elevation which were below DEM uncertainty. Validation of the stream length at Thomas Brook showed discrepancies of 3.7 to 24.1% for the 1 to 50 m DEMs, compared to independent field observations. Sensitivity of SWAT derived hydrological outputs to DEM spatial resolution were determined through a scaling analysis of DEMs (1 - 50 m) at Thomas Brook watershed, over a five year simulation period. Results indicated monthly water yield was insensitive to DEM resolution, unless a change in area was also present. Sediment yield from the 50 m DEM showed a 24% reduction compared to the 1 m DEM. The 5 - 50 m DEMs also showed a reduction in channel deposition of 45 - 90 t, compared to the 1 m DEM.

Sensitivity of terrain attributes, watershed attributes and hydrological outputs to LiDAR measurement errors were determined at the Thomas Brook watershed through the propagation of LiDAR sensor measurement errors with Monte Carlo simulations. Results showed that the uncertainty in the DEM, slope, and aspect were below 0.06 cm, 1.5° and 24.1° in 97.5% of grid cells, respectively. Watershed area and stream length resulted in relative standard deviations of <1% and 1.5%, respectively. However, sensitivity of watershed area increased in regions with elevation changes below DEM uncertainty and stream length uncertainty increased with decreasing stream length. SWAT simulated flow and sediment showed minor sensitivity to LiDAR measurement error in high flow months, and increased as flow decreased. Simulated sediment showed higher sensitivity to LiDAR measurement errors than flow, due to changes in the HRU slope class, which can shift the dominant HRU (Hydrological Response Unit) if a minimum HRU threshold area is implemented.

LIST OF ABBREVIATIONS AND SYMBOLS USED

ψ	Aspect
α	Power law constant / slope of log-log linear regression
a	Power law constant / y-intercept of log-log linear regression
A_{ch}	Channel cross-section
ALTM	Airborne laser terrain mapper
$area_{HRU}$	Area of an HRU (ha)
ASTER	Advance spaceborne thermal emission and reflection
b	Slope of linear regression line
BMP	Beneficial management practices
$conc_{max}$	Maximum concentration of channel sediment
$conc_{sed}$	Concentration of channel sediment
c_{sp}	User defined sediment transport coefficient
C_{USLE}	USLE cover management factor
CN	Curve number
CV	Coefficient of variation
D	Fractal dimension
D_{av}	Average fractal dimension
DEM	Digital elevation model
e	Simulated elevation coordinate error
Σ	Covariance matrix
ET	Evapotranspiration
GLOPOV	General law of propagation of variance
GPS	Global positioning system
HRU	Hydrological response unit
IDW	Inverse distance weighting
J	Jacobian matrix
K_{USLE}	USLE soil erodibility factor
LiDAR	Light detection and ranging

L_{ch}	Length of the channel
LS_{USLE}	USLE topographic factor
L_{slp}	Sub-basin slope length
m	Power in USLE topographic factor
MA	Moving average
MUSLE	Modified universal soil loss equation
N	Set number
n	Manning's roughness coefficient
NED	National elevation dataset
NN	Natural neighbour
NSE	Nash-Sutcliffe coefficient
PBIAS	Percent bias
p	Point number
P_{USLE}	USLE erosion practice factor
q_{peak}	Peak runoff rate
Θ	Slope angle (rad)
Θ_i	Incidence angle
λ	Slope length
P_{ch}	Wetted perimeter
prf	Peak rate adjustment factor
q_{ch}	Channel flow rate
Q_{surf}	Surface runoff volume (mm)
R_{ch}	Hydraulic radius
RD	Relative difference
RMSE	Root mean square error
R_{runoff}	Rainfall runoff factor
RSR	Standard deviation ratio
RTK	Real time kinematic
R_{USLE}	USLE rainfall runoff factor
r_z	Residual elevation error
S	Slope (°)

s_t	Standard deviation of monthly SWAT outputs
σ_{DEM}	DEM uncertainty
σ_S	Grid based slope uncertainty
σ_ψ	Grid based aspect uncertainty
$\{S\}$	Set of three dimensional Cartesian coordinates
SCS	Soil Conservation Service
sed	Soil loss (t/a)
slp	Average slope of a subbasin
slp_{ch}	Channel slope
spexp	Channel processes coefficient
SRTM	Satellite radar topography mission
SWAT	Soil and water assessment tool
t	Time in months
t_{conc}	Time of concentration
t_{ch}	Channel time of concentration
TIN	Triangular irregular network
t_{ov}	Overland flow time of concentration
u	Unit vector
UK	Universal Kriging
USDA	United States Department of Agriculture
USGS	United States Geological Service
USLE	Universal soil loss equation
v	GPS validation point
v_c	Flow velocity
V_{ch}	Volume of water in the channel
$v_{ch,pk}$	Peak channel velocity
x	x Cartesian coordinate
x_t	Monthly SWAT output
y	y Cartesian coordinate
z	z Cartesian coordinate

ACKNOWLEDGEMENTS

This dissertation is the culmination of knowledge and skills acquired since my childhood. To that end, my eternal thanks must be given to my parents, Paul and Ruth Goulden, and brother, Adam Goulden. Nobody has shaped my thinking and approach to problem solving more than my family. I would not have completed, nor endeavored to complete, such a monumental task without their extensive support.

I am quite fortuitous to have been accepted for supervision by an outstanding committee. My co-supervisors, Dr. Rob Jamieson and Dr. Chris Hopkinson have provided support through the teaching and mentorship beyond their duties as academic supervisors. Chris has guided me since the beginning of my research career, and his encouragement can be credited with keeping me on my successful journey through academia. I would like to acknowledge the fundamental support he provided, both financial and academic, which allowed for completion of two graduate degrees. But also, I would like identify the importance of the many discussions in a range of topics outside of the realm of the PhD research, which have helped me develop as a person. I must also express my gratitude for the responsibilities and opportunities Chris provided throughout my research. The invitation to attend conferences, support field work campaigns, and join committees, shows his commitment to student success. I would also like to thank Rob for the mentorship and financial support provided throughout my PhD research. Rob introduced me to the science of hydrology and afforded me the freedom to pursue my inter-disciplinary interests. His has served as an ideal role model of professorship, one which I would hope to emulate. The invitation to sit in his wonderfully managed research group, which is surely a blueprint for graduate student learning and achievement, made my PhD an enjoyable experience. I would like to thank Dr. Shannon Sterling for her insightful and constructive comments during the review of my dissertation. I learned a great deal through discussions and during dissemination of notes; these contributed to raising my research to a higher level. Also, I would like to thank Dr. Ken Wilke for his useful and perceptive comments during committee meetings, which kept me on track for completion.

I would also like to thank fellow graduate students who have helped me throughout the learning process. Specifically, I would like to thank my partners of PhD candidacy within the lab; Andrew Sinclair, and Greg Piorkowski. These colleagues engaged in discussions pertaining to research, but also in successfully navigating the non-research components of PhD completion. I am thankful to Dr. Lisa Wedding, for expanding my views on science, and for demonstrating the holistic nature of a career in science. I would also like to thank several others in the research group at Dalhousie, and the Applied Geomatics Research Group (AGRG), who have participated in many conversations, and fieldwork campaigns; Colin Ragush, Erin Mentink, Jenny Hayward, Allyson Fox, Neville Castro, Heather Morrison, and Laura Chasmer.

I would also like to acknowledge the financial support from the National Sciences Engineering and Research Council (NSERC), the Atlantic Canada Opportunities Agency (ACOA), the AGRG, the Rosetti Scholarship foundation, Exxon Mobil, and the Faculty of Graduate Studies at Dalhousie University.

CHAPTER 1 INTRODUCTION

Hydrological models contribute important information for designing policy to promote environmentally and economically sustainable management of water resources. A recent example is the Canadian WEBS (Watershed Evaluation for Beneficial Management Practices, Stuart et al. 2010) program, a federally funded watershed research initiative administered through Agriculture and Agri-Food Canada with a stated objective of *"assessing the environmental and economic performance of selected agricultural beneficial management practices (BMPs)"* (Stuart et al. 2010). In the execution of this objective, hydrologic modeling was considered one of the primary information sources capable of advancing the understanding of the watershed systems of interest and assigning BMPs. To ensure hydrologic models will contribute effective and defensible BMP policy actions, any source of model uncertainty should be well understood and quantified. One source of hydrological model uncertainty can be attributed to the DEM (Digital Elevation Model), a primary input data layer required to describe the landscape topography, and facilitates watershed delineation and parameterisation of process based hydrological models.

LiDAR (Light Detection and Ranging) is an active remote sensing technology used to observe topographic information to describe the Earth's surface. LiDAR technology has experienced robust commercial expansion in the past decade, and is replacing competing remote sensing technologies as a source of digital topographic information for development of DEMs. The adoption of LiDAR as a leading source of topographic information is evidenced by the initiation of several large scale federal mapping initiatives. Currently, approximately one-third of the continental United States has been surveyed with LIDAR (Stoker, 2013), and several countries have achieved nationwide survey coverage such as Denmark, Switzerland, and the Netherlands. The popularity of LiDAR technology can be traced to its unique ability to simultaneously provide dense (> 1 pt/m^2) and accurate ($<$ dm) coordinate samples of the physical terrain, even beneath forest canopy, which can be used to create DEMs with spatial resolution at the metre level. To date, the sensitivity of watershed attributes, and

simulated hydrologic outputs, to uncertainty in fine resolution LiDAR DEMs has not been well established. As the availability of LiDAR DEMs is becoming ubiquitous through publically funded national survey campaigns, it is being adopted by the hydrological modeling community. Therefore, there is a current need to describe hydrological model uncertainty associated with the implementation of fine resolution LIDAR DEMs in order to understand the limitations of policy initiatives derived from hydrological models. A comprehensive understanding of the sources and magnitude of uncertainty will also contribute to the development of best practices and guidelines for diligent use of LIDAR information in the hydrological sciences, limiting the potential for management decisions based on information of insufficient quality. Currently, best standards and practices for use of LiDAR for hydrological modeling are rare, due to the lack of research describing LiDAR derived uncertainty.

The development of best standards and practices for other application areas does exist, setting a precedent for the need to develop similar guidelines for hydrological analysis. For example, the Federal Emergency Monitoring Agency (FEMA) has developed best standards and practices for the use of LiDAR in the national flood risk assessment insurance program. Similarly, the ASPRS (American Society of Remote Sensing) and the FGDC (Federal Geographic Data Commission) have guidelines for quality assurance of LiDAR observations. While this dissertation does not intend to provide an exhaustive set of guidelines for use of LiDAR DEMs with respect to hydrological analysis, it contributes to this goal through the quantification of uncertainty of hydrological products. The workflow which translates LiDAR observations through to predictions of hydrological processes generally includes generation of grid based digital elevation model, grid based slope and aspect maps, delineation of watershed area and stream networks, and processing with a hydrological model. Knowledge of how each of these data layers will react to LiDAR derived DEM uncertainty will aid in recommending best standards and practices of LIDAR for use in the hydrological sciences.

The research objective of the dissertation is to investigate the sensitivity of topographic attributes, watershed attributes and simulated hydrological outputs to DEM uncertainty from two sources, 1) the spatial resolution of the DEM and 2) the elevation uncertainty of individual DEM grid nodes. The first half of the dissertation (Chapter 2

and Chapter 3) describes the sensitivity of watershed attributes, including watershed area, the channel network, and topographic derivatives (slope and aspect). These inputs are universally required for process-based hydrological models, allowing these results to be useful to a broad cross-section of modeling efforts. Specifically, Chapter 2 investigates the sensitivity of watershed boundary and stream network delineation to DEM spatial resolution ranging from 1 to 50 m, as well as the interpolation of LiDAR three dimensional coordinates to DEM grid elevations. The sensitivity of watershed attributes is interpreted through a DEM scaling analysis in three distinct topographic environments. A scaling analysis will reveal two important conditions related to grid cell size, 1) scale dependent irregularities, and 2) scaling relationships, in relation to hydrological quantities of interest. The existence of scale dependent irregularities or scaling relationships allows inference on the optimum grid scales for watershed boundary and stream network delineation. Chapter 2 also includes an accuracy assessment of stream length modeled from DEMs with varying resolutions. Modeled stream lengths were compared against the field measured stream length obtained from high accuracy RTK GPS observations. The field verified stream length provides an independent verification of the ideal grid cell size for modeling stream length. A scaling relationship between DEM grid cell size and stream length is also investigated, which allows stream lengths to be systematically scaled between resolutions.

Chapter 3 investigates the sensitivity of topographic attributes (slope and aspect) and watershed attributes (stream length, watershed area) to the elevation uncertainty in LiDAR derived DEMs. The error in individual LiDAR coordinates is obtained from a novel error propagation algorithm based on the sensor hardware measurement errors and terrain conditions. The spatial distribution of uncertainty in the DEM, grid-based slope and grid based aspect are determined through Monte Carlo error propagation techniques and related to the LiDAR flight configuration and terrain conditions. Uncertainty in the delineated watershed boundary and stream network is also investigated with the aim of identifying regions where a high incidence of uncertainty can be expected.

The latter half of the dissertation (Chapter 4 and Chapter 5) focuses on the sensitivity of DEM uncertainty to the SWAT (Soil and Water Assessment Tool), a process based semi-distributed watershed model. Due to the unique algorithmic

conditions of the SWAT, the results are generally confined to only this model. However, the methodological framework is valid for furthering the analysis to additional process based hydrological models. Chapter 4 investigates the sensitivity of the simulated flow and sediment yield in the SWAT (Soil and Water Assessment Tool), a semi-distributed watershed model, to DEM grid cell size. The investigation of the sensitivity separates the role of the DEM to three distinct functions, 1) defining the hillslope scale, 2) the extraction of a hydrologic network, and 3) watershed boundary delineation. The primary investigation of Chapter 4 surrounds the response of the SWAT model to DEMs with decreasing grid cell sizes, which reach a minimum of 1 m, and whether the increase in detail of topographic information is beneficial for the SWAT model design. A secondary investigation determines whether each DEM role is optimized at the same resolution.

Chapter 5 investigates the sensitivity of the SWAT to LiDAR measurement errors. LiDAR measurement errors were propagated through to DEM using the same algorithm implemented in Chapter 3. Uncertainty in SWAT flow and sediment were determined with a Monte Carlo approach, which required the creation of several SWAT models with unique DEMs. Results were compiled at several monitoring stations within the Thomas Brook watershed to assess the influence of LiDAR measurement error at varying spatial scales. Chapter 6 provides a summary of the main conclusions and novel contributions, as well as directions for continuation of the research.

CHAPTER 2 SENSITIVITY OF WATERSHED ATTRIBUTES TO SPATIAL RESOLUTION AND INTERPOLATION METHOD OF LIDAR DEMS IN THREE DISTINCT LANDSCAPES

2.1 Introduction

To allow modeling of land surface patterns and processes, continuous topography must be simplified to a set of discrete values for virtual representation. The process of discretizing topography from measured data will inevitably introduce algorithmic and scale dependent biases. A DEM (Digital Elevation Model) is a common virtual form of topographic information required for automated delineation of watershed boundaries and stream networks (O'Callaghan and Mark, 1984; Band, 1986; Jensen and Dominigue, 1988; Tribe, 1992; Martz and Garbrecht, 1993), because it indicates gravitational potential gradients that control the flow of surface water. The discrete structure commonly taken by a DEM is a grid of elevations at a constant horizontal spacing in both *x* and *y* directions (Moore et al., 1991). The horizontal distance between grid locations is referred to as the spatial resolution and represents the minimum size of an object that can be identified within the DEM and is representative of the DEM scale. LiDAR (Light Detection and Ranging) has emerged as one of the most popular tools for acquiring high resolution DEM information, as shown by its sustained commercial growth (TMSI, 2005; Carey and Associates, 2010). In addition, LiDAR derived DEMs show promise for expanded future use given large scale initiatives to acquire LiDAR coverage for entire countries (e.g. Stoker et al., 2008). With the availability of LiDAR increasing rapidly, appropriate analysis is required to properly assess the implementation of fine resolution DEMs for development of watershed boundaries and stream delineations. These products require attention because they are primary data layers for use in hydrological models, which provide critical information for the efficient management of water resources.

2.1.1 Previous relevant research of hydrology and LiDAR DEMs

Research has begun to assess the benefits of LiDAR technology for watershed characterization and analysis. For example, Li and Wong (2010) compared LiDAR DEMs at spatial resolutions of 2, 10 and 30 m, a Satellite Radar Topography Mission (SRTM) DEM at 30 m of spatial resolution, and National Elevation Dataset (NED) DEMs at spatial resolutions of 10 m and 30 m for the purposes of drainage network extraction and flood simulation. It was found that the 2 m LiDAR DEM provided drainage networks that were the most accurate when compared to networks from the National Hydrography Dataset (NHD). However, the LiDAR drainage networks were less accurate than the NED DEM derived drainage networks at equivalent resolutions (10 m and 30 m). Hopkinson et al. (2009) analyzed watershed attributes using three data sources (LiDAR, photogrammetry, public digital contour data) at two resolutions (5 m, 25 m) and found that a watershed area derived from the digital contour derived DEM was over-estimated by 15% compared to a LiDAR derived DEM. It was determined that the overestimation was related to the ability of the LiDAR acquisition system to more accurately depict the terrain beneath the forest canopy as the low data density of the photogrammetric and contour sources created erroneous flow paths in forested areas. The overestimation of area was not related to DEM resolution, but the accuracy and sampling of the terrain surface represented in the DEM. In a similar study of a watershed in the foothills of the Rocky Mountains, Murphy et al. (2008) compared a drainage network from a 1 m LiDAR DEM and a 10 m photogrammetrically derived DEM. It was found that the photogrammetric DEM excluded or reduced the length of first order streams and contained significant spatial errors when compared to GPS field sampled observations of the stream channel. This indicated that the 1 m LiDAR derived DEM provided the most accurate characterization of the stream network. In addition, the LiDAR DEM produced a delineated watershed area, which when analyzed through a visual inspection was 15% larger and with more detailed boundaries, than that derived from the photogrammetric DEM. Remmel et al. (2008) compared a 20 m photogrammetrically derived DEM with a 5 m LIDAR DEM re-sampled to 2.5 m. It was found that the high spatial resolution provided by the LiDAR DEM allowed a better prediction of smaller stream segments,

improved definition on watershed extents and provided details on areas of soil saturation, which could improve management decisions of forest harvests. Barber and Shortridge (2005) reported that LiDAR derived DEMs offered limited advantage for basin delineation over medium resolution DEMs as source and resolution resulted in only minor differences. The study compared a LIDAR DEM at spatial resolutions of 6 m and 30 m versus a 30 m NED DEM. They noted low relief landscapes as an exception that would benefit from improved elevation accuracies and resolution of LIDAR derived DEMs.

The existing literature has concurrently focused on comparing the source of DEM information (e.g. LiDAR vs. photogrammetry) and spatial resolution for the purposes of watershed and stream network delineation. In the assessment of spatial resolution, the variation has been limited to at most three different levels. The majority of studies conclude that fine resolution LIDAR DEMs will offer the best results compared to lower resolution DEMs from alternative sources; however, an optimum DEM resolution for LiDAR specific DEMs cannot be concluded due to the complicating factors of alternative data sources. Knowledge of the optimum DEM resolution of LiDAR DEMs is desirable because it allows for efficient and accurate modeling of watershed attributes, yet minimizes acquisition costs and computational burden.

The determination of an optimum spatial resolution in the generation of DEMs requires careful consideration because the spatial resolution defines the hillslope scale, which will influence the quantification of watershed attributes or modeled processes. A scaling analysis, consisting of multiple determinations of a modeled process through a controlled modification of the DEM resolution, can reveal scale-dependant irregularities as well as determine the existence of repeatable patterns across multiple scales (Atkinson and Tate, 2000). Knowledge of an irregular response of a modeled process to a particular scale can guide users in optimizing DEM resolution to suit their modeling needs. Identifying repeatable patterns across multiple scales can indicate whether a process is scale invariant, and can be modeled without explicitly requiring data at a specified resolution. LiDAR data offers an effective tool for such a scaling analysis because it provides sufficiently dense raw elevation information to enable the production of DEM elevations across previously unavailable fine spatial resolution supports.

Useful scaling relationships between the resolution of a DEM derived stream network and stream network length have been identified in the literature (Tarboton et al., 1988; Hjelmfelt, 1988; La Barbera and Rosso, 1989) and have shown to be effectively modeled through fractal properties. Traditionally, changes in stream network resolution were imposed on DEMs of constant resolution by modifying the threshold area for stream initiation, as by Tarboton et al. (1988) who implemented a scaling analysis with a 30 m resolution DEM. The stream initiation threshold controls the number of required cumulative cells draining to a common point to define the first instance of channel flow. Decreasing the stream initiation threshold has the effect of increasing the resolution of the stream network and vice versa (Tarboton et al., 1988; Helmlinger et al., 1993); therefore, the stream initiation threshold area can be used to set a finite scale to the landscape (Montgomery and Dietrich, 1988; Montgomery and Dietrich, 1992). Two distinct scaling relationships have been observed between the resolution of the stream network and stream length. One value for entire drainage networks, which can be modeled with a fractal dimension approaching two, and one for single stream channels, which can be modeled with fractal dimensions between 1.04 and 1.07 (Tarboton et al., 1988). Little analysis has been provided on scaling relationships between stream network resolution and DEM resolution explicitly through a change in DEM cell sizes from source data. Some preliminary analysis on single stream lengths (Hemlinger et al., 1993; Garbrecht and Martz, 1994; Wang and Yin, 1998, Thieken et al., 1999) has shown a systematic decrease with DEM spatial resolution as fine details of the stream channel are lost in coarse resolution DEMs.

The selection of DEM interpolation method is also a critical in the generation of LIDAR derived DEMs and has shown to affect DEM accuracy (Aguilar, 2005; Chaplot et al., 2006; Bater and Coops, 2009; Guo et al., 2010). Interpolation routines are required to determine the elevation of DEM grid nodes from raw LiDAR observations, which distribute in a pseudo-random ground pattern related to flight configurations and post-processing filtering routines. Traditional DEM interpolation algorithms are designed for determining grid node elevations from intermittent and sparse source data and not dense raw elevation point distributions typical of LiDAR surveys. As a result, the traditional goal of ‘interpolating’ elevation observations to determine DEM grid nodes is often more

appropriately described as ‘re-arranging’, ‘averaging’ or ‘aggregating’ observations in the LiDAR scenario since DEM grid nodes can be spaced further apart than source data. Therefore, optimum interpolation approaches exploit the available redundancy in the source data to reduce random vertical errors, which can conservatively reach decimetre levels (Glennie, 2008; Goulden and Hopkinson, 2010a), and also to maintain computational efficiency (Pfeifer and Mandlburger, 2009). The choice of interpolation method of raw elevations has not been well studied in the context of determination of watershed extents and stream channel delineation. The choice of interpolation method for DEM generation is often made by LiDAR service providers on the basis of efficiency in data processing and not for optimization of the accuracy of the intended DEM products. For example, Remmel et al. (2008) indicated the LiDAR DEM implemented in their study was created with an unknown interpolation method implemented by the service provider.

A useful approach for characterizing DEM suitability for drainage network extractions was introduced by Gyasi-Agyei et al. (1995) who stated that the ratio of the average pixel elevation drop to the DEM vertical resolution should be less than or equal to one. Implementing such a ratio in the LiDAR scenario is difficult because research dedicated to the quantification of a LiDAR DEM precision is currently active with recent studies identifying errors as non-linear combinations of several variables. For example, Glennie (2008), Goulden and Hopkinson (2010a) and Goulden and Hopkinson (2010b) have investigated the precision of sensor hardware, Bowen and Waltermire (2002), Hodgson and Bresnahan (2004), Hopkinson et al. (2005), and Reutebuch et al. (2003) have investigated external error sources such as terrain slope and vegetation and Aguilar (2010) and Guo et al. (2010) have reported on effects due to interpolation. Therefore, a rigorous quantification of DEM precision derived from LiDAR is not available and current estimates must rely on documented empirical assessments.

2.1.2 Objectives

The purpose of this study it to investigate optimum DEM generation procedures for fine-scale LiDAR-derived DEMs for application to the determination of watershed boundaries and stream network length determined in ArcHydro (Maidment, 2002). The

study is executed through several objectives: (i) to determine if fine spatial resolution DEMs derived from LiDAR (1 m to 50 m) show scale-dependent irregularities, which affect the determination of watershed area, (ii) to determine if stream length displays a systematic relationship with changes in DEM spatial resolution and allows scaling through a fractal relationship, (iii) to identify the most appropriate DEM resolution for representing stream length, and (iv) to determine if DEM interpolation method will affect these relationships. The respective hypotheses are that (i) determinations of planimetric watershed area will show unpredictable variations due to the introduction of scale dependent features such as anthropogenic landscape modifications (roads), or natural gullies or valleys in the landscape as resolution is increased, (ii) that stream length will increase with an increase in spatial resolution as additional details in the stream are resolved, and that this relationship can be described with a fractal dimension, (iii) the most appropriate resolution for characterizing stream length is the highest resolution available due to the ability to represent fine details and, (iv) that the interpolation method can result in subtle changes in elevation, which will affect watershed area and stream length in regions with minor changes in relief. In addition, it is hypothesized that interpolation methods, which do not effectively reduce noise, could cause erratic behavior in the flow direction, thereby increasing stream sinuosity and total length.

As the relative benefits of using LiDAR-derived DEMs have varied across different landscape types (Barber and Shortridge, 2006; Jones et al., 2008), the analysis was conducted with three case studies displaying distinct landscapes: (i) Mosquito Creek, an alpine environment with large elevation change (~2000 m), (ii) Scotty Creek, a boreal wetland environment with minimal elevation (~25 m) change and (iii) Thomas Brook, a hill to valley floor site with moderate elevation change (~200 m). These landscapes types were selected because the Mosquito Creek and Scotty Creek are representative of end-members in relief variation and Thomas Brook represents an intermediate level of relief variation with some anthropogenic modifications. Validation data for verifying DEM-derived stream lengths is provided for the Thomas Brook in the form of field surveyed stream locations. The validation data provide an estimate of the true stream length and indicates an ‘ideal’ DEM resolution to model the most accurate estimate of stream length. With knowledge of the ideal resolution and an associated scaling relationship, stream

lengths determined from DEM information obtained from public sources with a pre-determined spatial resolution could be scaled to the ideal resolution to improve accuracy. GPS validation data of the stream network is not available for Mosquito Creek and Scotty Creek due to logistical constraints of access to their remote locations.

2.2 Background to ArcHydro

ArcHydro, (Maidment, 2002) is an add-on to ArcGIS© (ESRI, 2003) that enables efficient delineation of watershed extents and stream networks from DEMs. The software package is well-used within industry, which ensures the analysis presented here will be relevant to a broad cross section of the community. Background information on the details of the algorithms for the watershed delineation process can be found in Jenson and Dominigue (1988) and are well described and widely used in existing literature. An important consideration to the ArcHydro framework is that flow direction is calculated using the D8 algorithm (O'Callaghan and Mark, 1984), which directs flow in one of eight cardinal directions to a single neighboring cell in the DEM grid lattice that shows the steepest descent. More sophisticated algorithms exist that permit flow to be partitioned between multiple cells, such as those found in Quinn et al.(1991), Costa-Cabral and Burges (1994), Tarboton (1997), Qin et al. (2007) and Seibert and McGlynn (2007). Partitioning of flow to multiple cells improves on documented deficiencies of the D8 algorithm, such as the imprecision imposed by directing flow to only eight directions as well as the existence of unrealistic parallel flow paths in convergent topography (Fairfeld and Leymarie, 1991). Despite its drawbacks, the D8 algorithm was maintained for this analysis because it is simple and efficient to execute, which is an important consideration for fine resolution LiDAR DEMs (Murphy et al., 2008) and is the only option available in ArcHydro software package. Furthermore, Tarboton and Ames (2001) suggest the use of the D8 algorithm when focusing on analysis of drainage networks, to prevent braided stream channels and unrealistic flow dispersion in flat landscapes. Additionally, McMaster (2002) showed that the spatial accuracy of a stream network had little dependency on the choice of either the D8 or D∞, a multiple flow direction algorithm by Tarboton (1997).

During the definition of stream channels in the ArcHydro algorithm, the user must supply a value for the stream initiation threshold. Competing methods exist, such as slope-dependent critical support areas (Dietrich et al., 1992) and a recent method using geodesic paths that has been suggested for use with high resolution LiDAR DEMs (Passalacqua et al., 2010); however, the area threshold is the only option available within ArcHydro. Automated methods are available for predicting appropriate thresholds from the DEM (Tarboton, 1989); however field information often provides the best information for determining appropriate values for channel initiation parameters (Montgomery and Foufoula-Georgiou, 1993).

2.3 Methods

Spatial resolutions were chosen at levels of 1, 5, 10, 25 and 50 m. The 1 m resolution limit was selected to because it is the finest resolution allowed by the raw data, while the 50 m limit was selected because it was extended the analysis past the 30 m resolution limit in several previous studies. Five unique interpolation routines were also used to generate the DEMs, including Inverse Distance Weighting (IDW), Moving Average (MA), Universal Kriging (UK), Natural Neighbour (NN), and a triangular irregular network (TIN). All DEMs were generated in Golden Software's Surfer© application from raw ground filtered LiDAR observations. In total, 75 DEMs were generated to include the five interpolation methods, five spatial resolutions and three case study sites.

2.3.1 Study Sites

2.3.1.1. Scotty creek

Scotty Creek is a Northern Boreal wetland environment located in the Northwest Territories of Canada approximately 50 km south of Fort Simpson, NWT (Figure 2.1a) at approximately 300 m a.s.l. It is characterized by low relief with a drainage structure that contains surface flow connecting several lakes. Peat plateaus and wooded upland characterize the vegetation and the soil is dominated by an organic layer that is approximately 8 m thick (Quinton et al., 2003). Underlying permafrost exists at a depth of approximately 0.6 m in late summer and covers a mixture of clay and silt (Ayelsworth

and Kettles, 2000; Quinton et al., 2003; Quinton et al., 2008). An elevation change of approximately 20 m exists over the total area of 24.5 km^2 and 95% of slopes are less than 6.6° indicating the general trend of subtle changes in relief (Figure 2.1a). The LiDAR survey for Scotty Creek was performed in August of 2009 at a flying height of approximately 1500 m above ground level. The airborne survey configurations of the LiDAR sensor provided an average distance between the closest neighboring observations at several sample locations of 0.85 m with 95% of the points being within 1.30 m of another observation.

Table 2.1 - Topographic attributes and LiDAR point density of study sites

	Area (km^2)	Elevation Range (m)	95th percentile of slope histogram (°)	Point density (pts / m^2)
Thomas Brook	7.02	206	18	0.75
Mosquito Creek	46.33	1190	59	0.31
Scotty Creek	22.69	15.3	6.6	0.63

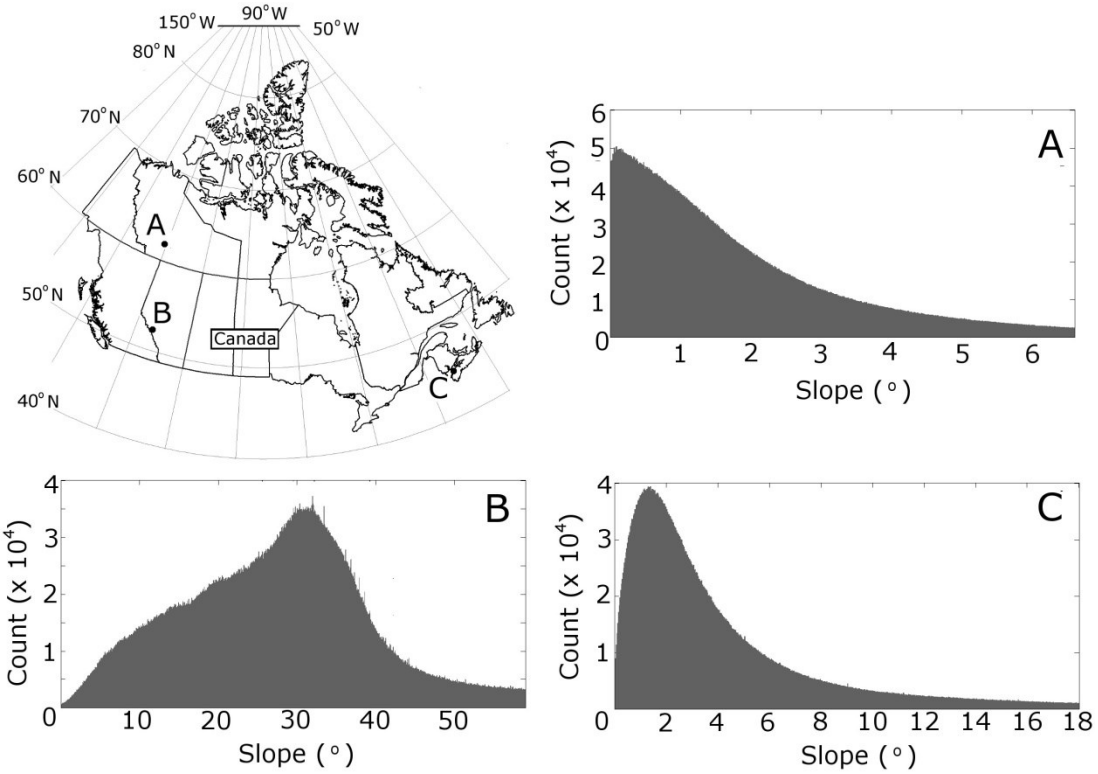

Figure 2.1 Geographic location of study watershed sites and associated slope histograms. Each slope histogram terminates at the 95th percentile; A) Scotty Creek; B) Mosquito Creek; C) Thomas Brook.

2.3.1.2. Mosquito Creek

Mosquito Creek watershed is located north-west of Banff, Alberta, Canada and forms part of the headwaters of the Bow Valley (Figure 2.1b). It is an alpine environment with an average elevation of 2500 m a.s.l. The dominant land cover is forest at lower elevations with a thin soils layer approximately 0.25 m in depth. In the upper elevations the terrain is predominantly exposed sedimentary carbonate bedrock, with areas of metamorphic sandstone, with small hanging glaciers on north-eastern facing slopes. A major geologic fault line runs from NW to SE through the basin, which exerts strong control over internal drainage characteristics (Hopkinson, 2002). The eastern side of the fault is characterized by highly incised drainage gullies in dolostone rock formations while the western side is characterized by quarzite rock with overlying forest and glacial tills (Hopksinson, 2002). The slope histogram of Mosquito Creek shows that 95% of the slopes at the site are below 59° with a peak at approximately 32°, showing the variable topography that exists in the alpine environment (Figure 2.1b).The LiDAR survey for Mosquito Creek was flown in August of 2010 at a 1700 – 2400 m a.g.l. The average distance between a point and its closest neighbor from a sample area of the Mosquito Creek survey was 1.1 m with 95% of the points taken within 1.9 m of another observation.

2.3.1.3. Thomas Brook

The Thomas Brook watershed is located near Berwick, Nova Scotia (Figure 2.1c). The headwaters begin on the southern side of a mountain at the northern end of the site and flow southerly into the Annapolis Valley. There are two main tributary branches that join at approximately one third of the distance from the headwaters to the outlet (Jamieson et al., 2003). Soils in the area are predominantly fine-grained reddish sandy loams (Cann et al., 1965) and the watershed consists of a mix of agricultural (~70%), residential and forested (~30%) land use (Brisbois et al., 2008). The majority of the watershed consists of gently sloping topography in the southern area along the valley floor (Figure 2.1c) and the majority of the slopes existing in the range of 0-6° and 95% of the slopes below 18°. The Thomas Brook LiDAR survey was acquired in August 2006.

The aircraft was flown at 900 m a.g.l and this resulted in an average spacing between an observation and its closest neighbor of 1.1 m and with 95% of the points having a neighbor within 1.5 m.

2.3.2 DEM preparation

2.3.2.1 Interpolation routines

The IDW algorithm is a univariate interpolator that weights observations based on their respective Euclidian distance from the DEM grid node being determined (Bartier and Keller, 1996). The weight associated with each sample elevation observation is determined through the inverse of the distance from the DEM grid node location raised to a selected power. The influence of surrounding points can be controlled by the value of the power exponent. High values of the exponent will more rapidly decrease the influence of observations at greater distances. A power of two was chosen as it is a typical value selected for interpolating elevations within previous studies (e.g. Chaplot et al., 2006; Guo et al., 2010). Only elevations located within a circular neighbourhood with a five metre radius around the DEM grid node were used. This spatial limit was chosen because elevation observations further than this distance may not be truly representative of the actual DEM grid node elevation and a sufficient number of sample elevations were always available within this limit. A large search radius also creates an overly smoothed terrain surface, which can lose important details of the topography. The IDW method is commonly used in LIDAR DEM processing because of its simplicity and efficiency for large data sets. The moving average (MA) interpolation method is identical in implementation to the IDW method except that the weights of all points within the search radius are equivalent.

The Universal Kriging (UK) interpolation routine has a well studied theoretical background within the field of geostatistics (see Cressie, 1993; Chilès and Delfiner, 1999). Studies which implement Kriging on LiDAR source data such as Lloyd and Atkinson (2002), and Guo et al. (2010) have identified that as raw data density decreases Kriging interpolators are advantageous within the context of DEM accuracy. However, as point densities approach those of typical LIDAR surveys there is negligible gain over

other simpler interpolation methods and large computational requirements. The UK algorithm assigns weights to surrounding observations based on their distance from the grid node as well as their spatial autocorrelation. The autocorrelation function is determined from fitting a semi-variogram model to estimate the correlation of surrounding elevation observations. UK is the most general form of point Kriging because it allows for a drift in the determination of the variogram (Chilès and Delfiner, 1999). A linear drift model for the mean was chosen, which was also implemented in Guo et al., (2010), as well as a linear variogram model. A search radius of five metres was selected as the neighbourhood for the UK algorithm for consistency with the IDW and MA algorithms.

The natural neighbour (NN) interpolation algorithm (Sibson, 1981) determines the interpolated point elevation by creating Theissien polygons associated with observed elevation values in the data set. The interpolated elevation is calculated as a weighted sum of the elevations of all other points in adjacent Theissien polygons. Weights are determined by the ratio of area lost from the pre-existing Thiessien polygons prior to the insertion of the point to be interpolated. The averaging algorithm in the NN routine differs from IDW, UK and MA in that no search radius is required. The triangular irregular network (TIN) interpolation scheme operates by constructing a set of contiguous triangles across the entire dataset, in which the triangular edges form linear connections between points. The algorithm is constrained by the condition that no triangle can contain a point in the dataset. Interpolated DEM grid node elevations are found by overlaying the horizontal grid point location onto the triangular mesh and extracting the elevation from the triangular facet plane it falls within. The TIN algorithm is traditionally well-used for generation of surfaces of topography because it honours the location of the data points, assumes minimal information about the terrain surface and identifies surface breaklines. The digital surface representation is often left as a triangular mesh and not converted to a grid based DEM. Although this conversion to a grid based DEM loses some advantages of the triangular mesh surface it is a required conversion for further processing.

2.3.2.2 Hydrological enforcement

Prior to hydrological analysis, DEMs require appropriate hydrological enforcement to properly characterize true field conditions. Pit filling was implemented on all DEMs according to the algorithm in ArcHydro, which raises the elevation of a pit to be equivalent with the lowest neighboring cell. Of the three study sites, Thomas Brook was the only watershed which was located in a developed area containing anthropogenic modifications to the landscape. Common anthropogenic features, which require hydrologic enforcement, are roads which pass over culverts and can incorrectly obstruct flow paths (Murphy et al., 2008). At these locations stream paths have to be 'burned' into the DEMs, to avoid artificial obstructions. The burning process consisted of identifying where culverts passed under roads and lowering the elevations of the DEM grid nodes across each road to the elevation of the outlet of the culvert. The location of all culverts in the Thomas Brook watershed, which required burning were confirmed through field visits to the site.

Scotty Creek contains no man-made structures; however, artificial and incorrect blockages exist at stream outflows near the edge of lakes where low-lying aquatic vegetation was not correctly removed during the filtering of non-ground raw elevation observations. It has been previously identified by Hopkinson et al. (2005) that an upward bias exists in LiDAR DEM elevations surrounding aquatic vegetation. This is due to the 1064 nm wavelength of the ALTM LiDAR sensor reflecting weakly, or being absorbed from water surfaces leaving only returns from the vegetative surface as potential ground points (Hopkinson et al., 2005). At Scotty Creek, this creates artificial obstructions to flow in the DEM where lake outflows drain into regions of marsh vegetation. The DEMs were visually interpreted to determine the location of true lake outflow points and channels were burned into the DEM to create a correct representation of flow pathways. The delineated drainage network also existed within lake boundaries and flow paths acted erratically in these areas due to increased noise levels in LiDAR return elevations over water surfaces (Hopkinson et al., 2011). Lakes were manually digitized into polygons and the associated stream lengths across the site were removed from the analysis to mitigate

errors in total stream network length estimate due to erratic flow paths in open water areas.

2.3.3. Stream delineation

Field reconnaissance was performed at Thomas Brook during August of 2010 to identify the location of the initiation of first order streams during base flow conditions as well as the location of any tributary junctions into the main stream channel. Stream initiation locations were identified based on the first existence of flowing water at the highest elevation on the hillslope. Several constant area thresholds were selected from a 1 m resolution DEM and a final value was chosen to be 1 ha, which best matched field verified locations of channel initiation, and showed the existence of the observed streams flowing into the main channel. The 1 ha threshold was implemented consistently for each unique combination of spatial resolution and interpolation method at each study site. Realistically, a threshold area will not remain consistent for each site; however, this assumption was necessary to allow for control in comparisons between the unique landscapes.

Due to an observed variability in watershed area, changes in the length of the entire drainage network were analyzed through drainage density, determined as a ratio of the total stream length to watershed area (Horton, 1932). The drainage density normalizes the stream length by watershed area and allows for a more suitable attribute for comparison between DEMs than stream length. No trends were obvious in drainage density results when comparing the spatial resolution and interpolation results individually. However, trends between the spatial resolution and drainage density became apparent when the interpolation results were averaged for each individual spatial resolution.

Variability was introduced in the relationship between spatial resolution and drainage density due to the necessity of a constant stream initiation threshold. Therefore, a single channel for all DEMs at each site was also extracted for length analysis. The single stream channel was chosen as the longest path of successively decreasing Strahler stream orders (Strahler, 1952) from the watershed outlet to the headwaters. Since the Thomas Brook watershed experiences a convergence of two main channels of equal

magnitude approximately one third of the distance from the watershed outlet, and because each of these main channels were surveyed in field validation, they were both included in the analysis. At Mosquito Creek and Scotty Creek only the single main channel was considered.

2.3.4 Thomas Brook GPS field validation measurements

A field validation was performed to determine the spatial accuracy and overall length of the stream network delineation in Thomas Brook. Validation included a ground survey of the main river channel, performed with a Real-Time Kinematic (RTK) GPS survey during June, July and August of 2011. The ground survey consisted of collecting cm level horizontal position and elevation observations along the centreline of the main channel in the watershed during base flow conditions. A small portion of channel near the outlet was neglected because it had been mechanically straightened and therefore did not represent a naturally evolving stream channel.

An estimate of the 'true' stream length was obtained by summing the linear distance between successive GPS observations. The accuracy of the predicted stream lengths determined from the DEMs at Thomas Brook was obtained by comparison with the length obtained from GPS field measurements. An estimate for the spatial accuracy of delineated streams was determined through a 'buffer analysis', which determined the percentage of the field surveyed GPS locations that fell within a 3 m wide buffer of the delineated stream in each DEM.

2.3.5. Determination of the fractal dimension of stream length

The existence of a scaling relationship between the DEM spatial resolution and the stream length was investigated by determining whether the variables took the theoretical form of a power function. In its most simple form, the power function is written as (Rodrìguez-Iturbe and Rinaldo, 1997):

$$g(x) = ax^{\alpha} \tag{2.1}$$

where $g(x)$ is the stream length, x is the DEM spatial resolution, and a and α are constants determined from experimental data. The fractal dimension (D) is related to the exponent in the power function as:

$$D = 1 - \alpha \tag{2.2}$$

The value for D can be similarly determined as the slope of a best fit line through a log-log plot of the spatial resolution and stream length. An estimate of the fractal dimension was obtained for the main channel stream length for all interpolation methods at Thomas Brook and Mosquito Creek. Variability in the main tributary channel at Scotty Creek prevented a reliable estimate of the fractal dimension. Therefore, the values for fractal dimension obtained from each interpolation method at Thomas Brook and Mosquito Creek were averaged to achieve a single site independent estimate (D_{av}). The scaling relationship defined by D_{av} was used to predict stream lengths, which would be obtained from the 1 m DEM from the length obtained from the 50 m resolution DEM. The accuracy of the re-scaled stream length estimates was described through a relative error to the stream lengths obtained from the stream delineations of the 1 m DEM.

2.4 Results and discussion

The results are organized into sections describing the watershed area, drainage density, and the single stream analysis, each including all three case study sites. Watershed area results discuss observed scale-dependent irregularities, as well as the suitability for hydrological analysis according to the Gyasi-Agyei et al. (1995) ratio. The suitability test was applied to Mosquito Creek and Scotty Creek, the two end-member case studies of possible relief variation. The drainage density section presents observed results on potential scaling behaviour of DEM spatial resolution with the length of the entire drainage network. The single stream section presents results of the spatial accuracy of the main channel stream delineations obtained through the buffer analysis, the accuracy of modeled stream lengths, the determinations of the fractal dimension, and the predicted 1 m stream lengths from 50 m stream lengths through the observed fractal scaling relationship.

2.4.1 Watershed areas

2.4.1.1 Thomas Brook

At Thomas Brook, the coarse spatial resolution DEMs tended to produce smaller watershed areas apart from the IDW and MA 50 m DEMs (Figure 2.2). The reduction in watershed area in coarse resolution DEMs is attributed to the exclusion of a section of the watershed in the south-western corner of the site (Figure 2.3), where the coarse resolution DEMs could not represent a drainage ditch and road blockage. The field verified drainage network flows easterly in a ditch along the northern edge of the road boundary until it reaches the outlet, correctly represented in the 1 m and 5 m DEMs. The DEMs, which were 10 m and lower in resolution, contained spacing between grid nodes that was larger than the 8 m wide roadbed. At some location along the roadway the lower resolution DEM grid nodes are located on adjacent sides of the road at elevations lower than the road surface. This allows an incorrect flow path across the road and causes 10% of the watershed to diverge to an incorrect outlet point. This error is a combination of both the DEM resolution and width of the roadbed. As the roadbed has a defined width of 8 m, the error is scale dependent. The 10 m DEM represents the finest resolution DEM tested, which could cause this error.

2.4.1.2 Scotty Creek

Area estimates for the Scotty Creek watershed are highly variable among both spatial resolution and interpolation methods (Figure 2.2). The relative change in area reached 53%, well above the levels of increase observed at either Thomas Brook or Mosquito Creek. This result corroborates existing evidence that determination of watershed attributes is difficult in low relief landscapes. For example, Lohani and Mason (2001) identified that unacceptable levels of error of commission and omission existed in the determination of fluvial channels in tidal flats with a LiDAR derived DEM and the D8 algorithm. They identified that errors were due to a high incidence of random error and distinctive morphological characteristics of the channels in tidal flats, such as enclosure by raised banks (Lohani and Mason, 2001). Uncertainty in watershed area is introduced at Scotty Creek through measurement error, resulting from low-lying

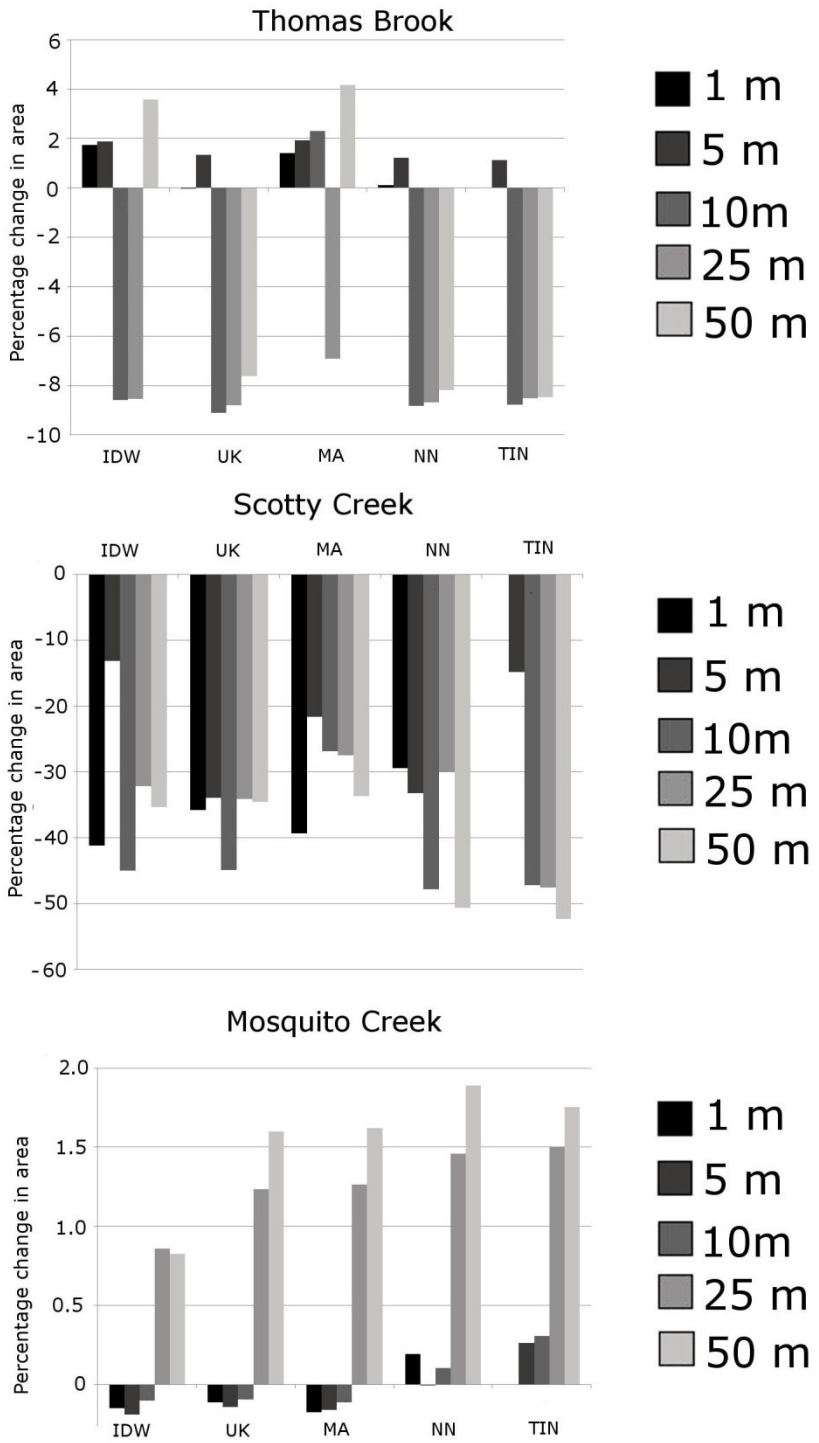

Figure 2.2 **Change in watershed area for each interpolation method and spatial resolution as compared to the area determined from the TIN interpolation method at a 1 m spatial resolution for each study site.**

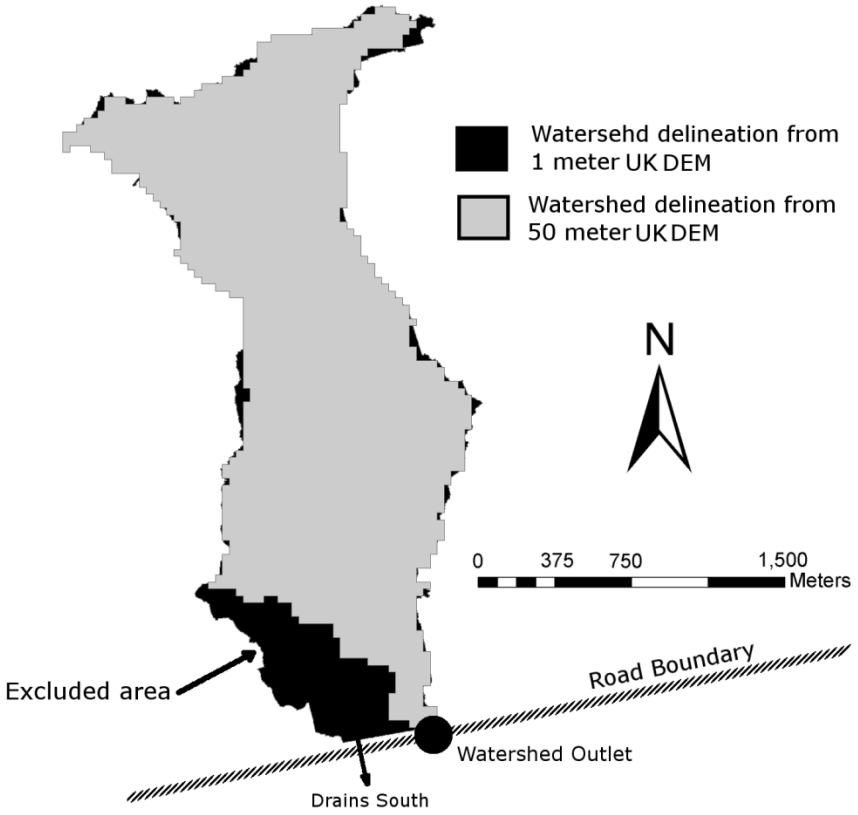

Figure 2.3 Watershed delineation of 1 m IDW DEM and 50 m IDW DEM.

vegetation and surface saturation, which biases laser return signals (Hopkinson et al., 2005). The direction of flow paths and inclusion of areas is biased by elevation uncertainty introduced through non-ground objects, which remained after filtering, or measurement error introduced through laser reflections with a low signal to noise ratio returned from saturated surfaces. Subsequently, irregularities in area result in random variability and do not show obvious scale dependence for the tested resolutions or relationship to interpolation method.

The lack of consistency in the estimates of area can be explained through the Gyasi-Agyei et al. (1995) suitability ratio. To quantify this value, an estimate of the DEM vertical error is required to estimate DEM precision. Considering the complicated interaction of error sources, conclusive error estimations across the Scotty Creek site are difficult to predict and no ground validation data is available for empirical error assessments due to the remote location of the site. Of the available previous studies, which focused on LiDAR error sources, the study performed by Hopkinson et al. (2005)

analyzed error in a landscape similar to that of Scotty Creek. In this study the standard deviation of height errors ranged from 0.10 m to 0.18 m depending on vegetation type, although larger errors have been observed in other vegetation types (Hodgson and Bresnahan., 2004). The 1 m TIN DEM of Scotty Creek resulted in the largest overall mean slope of 2.6°, which leads to an average drop of 0.05 m per pixel. Therefore, the ratio for this pixel drop to DEM precision, assuming an optimistic vertical precision (0.10m) observed by Hopkinson et al. (2005), is 0.5. This value is well below the unit ratio required for DEM suitability suggested by Gyasi-Agyei et al.(1995). Even under ideal flight and terrain conditions, the level of precision required to reach a suitability ratio near unity in this landscape is approaching achievable accuracy limits of current LiDAR sensors (Goulden and Hopkinson, 2010a). Localized terrain variation below the random error in DEM grid nodes will lead to incorrect and random deviations in flow paths and boundaries at the local scale. Therefore, the collected LiDAR data may not be suitable for detailed accurate hydrological flow path analysis in this landscape using a 1m DEM.

Increasing the DEM grid spacing increases the average elevation drop per pixel by allowing for larger potential changes in relief and relaxes the DEM error precision requirements in the Gyasi-Agyei et al. (1995) suitability test. For example, the 50 m TIN DEM resulted in an average slope of 0.25°, which corresponds to an average pixel drop of 0.22 m and a suitability ratio of 2.2, assuming optimistic error circumstances. The improved ratio may seem encouraging, however, the decrease in spatial resolution introduces additional uncertainty by ignoring variations in the landscape which are smaller than the grid cell size and this can have a large influence on the overall drainage area. If LiDAR is intended for analysis in this type of landscape, a potential solution is to increase the density of raw observations, which will reduce the magnitude of random error and increase the precision of individual DEM grid nodes. However, if elevation uncertainty is being introduced through surface cover such as or low lying vegetation an increase in data density may prove unsuccessful. To properly characterize the basin hydrology improved raw point filtering routines, or alternative stream network processing routines are required.

2.4.1.3 Mosquito Creek

The Mosquito Creek results show a relationship of increasing watershed area as the spatial resolution becomes lower (Figure 2.2). The overall magnitude of the change in area is approximately 2.0%. The trends are relatively consistent across all interpolation methods, in contrast to the results obtained at Thomas Brook and Scotty Creek. The slight increase in the watershed area at the coarse spatial resolution was due to the inclusion of a small additional area of the watershed (Figure 2.4). The deviation has a scale dependence as the fine resolution DEMs correctly represented a ridge, which caused a barrier to flow and excluded the small area while the coarse resolution DEMs permitted flow across the ridge. Despite the small deviation, the Mosquito Creek site shows consistency, which was not available at either Thomas Brook or Scotty Creek.

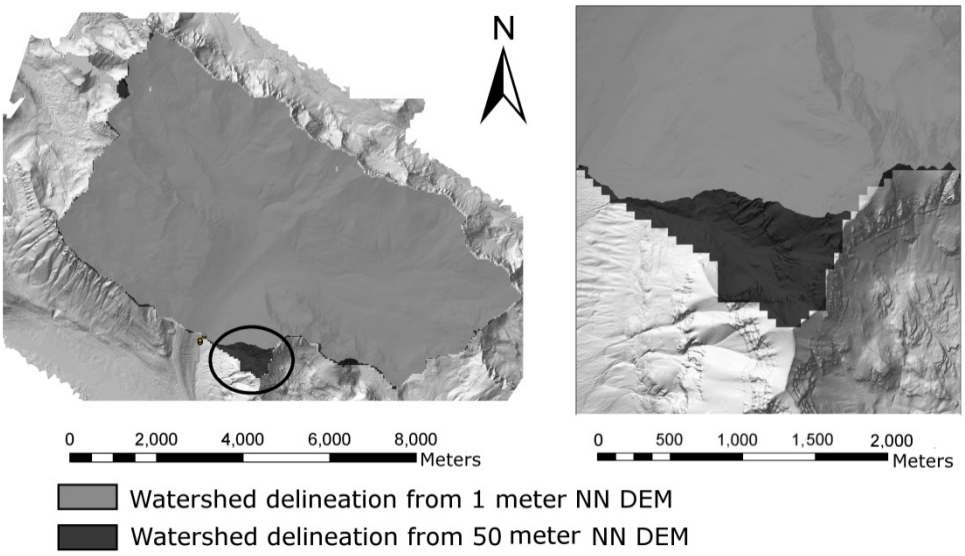

Figure 2.4 Mosquito Creek watershed delineation derived from the 1 m NN DEM overlaid on the watershed delineation derived from the 50 m NN DEM. A) overview of the entire watershed, B) magnified view of an area, which showed a discrepancy between the two delineations.

The consistency at Mosquito Creek can be related to the Gyasi-Agyei et al. (1995) ratio. The average slope across the entire site for the TIN DEM at a 1 m resolution is 25°, which corresponds to an average pixel drop of 0.47 m. Although LiDAR error levels are known to increase in sloped environments due to complications related to the interaction of the laser pulse with sloped terrain and inherent horizontal uncertainty, mean errors typically do not reach levels near 0.47 m. Therefore the 1 m DEM at Mosquito Creek

results in a suitability ratio of greater than one, indicating favorable conditions for hydrologic network extraction.

2.4.2 Drainage density

A relationship between interpolation method and drainage density did not exist with the exception of the MA method, which resulted in the lowest drainage density at each site. Therefore, focus is on the relationship between spatial resolution and drainage density. Scotty Creek was the only site to demonstrate the hypothesized decrease in drainage density with increasing DEM grid cell size (Figure 2.5).

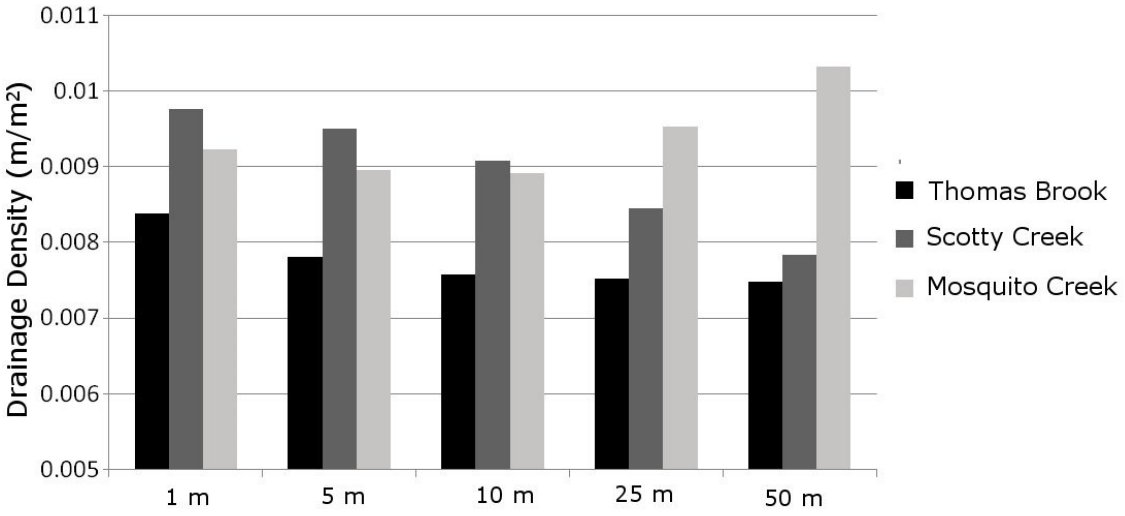

Figure 2.5 Drainage density of each watershed averaged across all gridding methods for each spatial resolution

Thomas Brook exhibits a decrease in drainage density as cell size increases initially; however, no significant further decreases occur at the 10, 25 and 50 m resolutions. Mosquito Creek shows a decrease at high resolutions (1, 5 m) followed by an increase at the 25 and 50 m spatial resolutions. The unexpected increase in drainage density occurs in the low resolution DEMs at Mosquito Creek is a result of an increase in total length of first order streams (Figure 2.6).

The increase in the total length of first order streams is a result of the convergent topography at Mosquito Creek, which facilitates attaining the stream initiation area threshold at higher elevations on the hillslope (Figure 2.6). In coarse resolution DEMs,

the threshold area is more easily met since fewer cells are required to collectively drain to a common point. The increase in the likelihood of a small number cells with a large area initiating a stream results in the increase in the length of first order streams in coarse resolution DEMs. Since Scotty Creek is characterized by divergent topography with subtle changes in relief, the likelihood of a meeting the contributing area threshold for stream initiation is low, even at coarse resolutions, and the length increase of first order streams did not occur. Therefore, the drainage density decreased as expected due to the loss of details in the drainage network at coarse resolutions. At Thomas Brook, the existence of moderate and subtle changes in relief resulted in drainage density results, which were not as extreme as that of Scotty Creek or Mosquito Creek. Therefore, the length of the entire drainage network is related to the resolution of the DEM, the choice of stream initiation threshold, as well as the topographic landscape characteristics within the basin. Due to the interaction between these variables, the hypothesized scaling relationship cannot be established between the drainage density of a stream network and changes in scale initiated through changes in spatial resolution.

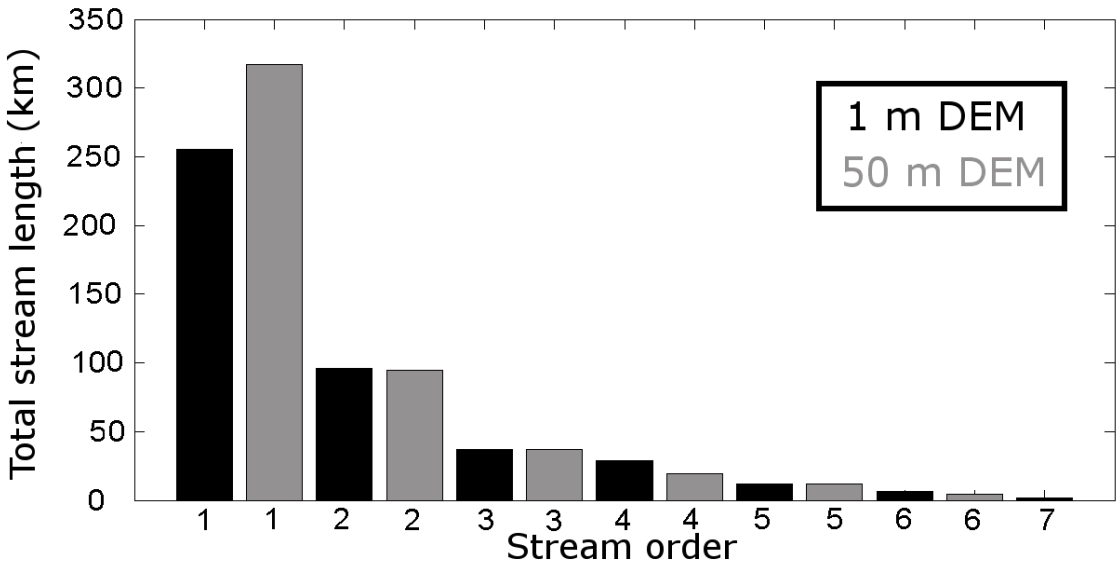

Figure 2.6 Total stream lengths of all stream orders for 1m and 50m spatial resolution DEMs for Mosquito Creek.

2.4.3 Single stream analysis

2.4.3.1 Spatial accuracy of Thomas Brook watershed stream delineation

The 1 m resolution DEM resulted in the most accurate stream delineation with approximately 71% of validation points falling within the 3 m buffer (Table 2.2). The MA interpolation method was the exception, resulting in the lowest accuracy among the 1 m resolution DEMs. The inaccuracy of the MA algorithm is attributed to a section of the stream in which the delineation followed an erroneous path compared to the field validated stream network (Figure 2.7a). The erroneous flow path occurred in an area of low relief and is due to a slight perturbation in elevation causing the stream to incorrectly deviate. At the 1 m level of spatial resolution the MA interpolation also tended to reduce the overall sinuosity of the stream network and additional inaccuracies occurred in sections of the river with substantial meanders (Figure 2.7b). The reduction in sinuosity of the MA method occurs due to the equivalent weighting of all raw data points in the determination of DEM grid node elevations, which created a smoothing effect. Inaccuracy at the 1 m level for the remaining interpolation methods was also a result of the underrepresentation of meanders in the streams because of the inability of the DEMs to represent the stream channel at resolutions finer than the 1 m cell size. As the DEM resolution became increasingly coarse, finer details were further lost and the accuracy continually degraded, as shown in Table 2.2. At the 50 m resolution the DEM stream delineations generally contained only 7% of the validation points.

Table 2.2 Spatial accuracy of stream delineations in Thomas Brook where the percentage represents the number of validation points that fell within a 3 m stream buffer.

	1 m (%)	5 m (%)	10 m (%)	25 m (%)	50 m (%)
IDW	71.5	40.1	22.2	10.0	6.3
Kriging	71.6	51.0	22.9	13.5	7.2
MA	48.1	45.6	28.6	14.5	7.7
NN	71.0	52.0	23.0	13.7	7.2
TIN	71.2	52.5	22.3	13.4	7.2
Mean w/o MA	**71.3**	**48.9**	**22.6**	**12.7**	**7.0**

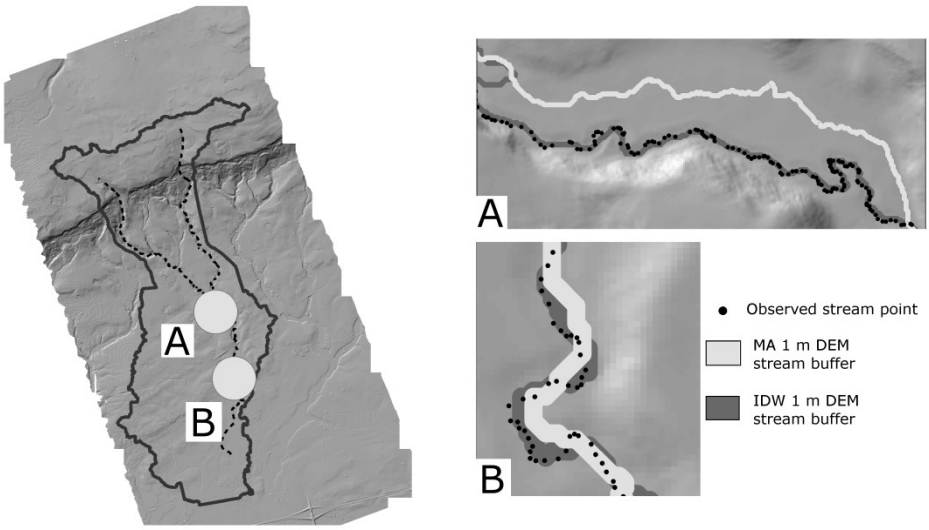

Figure 2.7 Buffer analysis of the field validated stream locations and delineated streams. A) illustrates the offset between the section of stream derived from the 1 m MA DEM and that surveyed in the field, B) illustrates errors in the MA 1 m stream position due to reduced sinuosity.

2.4.3.2. Stream length

The sum of the linear segments between GPS validation points resulted in a total distance of 10,403 m, longer than any of the delineated stream lengths found from the DEMs. The 1 m DEMs produced the most accurate estimation of the overall stream length (Table 2.3). Similar to the spatial accuracy results, the 1 m DEM generated with the MA interpolation algorithm was the most inaccurate and was removed from the calculation of average error. The remaining lengths resulted in an average error of only 3.7%. This suggests that for watersheds at the scale of Thomas Brook (~680 ha) the most accurate DEM resolution for stream length analysis is less than 1 m. The 50 m DEMs resulted in a length that was shorter than the field verified stream length by nearly 25%. Therefore, we can expect that simulated hydrological outputs using typical watershed runoff modeling approaches, such as peak runoff volume and timing, or sediment yield will incur systematic calibration or prediction errors commensurate with the weighting of the stream length parameter. For example, peak timing will tend occur earlier with shorter stream lengths along with an increase in peak magnitude.

Table 2.3 Percentage error of main channel stream length at Thomas Brook calculated as the ratio of the difference between the DEM observed stream length and the field verified stream length.

	1 m	5 m	10 m	25 m	50 m
IDW	3.6	11.1	16.6	24.5	25.1
Kriging	3.8	9.1	15.2	22.3	24.6
MA	9.3	12.8	16.9	23.2	24.5
NN	4.1	9.3	15.2	22.2	23.4
TIN	3.4	9.0	16.0	22.0	23.4
Mean w/o MA	**3.7**	**9.6**	**15.8**	**22.8**	**24.1**

2.4.3.3 Prediction of stream lengths

A scaling relationship between spatial resolution and main channel stream length was observed at Thomas Brook (Figure 2.8a) and Mosquito Creek (Figure 2.8c). The relationship was not identifiable at Scotty Creek (Figure 2.8b) because uncertainty introduced by LiDAR sensor measurement error caused deviations in stream location between the different resolutions. Table 2.4 summarizes the fractal dimension found for each interpolation method at Thomas Brook and Mosquito Creek as well as the average fractal dimension of all interpolation methods. The average fractal dimension (D_{av}) between all interpolation methods at both Thomas Brook and Mosquito Creek was determined to be 1.059, which agrees with previous determinations for single stream channels, such as those reported by Tarboton et al. (1988) to be between 1.04 and 1.07.

Table 2.4 Fractal dimension of stream length due to scaling of spatial resolution

Interpolation Method	Thomas Brook	Mosquito Creek
IDW	1.070	1.052
Universal Kriging	1.066	1.049
Moving Average	1.051	1.061
Nearest Neighbour	1.062	1.061
Triangular Irregular Network	1.062	1.055
Average	1.062	1.056

Since the 1 m DEM resulted in the most accurate stream lengths at Thomas Brook, the D_{av} (1.059) was used to re-scale stream lengths generated from the 50 m resolution DEMs to values that would be expected to be generated from 1 m resolution DEMs (Table 2.5). This exercise was undertaken to demonstrate how fractal relationships could be used to "correct" stream lengths generated using coarse resolution DEMs. Table 2.5 contains a length error (in units of metres) and an error percentage of estimates of 1 m DEM stream lengths obtained from re-scaling the 50 m DEM lengths using D_{av}. At both the Thomas Brook and Mosquito Creek sites the predicted stream lengths are within 5% of the lengths delineated from the 1 m DEM directly. The estimate from the MA interpolation algorithm was the least accurate at Thomas Brook, this is not surprising considering the spatial inaccuracies that were previously identified. In both the Thomas Brook and Mosquito Creek sites the TIN and NN interpolation methods resulted in the most accurate predictions. Scotty Creek showed the least accurate overall predictions, which were in some cases approximately 10% higher in error than predictions at Thomas Brook and Mosquito Creek. The poor performance at Scotty Creek can be attributed to the previously identified complication of the stream paths not following repeatable channels. Also, it is possible that a different optimum value of fractal dimension would be obtained for this landscape had the appropriate stream data been available. Despite these complications, a reasonable estimate (< 14% difference) of the lengths obtained from the high resolution DEMs could be obtained from the low resolutions DEMs at Scotty Creek.

Table 2.5 Absolute error in 1 m estimates based on average estimates of fractal dimension.

Interpolation Method	Thomas Brook	Mosquito Creek	Scotty Creek
IDW	218 (2.2%)	237 (2.4%)	177 (1.5%)
Universal Kriging	125 (1.2%)	427 (4.2%)	1892 (13.7%)
Moving Average	453 (4.8%)	143 (1.5%)	1434 (13.6%)
Nearest Neighbour	67.0 (0.7%)	21 (0.2%)	1577 (11.4%)
TIN	9.5 (0.1%)	167 (1.6%)	1015 (7.7%)
Average	175 (1.8%)	199 (2.0%)	1219 (9.6%)

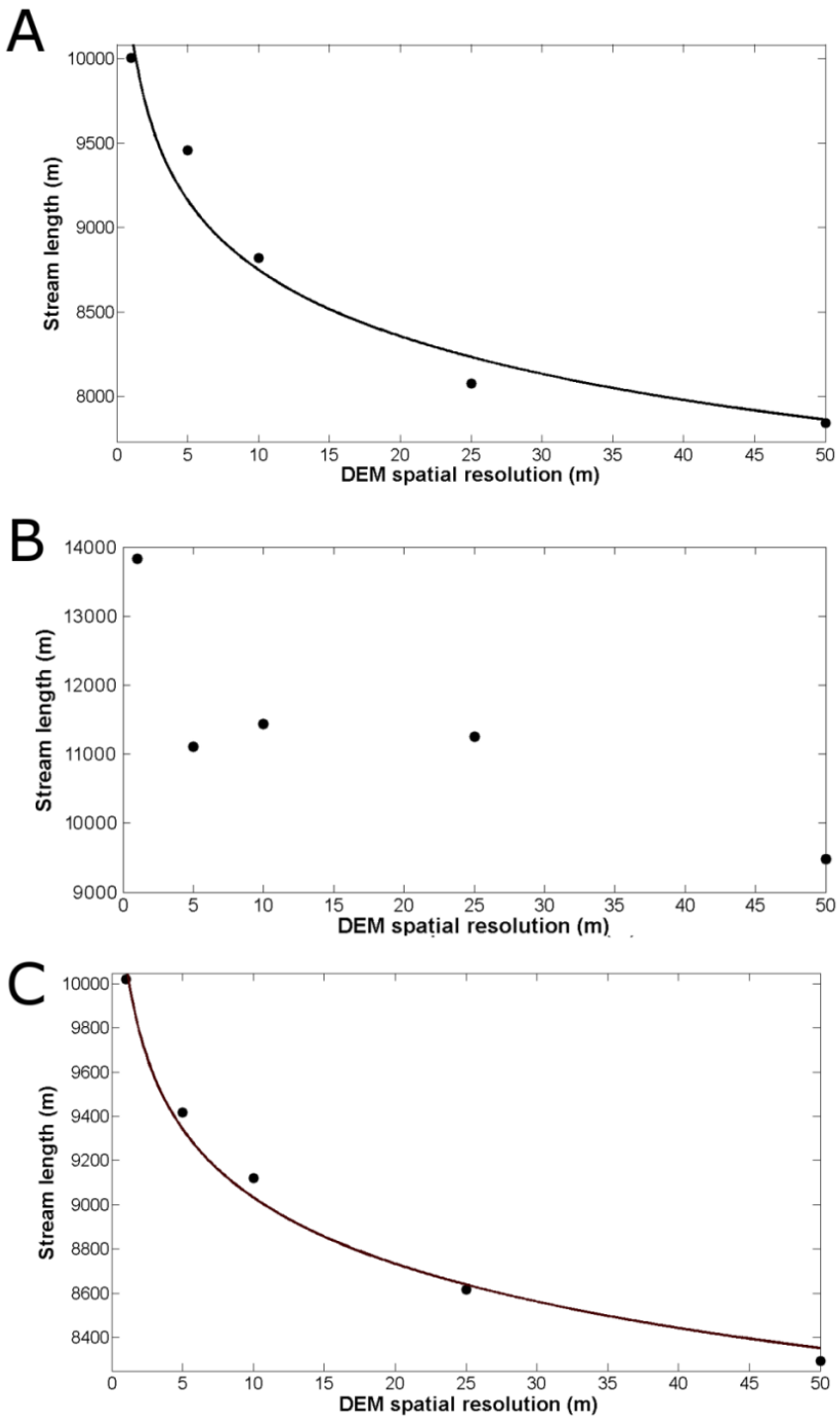

Figure 2.8 **Variation of DEM spatial resolution with main channel stream length for the Universal Kriging interpolation method, at A) Thomas Brook, B) Scotty Creek, C) Mosquito Creek.**

2.5 Conclusion

Choices surrounding the generation of LiDAR derived DEMs, including the spatial resolution and interpolation method, will affect the representative scale of the topography and elevation of grid nodes. The spatial resolution will contribute to variability in DEM based watershed attributes such as basin area, stream location and stream length, while the interpolation method can affect the stream location and length. These attributes are important inputs to distributed parameter watershed models, capable of simulating the hydrologic response of a basin, and developing sustainable environmental planning initiatives. This research investigated i) the existence of DEM scale dependent irregularities between watershed extents and stream length in three topographically distinct landscapes, ii) a fractal scaling relationship between DEM resolution and stream length, iii) the ideal scale for determining the stream length in the Thomas Brook Watershed, and iv) the sensitivity of watershed area and stream attributes to the DEM interpolation method.

At Thomas Brook watershed it was found that watershed area exhibits dependence on DEM spatial resolution due to landscape features, which become identifiable at different DEM resolutions. These irregularities occurred due to coarser DEM resolutions (10-50 m), which created an incorrect drainage path across a road and resulted in more than 10% of the true watershed area diverting to a separate outlet. Therefore, in areas with urban features the highest resolution DEM available is recommended as long as appropriate hydrologic enforcement is applied to correct anthropogenic modifications of the landscape. At the Mosquito Creek site a small portion of the watershed near the selected outlet was included in the coarse resolution DEMs (50 m), which caused a slight increase in the overall area (~2.5%). Since only minor changes were observed, if watershed area is the only attribute of interest in an alpine environment a high spatial resolution DEM is not required and the selection of spatial resolution should be based on efficiency and ease of data processing. Scotty Creek exhibited the largest overall variation in watershed area containing differences of up to 53% in area. The high variability at the Scotty Creek site was not due to scale dependent irregularities, but was related to the variability of elevation estimates at DEM grid nodes. DEM grid node variability was introduced by land cover conditions, such as low lying vegetation

and saturated ground surfaces. Conservative rules for DEM suitability recommended by Gyasi-Agyei et al. (1995) detected that 1 m LiDAR DEMs in this environment were insufficient for extraction of stream networks given their uncertainty. If fine resolution LiDAR DEMs are needed in this type of boreal tundra landscape for hydrological analysis, emphasis should be placed on reducing vegetation cover noise and on hydrological pre-conditioning of the DEM. Watershed analysts should be aware that the high resolution afforded by LiDAR derived DEMs will reduce the uncertainty in the determination of watershed area in low relief environments if the noise in DEM grid determinations is lower than the relative changes in elevation.

The total length of a drainage network, as represented by drainage density, was hypothesized to decrease as the DEM spatial resolution became increasingly coarse due to the loss of fine scale details in the stream network as previously observed in (Hemlinger et al., 1993; Garbrecht and Martz, 1994; Wang and Yin, 1998, Thieken et al., 1999). This phenomenon was initially observed across all resolutions for Scotty Creek and at resolutions of 1 to 25 m for Thomas Brook and 1 to 10 m for Mosquito Creek. However, as DEM resolution decreased further at Mosquito Creek, the drainage density began to increase due to an average lengthening of first order streams. This is a result of the convergent alpine topography at Mosquito Creek increasing the likelihood of stream initiation. The consistent decrease in drainage density to DEM resolution observed at Scotty Creek was due to the divergent topography preventing surface flow accumulation and stream initiation. The results of this research have shown that, in addition to the DEM resolution and stream initiation threshold, the topographic characteristics will also exert influence on the total length of the drainage network, which prevents the determination of a generalized scaling relationship.

A comparison of a field observed and DEM simulated main channel stream lengths from each resolution DEM at Thomas Brook showed that the 1 m resolution DEMs produced the most accurate length, but was approximately 3-5% short. The 1 m DEMs also showed the highest spatial accuracy through a buffer analysis of the field verified stream location. If stream network length and spatial accuracy are critical attributes to be developed from the DEM, than the highest resolution of data available is recommended, as the 1 m DEM represented the best available DEM resolution at Thomas

Brook. A hypothesized scaling relationship between grid resolution and main channel stream length, described by a fractal dimension, was shown to exist. The fractal relationship can be exploited to estimate stream lengths at any given scale. The scaled estimates of stream lengths at the 1 m DEM resolution showed an agreement of less than 5% to those delineated from the 1 m DEM.

The existence of scale dependent irregularities indicates that careful consideration of the major features within a site should be undertaken prior to selection of DEM spatial resolution. Additional scale dependent irregularities could exist in other landscapes or surface conditions, which were not identified from the three sites tested here. Further scaling analyses in a broader cross-section of sites with unique features would be beneficial to reveal further irregularities at distinct scales. This would provide more robust information for watershed analysts when selecting or acquiring DEM information for a site of interest. Although the 1 m DEM was identified to result in the best representation of the stream length in Thomas Brook, larger scale watersheds with higher stream orders may not show similar results. Further field investigations would be beneficial in estimating the ideal scale for stream length analysis in larger scale basins with different landscape and topographic conditions prior to implementing the scaling relationship. If the ideal scale can be determined, this relationship has practical application to distributed watershed modeling as the stream length can be scaled from the resolution of the available DEM to the ideal resolution. Corrected stream lengths will improve model parameterisation and performance and lead to more accurate simulated hydrological model outputs. Higher accuracy simulated outputs will provide improved information for designing environmentally sustainable planning strategies and policy.

CHAPTER 3 SENSITIVITY OF DEM, SLOPE, ASPECT AND WATERSHED ATTRIBUTES TO LIDAR MEASUREMENT UNCERTAINTY

3.1 Introduction

A virtual representation of land surface topography is a fundamental data source for paramaterizing rainfall-runoff models as terrain morphology influences surface flow processes. The common form of a virtual terrain surface is a grid cell based DEM, which can be used to determine topographic attributes such as slope (S) and aspect (ψ) (Gallant and Wilson, 2000), and watershed attributes such as basin area and stream network topology (Jensen and Dominigue, 1988; Martz and Garbrecht, 1993). As a measured input, the DEM is subject to various sources of error (Gong 2000; Fisher and Tate, 2006; Wechsler, 2007), therefore, users should exercise appropriate due diligence should be undertaken to understand the reliability of the DEM as well as derived topographic and hydrological products. Despite knowledge of the existence of DEM errors, Wechsler (2003) identifies that the majority of DEM users do not account for uncertainty in DEMs or derived topographic parameters. Ignorance of DEM uncertainty and its influence to hydrological model predictions can promote false conclusions and undermine decision making for water resource planning initiatives.

Due to their high spatial resolution and accuracy, LIDAR (Light Detection and Ranging) derived DEMs are increasing in usage for derivation of hydrological products as demonstrated by recent research endeavors (e.g. Barber and Shortridge, 2005; Murphy, 2008; Remmel, 2008; Hopkinson, 2009; Li and Wong, 2010; Beeson et al., 2012; Li et al., 2011). As LiDAR derived DEMs are being increasingly used by the hydrological modeling community, there is a need to assess the sensitivity of hydrological products to LiDAR measurement errors. Several studies have empirically demonstrated the existence of errors in LiDAR observations (Huising and Pereira, 1998; Reutebach et al., 2003; Hodgson and Bresnahan, 2004; Hodgson et al., 2005; Csanyi and Toth, 2007; Goulden and Hopkinson, 2010a), however, no studies have propagated these errors into the determination of a LiDAR DEM and derived products, such as primary topographic

attributes, or delineated watershed extent and stream networks. A study was performed by Lindsay (2006), which investigated the sensitivity of DEM elevation errors to hydrologic network extraction with a high resolution LiDAR DEM. Four methods of hydrologic network extraction were investigated, including two valley recognition techniques, and two channel initiation techniques. Within his analysis, DEM elevation uncertainty was simulated using several **assumed** RMSE values, including 0.10, 0.50, 1.00 and 5.00 m. These values may not represent the true error characteristics of the DEM.

To obtain three dimensional ground coordinate errors, primary LiDAR sensor measurements can be propagated through the LiDAR direct geo-referencing equation (Vaughn et al., 1996). Primary measurements include the sensor position and attitude, a scan angle and a laser range. Primary measurement error takes the form of both systematic bias and random noise (Wolf and Ghilani, 1997). A systematic bias tends to affect all observations similarly, whereas random errors will be variable and unpredictable. The source of a systematic bias can often be identified, modeled, and eliminated, therefore, does not require treatment here. Random errors act in an unpredictable fashion and are unavoidable, therefore, effort is necessarily placed on quantifying and understanding their effects to derived DEM products. Procedures for placing statistically derived limits on observed three dimensional LiDAR positions due to random measurement errors have been developed by Glennie (2008), and Goulden and Hopkinson (2010a).

Goulden and Hopkinson (2010a) demonstrated that random measurement errors of primary LiDAR observations tend to propagate more severely into three dimensional coordinate observations as the scan angle and aircraft altitude increases. Previous empirical evidence has also identified that LiDAR errors will increase in areas of high terrain slope (Huising and Pereira, 1998; Hodgson et al., 2003, Hyyppä et al., 2005). Schaer et al. (2007) theoretically identified that an increase in LiDAR coordinate error in areas of high slope is related to the incidence angle between the laser pulse and the intercepted terrain (Θ_i). An increase in LiDAR coordinate error with an increase in Θ_i is caused by a spread of the laser energy across the terrain (Schaer et al., 2007; Morton and Young, 2012), which increases range uncertainty. Hodgson et al. (2005) also discuss an

increase in LiDAR elevation coordinate uncertainty in sloped environments according to the well-known Koppe formula, which predicts an increase in elevation error on sloped terrain due to the existence of horizontal error as

$$Error_{Elevation} = Error_{Horizontal} * \tan(S) \quad (3.1)$$

Despite the observed dependence of LiDAR errors on acquisition and terrain variables, no attempt has been made to illustrate the spatial distribution of error and its relationship to terrain conditions or LiDAR survey acquisition parameters.

The objective of this Chapter is to perform an uncertainty analysis of topographic attributes (slope, aspect) and watershed attributes (stream length, watershed area) to random primary LiDAR measurement errors in a high resolution LiDAR derived DEM. Additionally, observed uncertainty was related to survey acquisition parameters and terrain conditions in the form of Θ_i, and terrain slope, respectively. Slope and aspect are chosen as topographic derivatives for analysis because of their importance to stream network extraction and hydrological modeling. Slope is related to flow velocity, which affects peak flow timing and magnitude, as well as the erosive potential of surface flow. Aspect was included because of its importance in the derivation of watershed extent and stream networks. However, similar analysis could be further applied to additional topographic derivatives such as curvature or the topographic index. Watershed area and stream length are selected because they are common quantities for estimating rainfall-runoff relationships and are required for the parameterisation of a broad cross- section of distributed and semi-distributed hydrological models.

A visual qualitative assessment is provided for the uncertainty in the DEM grid node elevations (σ_{DEM}), slope (σ_S), and aspect (σ_ψ). The visualisation of uncertainty offers a tool for identifying regions with unsuitable uncertainty and provides easily interpretable information on the spatial pattern of uncertainty. A spatially explicit determination of the Gyasi-Agyei et al. (1995) metric, given by the ratio of DEM precision to the average pixel drop, is also provided. As originally proposed, the Gyasi-Agyei et al. (1995) metric was used to determine a global DEM suitability for stream network extraction. The metric was calculated as the ratio of DEM precision to the average elevation drop of DEM grid nodes. Given that the analysis presented here

generates a unique estimate of σ_{DEM} for each grid cell in the DEM lattice, it allows a spatially explicit assessment of the Gyasi-Agyei et al. (1995) ratio. Knowledge of the ratio on a cell specific basis allows estimates of hydrologic suitability due to varied terrain and acquisition criteria present throughout the DEM, which could allow users to detect regions with unacceptable levels of uncertainty for stream network extraction. The results of this uncertainty analysis will provide guidance for assessing the suitability of a LiDAR derived DEM as a source for DEM information by demonstrating the level of expected uncertainty in hydrological products. If the maximum level of uncertainly for a given project is known *a priori*, informed decisions can be made on LiDAR mission planning parameters to ensure uncertainty targets are met during data acquisition, or to plan alternative measures for collection of higher accuracy topographic information.

3.2 Methods

3.2.1 Study site

The study site chosen for the analysis is the 689 ha Thomas Brook watershed located near Berwick, Nova Scotia, Canada (Figure 3.1A). The site consists of a hill to valley transition with the headwaters beginning on a northern mountain at an elevation of 200 m a.s.l. Stream flow is southerly and drops to the valley floor of approximately 10 m a.s.l. The majority of the watershed exists on the valley floor where slopes derived from a 1 m DEM range between 0° and 5° (Figure 3.1B). As the watershed transitions from hill top to the valley floor slopes can be as high as 32°, although this is rare as 95% of slopes across the entire site are below 18° (Figure 3.1B).Two main channels are initiated at headwater locations on a northern mountain and join into a single channel on the valley floor at approximately two-thirds of the total length (Jamieson et al., 2003).

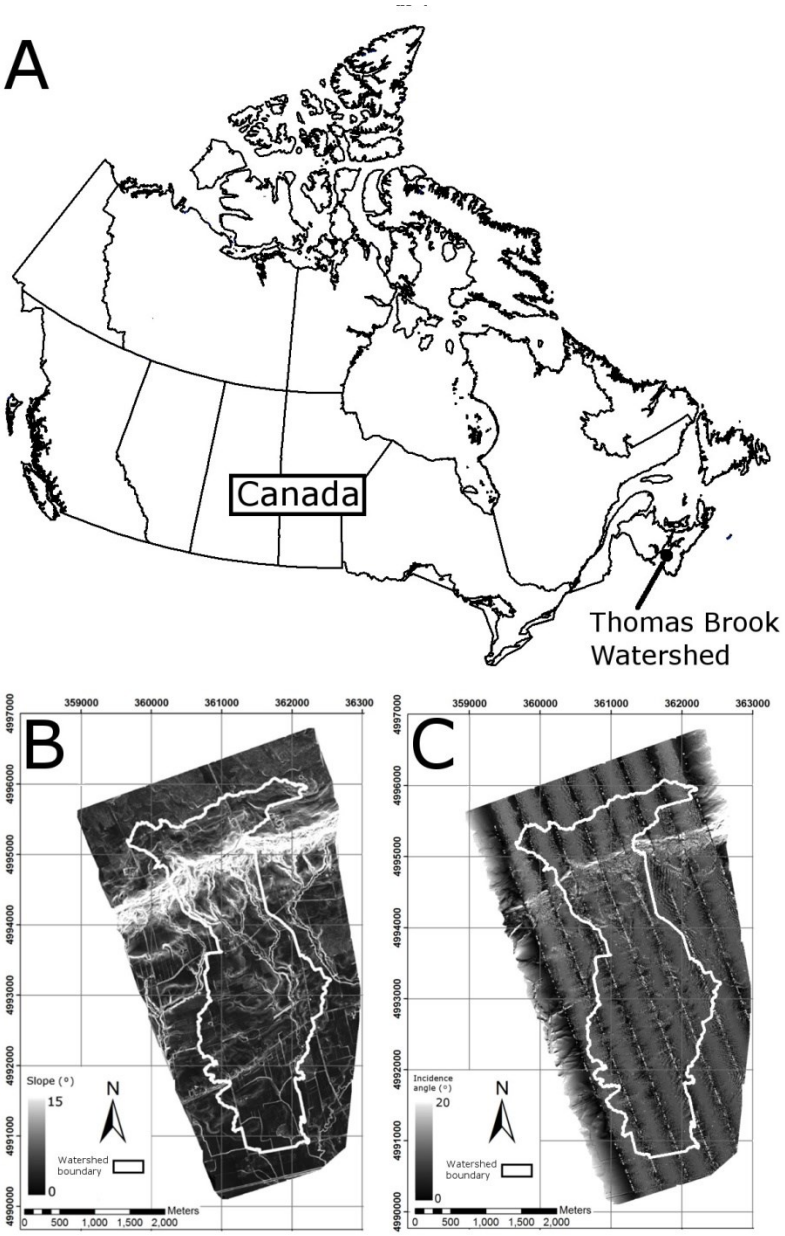

Figure 3.1 **A) The Thomas Brook watershed location within Canada, B) slope map obtained from a 1 m LiDAR DEM, C) map of resulting θ_i from the Thomas Brook LiDAR survey**

The LiDAR survey of the Thomas Brook watershed was performed in August of 2006 with an Optech ALTM 3100 system (Optech, 2004). The survey was flown at an altitude of 900 m a.g.l. and consisted of over 18 million points from 8 parallel linear swaths. The survey flight plan was designed so the edge of one swath reached the centre of the adjacent swath, resulting in 50% overlap between swaths. The scan angle was set

to 15°, which created values of θ_i that generally ranged between 0° and 15° on flat terrain (Figure 3.1C). The laser pulse was generated in narrow beam mode, which provides a beam envelop of 0.3 mRad at the *1/e* power level (Optech, 2004). The minimum spacing between neighboring points was less than 1.46 m for 95% of the observations and averaged 1.08 m. Echo returns from non-ground objects such as vegetation and buildings were removed in a classification and filtering routine available in Terra Scan, a proprietary LiDAR processing software package. RMSE (Root Mean Square Error) values for the aircraft trajectory used in execution of error models were obtained from Applanix's POSPac MMS (Applanix, 2013) trajectory processing software (Table 3.1).

Table 3.1 Average aircraft trajectory RMSE information provided by POSPAC MMS (Applanix, 2013) for the Thomas Brook LiDAR survey

Trajectory component	Mean estimated RMSE
X	0.025 m
Y	0.025 m
Z	0.040 m
Roll	17.3"
Pitch	17.0"
Yaw	92.7"

3.2.2 Estimation of DEM uncertainty

Initial predicted errors of elevation coordinates are determined by applying the General Law of Propagation of Variances (GLOPOV; Wolf and Ghilani, 1998) to the LiDAR direct georeferencing equation. Error propagation with the GLOPOV requires raw range and scan angle observations, detailed trajectory information including aircraft attitude (roll, pitch, yaw), three dimensional position and the associated errors of each of these observations (Goulden and Hopkinson, 2010a). The initial hardware errors are integrated with a model of the terrain slope, determined from the LiDAR observations, to predict additional errors due to terrain conditions following Goulden (2009). The resulting data set is a compilation of the original observed three dimensional point observations, each with modeled elevation coordinate error boundaries.

To propagate the error in elevation coordinates to the DEM, a Monte Carlo simulation procedure was implemented. Consider the original observed set of all LiDAR coordinate observations in the survey as $\{S_o\}$ and additional realizations as $\{S_N\}$, where N represents the realization number. Each $\{S\}$ will contain every three dimensional coordinate observation (x_p,y_p,z_p) in the LiDAR survey, where p represents the point number. An elevation error $(e_{p,N})$ is generated for each $z_{p,N}$ by randomly selecting a value from a normal distribution within the modeled error boundaries. Each $e_{p,N}$ was added to the appropriate elevation observation to realize all $\{S_N\}$ as follows;

$$(x_{p,N},y_{p,N},z_{p,N}) = (x_{p,o},y_{p,o},z_{p,o}+e_{p,N}). \quad (3.2)$$

One hundred potential $\{S_N\}$ ($N = 1 \rightarrow 100$) were simulated. From each $\{S_N\}$ a DEM was obtained through interpolation with a Triangular Irregular Network (TIN) surface at a grid spacing of 1 m. The TIN interpolation routine generates a surface by creating a set of triangular facets connecting neighboring coordinate observations in $\{S\}$. A grid based DEM is extracted from the TIN by obtaining the elevation from the triangular plane, which overlays each grid node location. The TIN interpolation routine was selected because it best honors the location of input elevations with minimal averaging. By honoring the true location of the data points, the TIN method will propagate a worst case scenario of $e_{p,N}$ to derived products. DEMs were chosen at a grid spacing of 1 m to best minimize uncertainty introduced through interpolation and to represent the finest available limit of resolution the density of coordinate observations allowed. The finest available limit of resolution is also advantageous because σ_{DEM} will most severely propagate into topographic attributes than in coarser resolutions (Erksine and Green, 2007). The values for σ_{DEM} were determined on a cell specific basis by calculating the standard deviation for each cell from all DEM simulations.

Theoretically, both spatial and temporal autocorrelation could exist in the errors of the primary LiDAR observations. However, adequate research into the development of models to describe the temporal and spatial auto-correlation of primary LiDAR observations has not been undertaken. For the analysis presented here, it is assumed that errors in the primary LiDAR observations are temporally and spatially independent. Empirical evidence has also suggested an increase in LiDAR errors in vegetated areas (Hopkinson, 2005; Hodgson et al., 2005; Reutabach et al., 2003), however, theoretical

error models to account for vegetative factors have not been investigated. Since hydrological analysis requires only returns from the ground surface it is assumed that vegetative error sources will have minimal impact on the results presented here.

3.2.2 Validation of predicted errors

To validate the modeled elevation error (σ_z), a comparison was made to elevation residuals (r_z). The r_z were found as the difference between the LiDAR elevations and elevations obtained from a higher accuracy source. The error modeling algorithm contains assumptions designed to produce 'worst case scenario' predicted errors, and therefore it is assumed that r_z will be below σ_z in 95% of cases, indicating the values for σ_z represent a two-sigma error boundary. To validate this assumption, a real time kinematic (RTK) GPS survey was executed in August of 2010. RTK GPS observations were selected as they can be determined to a higher accuracy than obtained through a LiDAR survey (< 2 cm). Validation information was observed on a flat roadway, a sloped roadway and a sloped forested area. The sites were chosen for their different landscape and slope conditions and because it was unlikely the ground surface had been disturbed since the 2006 LiDAR survey. A total of 100 three dimensional validation point coordinates (x_v,y_v,z_v) were collected and fell within three separate overlapping flight lines. Line 5, Line 6, and Line 7 contained 45, 45, and 50 GPS validation points respectively. Each flight line was considered to be an independent set of observations allowing three empirical validation datasets to be compiled. Since no validation point will be co-located with a LiDAR coordinate observation, r_z was determined as the elevation difference between a continuous terrain surface derived from the LiDAR observations and z_v, at x_v,y_v. The surface was generated using a TIN to best honor the location of the true data points, while also minimizing interpolation errors. To extract the appropriate σ_z for comparison with r_z a surface of the modeled elevation errors was also necessary. The surface was created with a TIN interpolation routine and σ_z was obtained from the modelled error surface at x_v, y_v. Prior to comparison of r_z and σ_z, a constant mean elevation error bias was averaged from each flight line and removed from r_z to isolate the random error component. The existence of a mean bias will not adversely affect results

presented in this analysis since all elevations will be affected similarly, and will not contribute additional uncertainty to the DEM and derived products.

3.2.4 Estimation of uncertainty in the DEM, slope and aspect

The DEM realizations were used to determine 100 slope and aspect grids in the ESRI ArcMap GIS (ESRI, 2003) software package, which uses the Horn method (Horn, 1981). The Horn method determines slope and aspect on a cell by cell basis for a DEM by creating a least squares fit of a plane for a cell's eight neighboring elevations. The equation of the plane is used to determine both the slope and aspect. The estimation for σ_S was quantified on a cell by cell basis as the standard deviation of each cell across all DEM realizations.

The determination of σ_ψ is not a straightforward calculation due to the cyclical nature of ψ; the north direction corresponds to 0° and 360°. To overcome this barrier, the following algorithm, following Oksanen and Sarjakoski (2005), was implemented. The aspect was reduced to horizontal east (x) and north (y) Cartesian vectors with a combined length equal to unity as follows

$$x = \cos(\psi) \tag{3.3}$$

$$y = \sin(\psi) \tag{3.4}$$

where the associated unit vector (u) can be expressed as

$$u = \sqrt{\bar{x} + \bar{y}} \tag{3.5}$$

where $\bar{x}$ and $\bar{y}$ are the mean of the east and north Cartesian vectors respectively. The formulation to solve for aspect from 3.3 and 3.4 is

$$\bar{\psi} = \begin{cases} arctan\left(\frac{\bar{y}}{\bar{x}}\right) \text{if} |\bar{y}| < |\bar{x}| \\ arctan\left(\frac{\bar{x}}{\bar{y}}\right) \text{if} |x| < |\bar{y}| \end{cases} \tag{3.6}$$

In order to derive the variance in aspect, the associated uncertainty in the x and y components must be propagated through (3.6) with the GLOPOV as follows,

$$\sigma_{\bar{\psi}}^2 = J_{\bar{\psi}} \Sigma_{xy} J_{\bar{\psi}}^T = \begin{bmatrix} \frac{\delta\bar{\psi}}{\delta x} & \frac{\delta\bar{\psi}}{\delta y} \end{bmatrix} \begin{bmatrix} \sigma_x^2 & \sigma_{xy} \\ \sigma_{xy} & \sigma_y^2 \end{bmatrix} \begin{bmatrix} \frac{\delta\bar{\psi}}{\delta x} & \frac{\delta\bar{\psi}}{\delta y} \end{bmatrix}^T, \tag{3.7}$$

where J is the Jacobian matrix, and includes the partial derivatives of (3.6) with respect to x and y. The Σ_{xy} matrix is the variance-covariance matrix containing the values for σ_x^2, σ_y^2 and σ_{xy}, which are obtained through the Monte Carlo simulations of the aspect grid determined from each DEM realization. After re-arrangement, the final formulation for σ_ψ^2 can be written as

$$\sigma_\psi^2 = \left(\frac{\bar{x}}{\bar{u}}\right)^2 \sigma_y^2 + \left(\frac{\bar{y}}{\bar{u}}\right)^2 \sigma_x^2 - \frac{2\bar{x}\bar{y}}{\bar{u}^2}\sigma_{xy} \tag{3.8}$$

which is a minor simplification of the final formulation given in Oksanen and Sarjakoski (2005). The estimation for σ_ψ was quantified on a cell by cell basis as the standard deviation of each cell across all DEM realizations.

The local cell by cell Gyasi-Agyei et al. (1995) metric was computed as the ratio of σ_{DEM} to the respective cell's elevation change, triangulated from slope, aspect and the cell size. For comparison, a global estimate of the Gyasi-Agyei et al., (1995) ratio for the LiDAR DEM of Thomas Brook was also computed. The global estimate requires an overall DEM precision and the mean slope of the DEM. The overall DEM precision was estimated from the standard deviation of r_e values obtained from the validation observations, and the average pixel drop was triangulated from the average slope of the original LiDAR DEM.

Results showed the Θ_i as a dominant factor in determining σ_{DEM} and σ_S. A linear piecewise relationship was fit to describe the behaviour of σ_{DEM} and σ_S due to Θ_i. The algorithm to determine the best fit model for the piecewise regression was developed from Vieth (1989). The Vieth (1989) algorithm determines the parameters of two continuous linear regression lines within two distinct domains of the independent variable (X) as follows

$$\begin{aligned} Y_1 &= a_1 + b_1 X_i \quad X \leq X_o \\ &= a_2 + b_2 X_i \quad X > X_o \end{aligned} \tag{3.9}$$

where X_o represents the estimated transition point of the linear regression lines, and a_1, b_1 and a_2, b_2, represent the slope and intercept of the first and second linear regression lines respectively. Following Vieth (1989), an analysis of variance (ANOVA) test was used to determine whether a single regression provides a statistically equivalent model fit as the piecewise model, with the following null hypothesis:

$$H_{o\ Piece}: a_1 = a_2 \text{ and } b_1 = b_2 \quad (3.10)$$

The test for H_{oPiece} was performed through comparison of a test statistic (F) with a critical value determined from the Fisher distribution following Vieth (1989). To assess the significance of each individual regression line in the piecewise regression, the ANOVA methodology was similarly applied to test the null hypothesis:

$$H_{o\ Line}: a = 0. \quad (3.12)$$

The critical value to test H_{oLine} is also obtained from the Fischer distribution. The tests for H_{oLine} and H_{oPiece} were performed at a 99% confidence interval.

The results of σ_ψ revealed a decreasing power law relationship with terrain slope of the form:

$$\sigma_\psi = e^a S^\alpha \quad (3.13)$$

To determine the parameters (a, α) of the power function a log transformation was applied to the values of slope and σ_ψ and fit with a linear regression line. The slope of the regression line represented β, while the intercept represented a. H_{oLine} was also applied to the log transformed linear regression model to determine the if the regression line was an appropriate model.

3.2.5 Analysis of uncertainty in watershed area and the stream network

Watershed area and the internal drainage network structure were determined from the DEM realizations using the ArcHydro tool (Maidmont, 2002) within the ESRI's ArcGIS (ESRI, 2003) framework. The ArcHydro framework follows an algorithm outlined in Jensen and Dominigue (1988) and utilizes a single flow direction constraint, which allows the continuation of surface flow from each cell in the DEM to one of eight surrounding neighbors. Within the algorithm, the only subjective input required by the user is the choice of area to define the stream initiation threshold. To determine the appropriate value for the stream initiation threshold a field reconnaissance was performed in the Thomas Brook watershed, which identified locations of stream initiation as well as the location of tributary channels entering the main channel. A 1 ha stream initiation threshold area was identified based on the location of running water found at the highest elevation areas of the basin.

The Thomas Brook watershed also includes anthropogenic modifications such as roads and culverts, which serve to disrupt natural flow paths on an unaltered DEM. To correct the flow paths to represent true field conditions a stream 'burning' methodology was applied, which inserts appropriate drainage pathways at culvert locations by manually lowering the elevation of road surfaces to the elevation of the culvert outlet. The locations of all culverts within the site were identified through field visits to the site. The uncertainty in watershed area and stream network length was calculated as their respective standard deviation from all simulations. A total of 25 simulations were used for the watershed analysis as the associated standard deviations of watershed area and total stream network length displayed negligible change (<5%) with additional simulations.

Results indicated that the variability in stream length was minor on the scale of the entire drainage network, but appeared to increase, as the analyzed area decreased. A relationship between the uncertainty in stream length and area was also investigated. This was accomplished by dividing the watershed into a grid of equal area square cells and determining the total stream length within each cell. The coefficient of variation for stream length was calculated for each cell and averaged across all the cells, which contained a stream. The coefficient of variation was converted into a relative standard deviation for reporting as a percentage. The side of the square grid cells analyzed were selected to be 100, 200, 300, 400, 500, 750, and 1500 m. The lower grid cell limit was selected because its area is equivalent to 1 ha, which is the minimum area for a single agricultural field within the watershed. The 1500 m upper limit was selected because it was the highest value, which could contain at least two adjacent cells that spanned the east-west extents of the watershed.

3.3 Hypothesis

It is hypothesized that σ_{DEM} will increase in high slope areas due to the potential for high Θ_i and due to increased levels of horizontal uncertainty manifesting as increased vertical uncertainty following Koppe's relationship. The σ_{DEM} is also expected to increase as the scan angle increases, therefore, σ_{DEM} will be at a minimum at the centre of a swath and increase toward the swath edge. The σ_S is expected to increase with an increase in Θ_i

and will be highest in areas of high slope where the potential for high Θ_i is greatest. In low slope conditions, σ_S will increase as the scan angle increases following the increase in σ_{DEM}. The σ_ψ is expected to show a strong relationship to the terrain slope, where σ_ψ will increase as slope decreases because minor variations in σ_{DEM} can easily rotate the plane determined from the Horn algorithm.

It is hypothesized that watershed area will not experience substantial changes relative to the total watershed area since only minor variations of inclusion or exclusion will occur along the watershed boundary. Stream channels will experience an increase in variation in both spatial location and length in regions of the DEM with low relief due to the associated increase of σ_ψ in these areas. Areas with elevation changes greater than σ_{DEM} will show consistency in stream location as σ_ψ is reduced.

3.4 Results and discussion

The results are separated into sections describing 1) the validation of the LiDAR elevation error models, 2) σ_{DEM}, 3) σ_S, σ_ψ, and the spatial distribution of the Gyesi-Ageyi et al. (1995) ratio, and 4) the uncertainty to watershed area and stream length. Visualization maps and histograms of σ_{DEM}, σ_S, σ_ψ, and the Gyesi-Ageyi et al. (1995) ratio are provided to allow for the qualitative assessment of the spatial patterns of uncertainty. The dominant variable in predicting the σ_{DEM} nodes and σ_S was found to be Θ_i, while the slope was the dominant variable in predicting σ_ψ. Scatter plots for these relationships and associated statistical tests are provided as a quantitative assessment of their relationships.

3.4.1 Validation of error models

The validation results from flight line 5 show 43 observations of a total of 45 (~96%) of r_z lying below the associated σ_z, which supports the 'worst case scenario' design intent of the error predictions (Figure 3.2). Flight line 6 shows 44 of 45 (~98 %) of r_z lying below the associated σ_z. Results from this line show that the r_z between points 0 and 25 are all below σ_z. These validation points are located on a portion of sloped

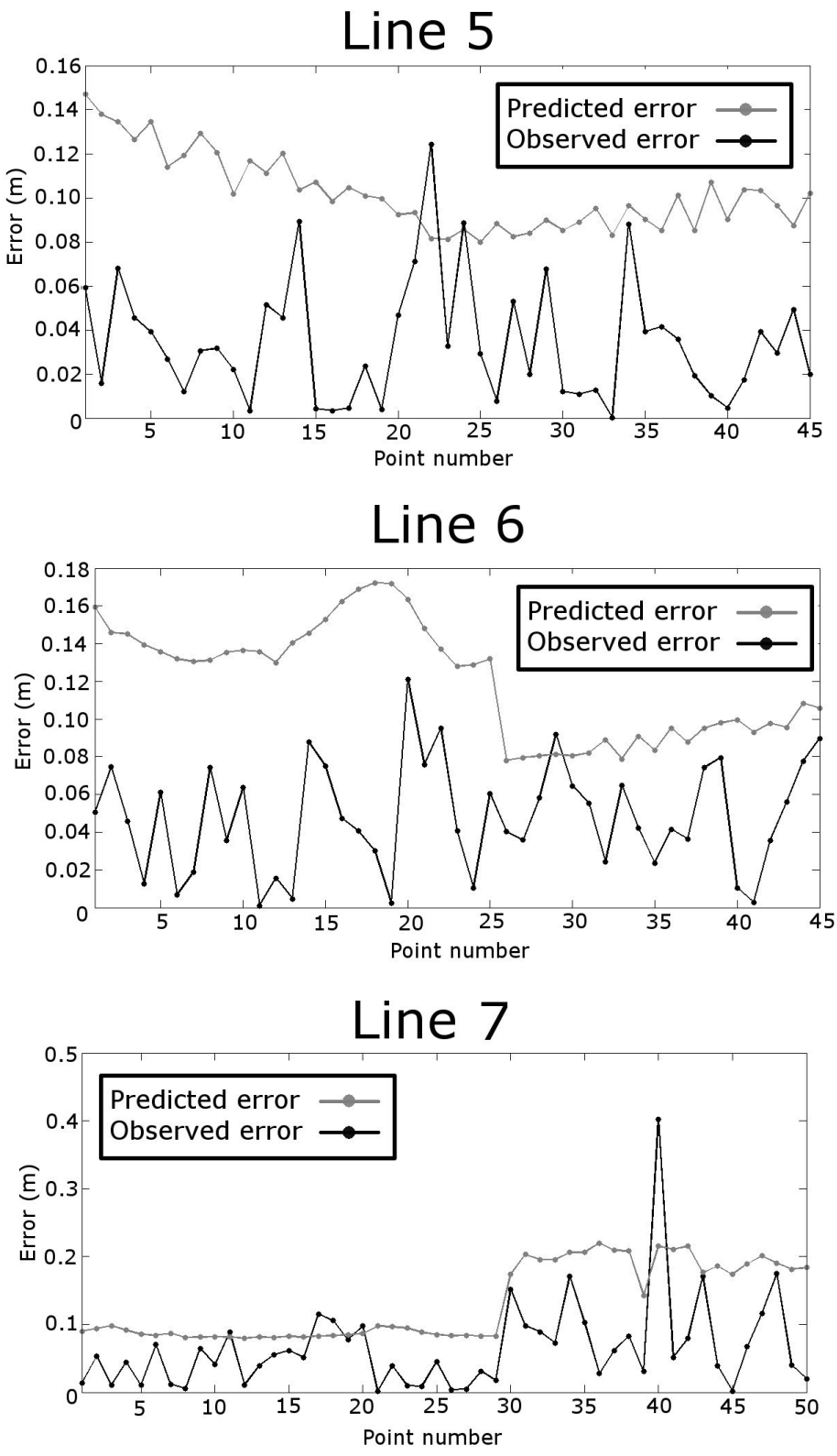

Figure 3.2 Validation of error models, which include observations from flight line 5, flight line 6 and flight line 7.

roadway. The low r_z in this area is potentially the result of a statistical absence of larger errors in the small sample set. It is also possible that the road surface and flight configuration in this area will consistently cause an over estimate of σ_z due to the worst case scenario design assumptions of the error prediction routine. Validation results in the latter portion of the flight line 6 data set (represented by points 26 to 45), located in the sloped wooded region, performed as expected with 19 of 20 (95%) of r_z falling below associated values of σ_z. The validation results from flight line 7 show 45 of 50 (90%) values of r_z lying below the associated σ_z (Figure 3.2), which are located on the sloped roadway and in the sloped wooded region. Also in flight line 7, the σ_z did correctly show a transition from an area of generally lower error (sloped roadway, points 1 to 29) to an area of generally higher error (sloped wooded area, points 30 to 50). In total, the error prediction routine across all flight lines resulted in 132 of 140 (94%) of r_z lying below σ_z.

3.4.2 Uncertainty in the DEM

A histogram of σ_{DEM} reveals that 95% of values range between 0.025 m and 0.060 m (Figure 3.3C). The histogram takes a unimodal shape with a skewness of 2.20. The positive histogram skew is a result of the increase in σ_{DEM} as slope increases in the upper reaches of the watershed. The high slope region in the northern area of the site can be visually identified as an area where an increase in error occurs relative to the southern, gently sloping regions (Figure 3.3A). A qualitative assessment of the σ_{DEM} map reveals a hypothesized striped pattern, which follows a NE-SW direction corresponding with the direction of the survey flight lines and the pattern of θ_i (Figure 3.3A).

The striped pattern is a result of the errors in the primary LiDAR observations propagating more heavily into the LiDAR derived elevation coordinates as the scan angle increases. Errors are minimized near the centre of the swath where θ_i approaches zero on the flat terrain of the valley floor. A profile line of σ_{DEM} perpendicular to the flight lines, and along flat terrain, generally ranges between 0.030 and 0.036 m between the swath

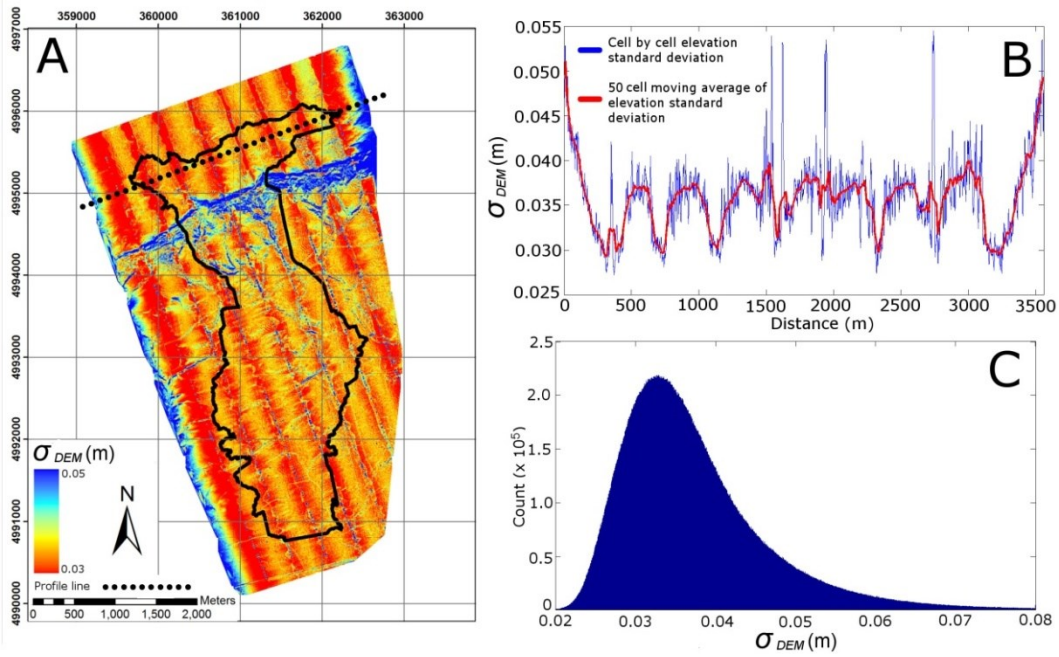

Figure 3.3 Distribution of DEM elevation error. A) color coded map of the DEM elevation error across the entire survey, B) profile of the error taken across the northern section of the watershed and C) histogram of the elevation standard deviations

centre and swath edges respectively (Figure 3.3B). This range identifies the expected increase in σ_{DEM} due to primary measurement observations without the influence of terrain slope.

The Θ_i of the laser pulse is related to the magnitude of σ_{DEM} (Figure 3.4A) within two distinct domains. A piecewise linear regression identifies that a change in slope of the regression lines occurs at an incidence angle of 15.6°. The piecewise regression function between Θ_i and the σ_{DEM} produced the following relationship:

$$\sigma_{DEM} = 0.0008\Theta_i + 0.030 \quad 0° < \Theta_i < 15.6°$$
$$= 0.0025\Theta_i + 0.004 \quad 15.6° < \Theta_i < 40° \qquad (3.15)$$

$H_{o\ Piece}$ was rejected indicating that the linear piecewise relationship provides a better model than a single regression line. $H_{o\ Line}$ was also rejected for each of the individual regression lines within the piecewise function indicating that the Θ_i is a significant predictor of σ_{DEM}.

The intercept of the regression line between 0° and 15.6° is 0.030 m, indicating this is the average σ_{DEM} that is to be expected under the ideal conditions of a Θ_i equal to

zero. This is 0.01 m less than the average RMSE of the elevation coordinate along the aircraft trajectory of 0.04 m (Table 3.1). This is to be expected because the contribution of the primary LiDAR observations error sources other than the RMSE of the trajectory elevation will be less than 10% as Θ_i approaches zero (Goulden and Hopkinson, 2010a). The 0.01 m reduction from the RMSE of the trajectory elevation and σ_{DEM}, at values of Θ_i near zero, occurs due to the averaging of elevation errors in the DEM creation process. This shows that the minimum DEM error is largely related to the elevation error of the trajectory, which is dictated by the geometric strength of the GPS satellite constellation during the survey, the quality of corrections received from the local GPS base station or GPS base station network, and the accuracy of the accelerometers in the IMU (Inertial Measurement Unit).

The break in the piecewise function at approximately 15.6° can be attributed to the LiDAR sensor scan angle setting of 15° during the survey. An aircraft with neutral attitude (0° of roll and pitch) observing flat terrain can create a maximum Θ_i equivalent to the scan angle. For Θ_i to exceed the scan angle, the aircraft must be experiencing a roll, pitch, observing sloped terrain, or some of combination these factors. The roll and pitch during the survey rarely exceeded 3.97° and 1.80° respectively, therefore, the increase in error at high Θ_i (>15.6°) is primarily due to the sloped terrain. This indicates that a more rapid increase of σ_{DEM} occurs due to a unit increase of Θ_i in sloped terrain than flat terrain. This is not surprising because the horizontal uncertainty also contributes additional elevation uncertainty in sloped terrain according to Koppe's relationship (eq. 1).

A solution to minimizing σ_{DEM} in sloped terrain conditions is to fly surveys parallel to the contours with a down-slope aircraft position. This allows an opportunity for the laser beam direction to be parallel with the terrain normal. A flight configuration, which would introduce the largest errors, would consist of flight lines parallel to elevation contours and an up-slope aircraft position. The upslope aircraft position would cause the pulse to intercept the terrain with a high Θ_i, spreading the laser energy across an expanded area of the terrain and increase laser errors. As the striping pattern suggests, the survey of Thomas Brook was generally flown perpendicular to the contours of the north mountain as opposed to parallel. A flight plan design perpendicular to the contours also

provides for a beneficial configuration, as θ_i will be dependent on the scan angle as opposed to terrain conditions.

3.4.3 Uncertainty in slope and aspect

The σ_S for each grid node resulted in 95% of the values ranging between 0.6° and 1.5° (Figure 3.5A). The histogram shows a unimodal distribution with a skew of 1.27. The skew is a result of increase in σ_S in the northern sloped areas where increases in θ_i occurred. The overall low magnitude of σ_S can be partially attributed to the determination of slope with the Horn algorithm. Since the algorithm determines slope by a least squares fit of a plane that passes through eight surrounding grid nodes, a reduction in σ_S through averaging occurs. Using 25 m DEMs, Raaflaub and Collins (2006) also found that σ_S is low with the Horn algorithm in comparison to other methods of slope calculation. They also noted that σ_S will be lower in situations of correlated values of σ_{DEM}. The σ_{DEM} will be spatially correlated in the DEMs tested here due to the common usage of raw LiDAR points in the generation of triangular facets in the TIN interpolation process. It should be noted that the resulting σ_S is only an indication of the variability due to LIDAR observation measurement errors and does not represent an absolute estimate of uncertainty in slope, which can also be influenced by algorithmic considerations (Raaflaub and Collins, 2006) and grid size dependencies (Chang and Tsai, 1991; Kienzle, 2004).

A qualitative assessment of the σ_S map reveals the striping patterns related to the flight line direction and identifies θ_i as a predictor of σ_S. Similar to the results for σ_{DEM}, the relationship between the θ_i and σ_S can be represented with a linear piecewise relationship (Figure 3.4B). The break in slope between the two regression lines is located at 16.4° and the piecewise equations can be described as

$$\begin{aligned} \sigma_s &= 0.0089\theta_i + 0.8670 \quad 0° < \theta_i < 16.4° \\ &= 0.0438\theta_i + 0.2968 \quad 16.4° < \theta_i < 40° \end{aligned} \tag{3.16}$$

$H_{o\ Piece}$ was rejected indicating that the piecewise linear relationship is more suitable than a single regression line. $H_{o\ Line}$ was also rejected for each individual regression line indicating that θ_i is a significant predictor for the uncertainty in slope. The intercept of

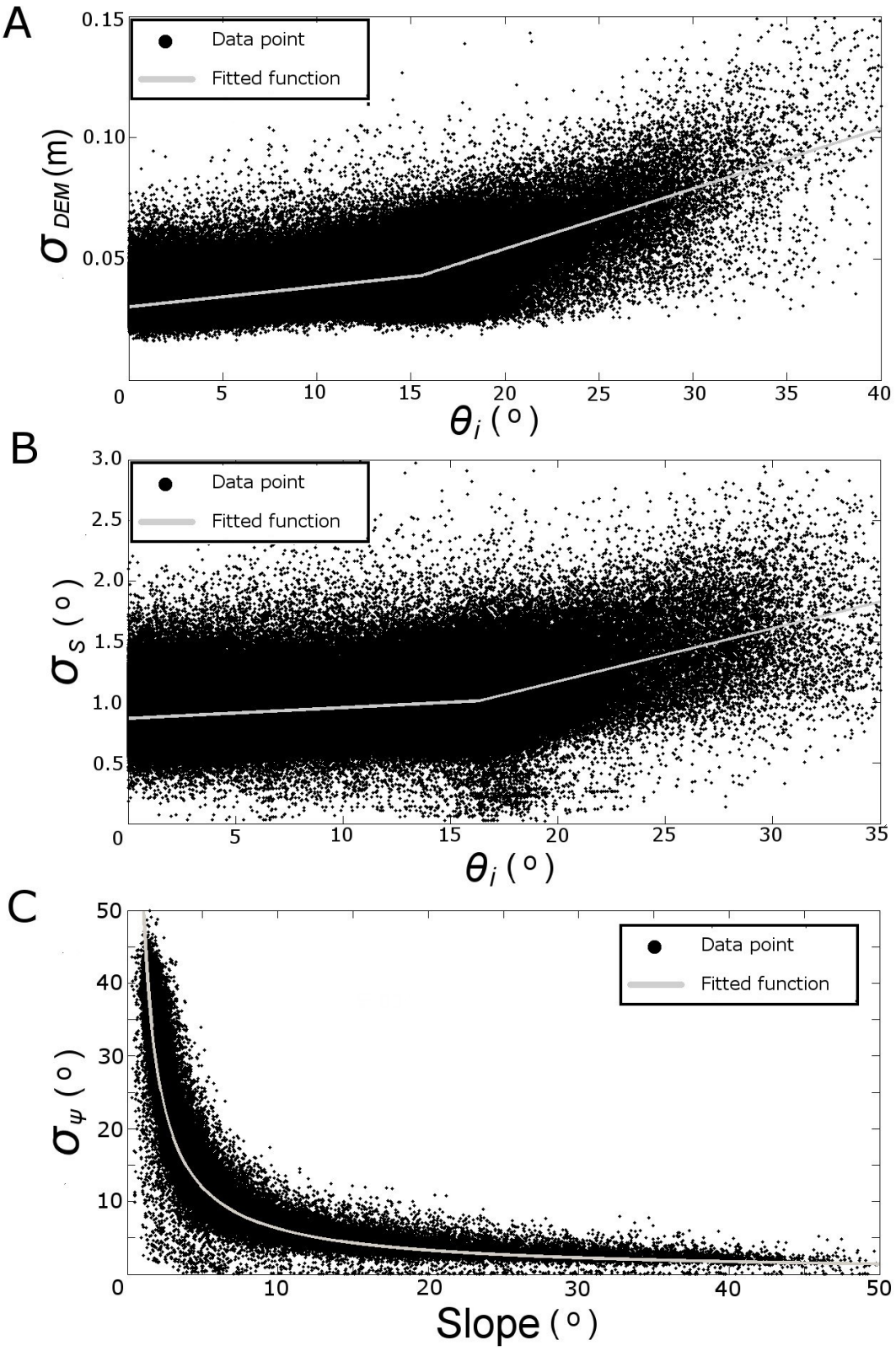

Figure 3.4 **A) Scatter plot of $\theta_i$vs σ_{DEM}, B) scatter plot of θ_i vs σ_S, C) scatter plot of slope vs σ_ψ.**

the line between 0° and 16.4° is 0.87°, indicating this is the minimum σ_S, which should generally be expected.

The transition point of 16.4° is related to the 15° scan angle selected for the survey. Similar to the results for the relationship between σ_{DEM} and θ_i, the breakpoint of the piecewise relationship near 15° indicates the beginning of an accelerated rate of increase of σ_S due to θ_i in sloped terrain. In areas with high slope, the striping pattern related to the flight lines is lost as the magnitude of the incidence angle is controlled by the terrain conditions as opposed to the scan angle. Therefore, terrain conditions will become the dominant factor in defining error patterns as the terrain slope increases and becomes the prominent factor in determining θ_i, and additional uncertainty is introduced through Koppe's relationship.

The resulting range for σ_ψ shows 95% of the values are between 2.7° and 24.1° degrees (Figure 3.5B). The histogram shows a bimodal distribution, in which the peak at approximately 10° corresponds to the σ_ψ obtained from the northern mountain, and the remaining values in the distribution represent the values of σ_ψ obtained from the valley floor. A qualitative assessment of the spatial patterns of σ_ψ reveal it closely matches the patterns of slope, which was also reported by Chang and Tsai (1991) and Oksanen and Sarjakoski (2005) for other DEM sources. The striped pattern evident in the maps of σ_{DEM} and σ_S was not evident in the map of σ_ψ indicating θ_i is not a dominant factor in controlling σ_ψ. The relationship between slope and σ_ψ formed a decreasing power function (Figure 3.5B):

$$\sigma_\psi = e^{3.9703} S^{-0.9282}. \tag{3.17}$$

H_{oLine} was rejected for the log transformed values of slope and σ_ψ, indicating the power law relationship forms a statistically significant model.

The high levels of σ_ψ are constrained to low slope conditions because minor variations in σ_{DEM} can easily manipulate the rotation of the plane determined with the Horn algorithm. Despite a higher σ_{DEM} in areas of high slope, the σ_ψ remains low due to large relative changes in elevation in the DEM grid nodes, which overcome σ_{DEM} and the plane determined from the Horn algorithm remains stable. The magnitude of σ_ψ is

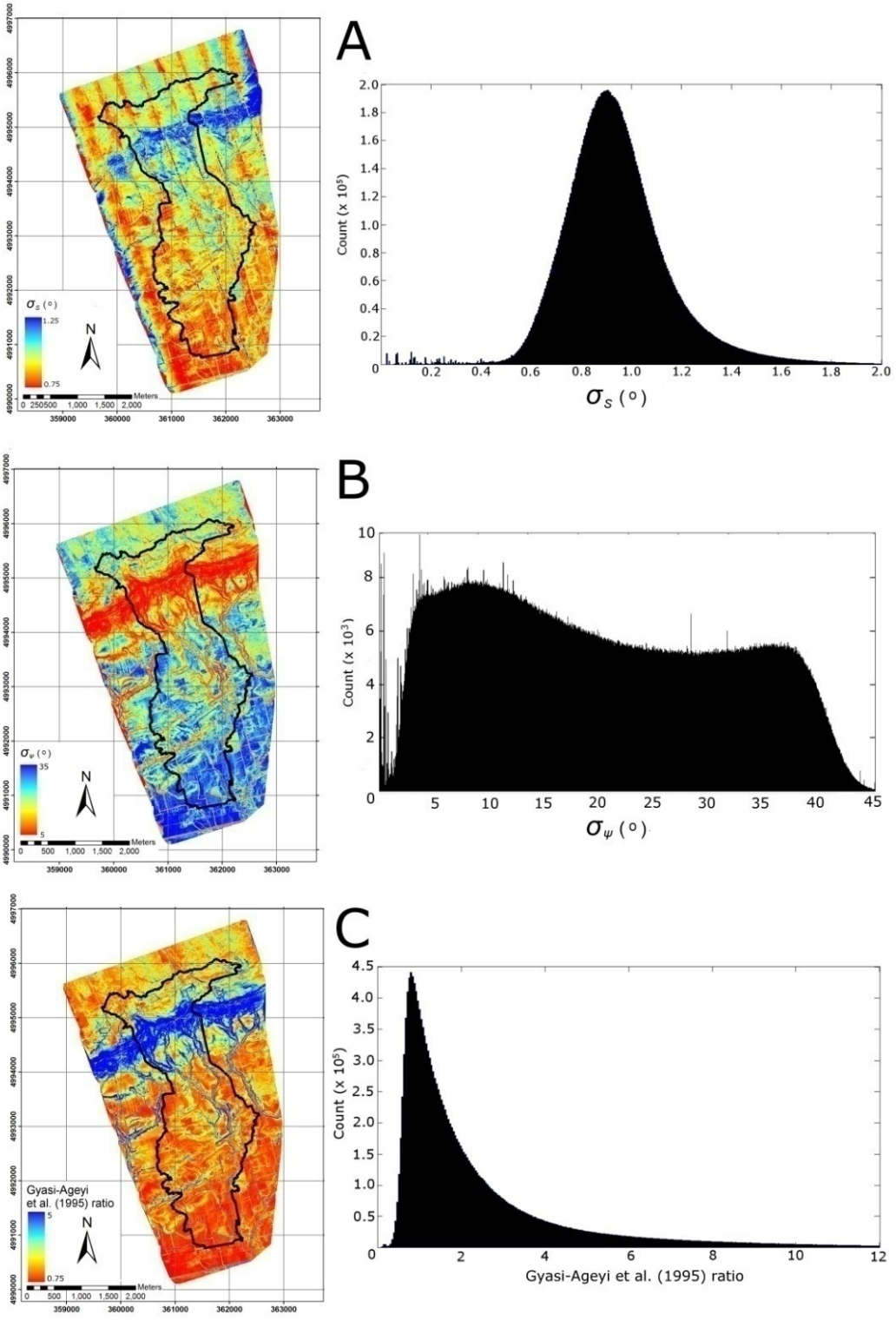

Figure 3.5 **Spatial patterns of A) σ_S, B), σ_ψ and C) the Gyasi-Agyei et al. (1995) ratio with associated histograms**

important to consider in terms of the evolution of the stream channel network throughout the DEM. The stream flow direction relies on the value of aspect to indicate which of the eight surrounding cells the flow will proceed to. Recall that each receiving cell contains an angular domain of 45°. In low slope environments σ_ψ is sufficiently large to frequently switch the receiving cell location and introduce uncertainty into the stream network topology. In higher sloped environments, this could also occur, but will be less likely since the mean aspect would have to be near the threshold direction, which divides flow between neighboring cells.

3.4.4 Spatial distribution of the Gyesi-Ageyi et al. (1995) ratio

Approximately one quarter of the DEM (25.2%) resulted in grid cells with a Gyasi-Ageyi et al., (1995) ratio below unity (Figure 3.5C). The entire DEM was characterized by a range in which 95% of the cell based Gyasi-Ageyi et al. (1995) ratio values were between 0.57 and 9.93. This indicates that, according to the local Gyasi-Agyei et al., (1995) ratio, approximately 75% of the 1 m LiDAR derived DEM has precision suitable for hydrologic network extraction. A global estimate of the Gyasi-Agyei et al., (1995) ratio resulted in a value of 1.413 following an overall DEM precision of 0.067 and a mean pixel drop of 0.095. The local estimates improves on the global estimate by allowing identification of specific areas of the DEM which may introduce unacceptable uncertainty for stream network extraction. As hypothesized, areas characterized by high slope resulted in the highest ratios despite the associated increase of σ_{DEM} in these areas. Regions with low slope tended to result in the lowest ratios even though σ_{DEM} tended to be lower in these elevation areas. The visualization map of cell specific Gyasi-Agyei et al., (1995) ratio values highlights areas with potential to introduce excessive uncertainty for stream network extraction.

3.4.5 Uncertainty in watershed area and stream network

The mean watershed area obtained from the 25 DEM realizations was 692 ha and the associated standard deviation was 5 ha, resulting in a variation of less than 1% of the

total area. This indicates that the determination of watershed area of the Thomas Brook watershed is not sensitive to the measurement errors in the LiDAR survey. The small level of variability was due to uncertainty in the boundary located in the south-east corner of the watershed, where the terrain experiences changes in elevation less than σ_{DEM}. One simulated delineation also contained an additional section in the north east corner of the survey, which is also an area characterized by minor changes in elevation. The disputed area in the north-east section also fell near the edge of a scan line where σ_{DEM} was increased and surpassed the local change in elevation.

Although watershed area was generally stable at the Thomas Brook site, there is evidence that sensitivity of watershed area to LiDAR measurements exists where σ_{DEM} is larger than changes in elevation, which can be identified by the local Gyasi-Agyei et al., (1995) ratio. Therefore, if a site contains sections with changes in elevation less than typical error levels ensuring the observations are sufficiently dense in these regions will reduce the uncertainty introduced through measurement and provide more consistent results.

The average stream network length was 61.8 km and the associated standard deviation of the length was 0.95 km, approximately 1.5% of the total length. The uncertainty in the stream network length was minor due to the random nature of σ_z, which led to the existence of random behavior in σ_{DEM}. The random values of σ_{DEM} resulted in slightly varied channel configurations, but as hypothesized, on a spatial scale of the entire basin they tended to sum to a similar overall length. Within areas characterized by high slope and high values of the Gyasi-Ageyi et al. (1995) ratio, the stream channels tended to follow consistent paths (Figure 3.6A). Uncertainty in the stream network configuration was evident on the field scale near areas of channel initiation (Figure 3.6B). Similar to results reported by Lindsay (2006), the stream locations in these areas tended to be variable because channel incisions with bank heights greater than σ_{DEM} did not exist. Areas near the initiation of streams were also typically characterized by low values of the Gyasi-Ageyi et al., (1995) ratio (Figure 3.6B).The stream initiation is affected by variability in aspect because similar grid cells will not cumulatively contribute to stream initiation at the same location for each DEM realization (Figure 3.6B). The difference in the location of stream initiation further increases the

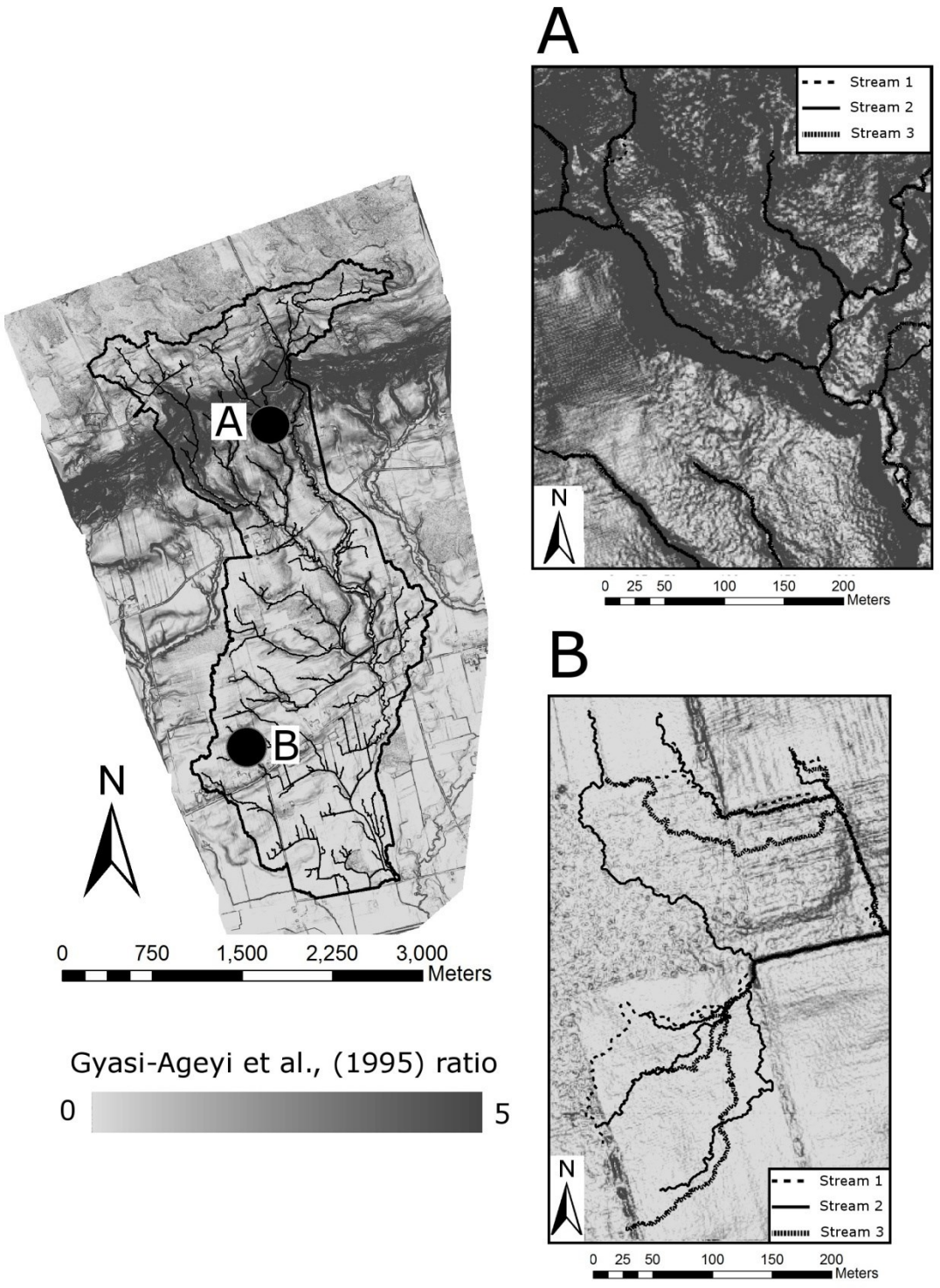

Figure 3.6 **Steam network delineation uncertainty with grid cell based Gyasi-Ageyi et al., (1995) ratio. A) Displays the stream network delineation from three different DEM realizations in an area with high slope, and B) shows a field plot in an area of low slope with stream channels delineated from three different DEM realizations.**

variability in the length and position of first order streams. As the stream channel advances to higher orders the variability in position and spatial location is reduced as channels become more deeply incised and well defined. In these areas, bank slopes possessed elevation changes higher than σ_{DEM}, reducing the opportunity for stream direction uncertainty.

As hypothesized, the variability in stream length tended to increase as the area decreased (Figure 3.7). At the field scale (1 ha), the stream lengths resulted in a relative standard deviation of approximately 28%. Therefore, in hydrological models with a small spatial domain, the uncertainty introduced by LiDAR measurement errors could introduce substantial uncertainty into relationships requiring flow path length as a parameter, such as sediment transport processes in concentrated flow channels. The relative standard deviation of stream length did not result in a 5% relative standard deviation until the area reached 2.25 km^2, which was also the limit for the grid cell areas tested. However, the relationship appears to reach a horizontal asymptote near 5% and substantial increases in the relative standard deviation do not begin until approximately 0.5 km^2. This level of uncertainty could also be relevant for users of watershed scale hydrologic models. Distributed and semi-distributed models typically sub-divide a watershed into several smaller spatial units (sub-basins or grid cells). Hydrology is analyzed separately within each spatial unit and materials are routed to a selected outlet. Unacceptable levels of uncertainty could be introduced to the hydrological outputs at the sub-basin or grid cell scale and propagate to the selected watershed outlet. Smaller sub-basin and grid cells with minor changes in elevation, and near headwater locations should be identified as those with a high likelihood of introducing uncertainty to modeled outputs. Jha et al. (2004), provided recommendations for sub-basin sizes in the SWAT (Soil and Water Assessment Tool, Arnold, 1998), recommending that sub-basins have a relative size between 2 and 5% of total watershed area, depending on the hydrological output of interest. For the Thomas Brook watershed, 5% of the total watershed area would be approximately 35 ha. Sub-basins of this recommended size could contain a relative standard deviation of ~20% for the stream length, which may not be an acceptable level of uncertainty. This indicates that the absolute area of sub-basins are an important consideration during division of a watershed into smaller spatial units for

distributed modeling purposes. Consideration of subbasin area only in terms of the ratio to overall watershed area could lead to undesirable levels of uncertainty in the stream network.

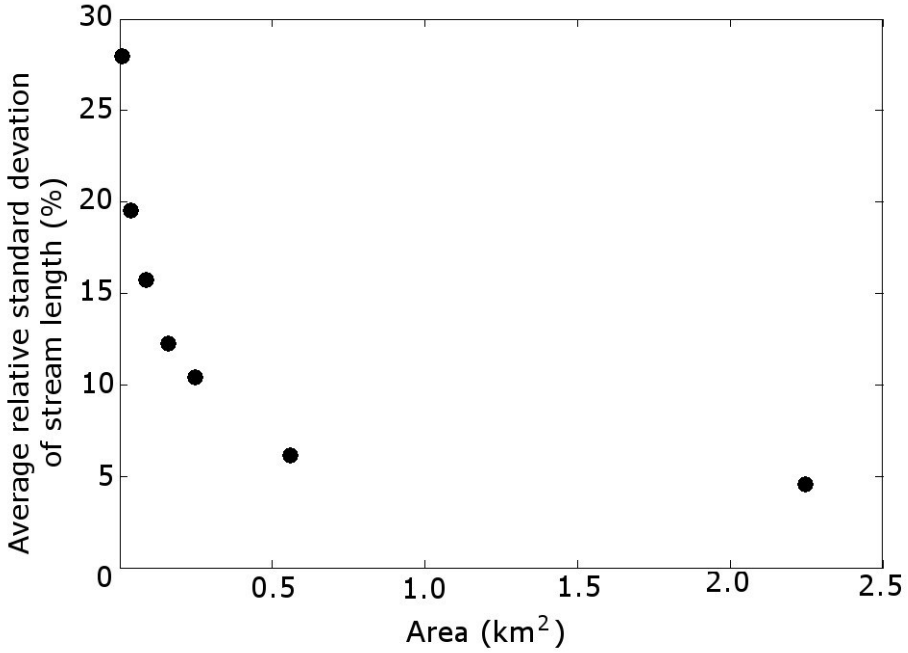

Figure 3.7 Area vs average relative standard deviation of stream length

3.5 Conclusion

This study investigated the sensitivity of random measurement error of primary LiDAR observations to the derivation of a DEM, as well as primary topographic attributes (slope, aspect), and watershed attributes (area, stream length and position). Topographic and watershed attributes are ubiquitous data sources for paramaterizing hydrological models, allowing results to applicable to a range hydrological products. Therefore, a comprehensive understanding of the sensitivity of LiDAR measurement errors to terrain and watershed attributes is important for conscientious development of water resource planning strategies. The analysis was focused on demonstrating the overall magnitude of uncertainty, which could be introduced by the random error in primary LiDAR observations, as well as the resulting spatial patterns of uncertainty, and their relationship to survey acquisition parameters and terrain conditions.

LiDAR derived DEMs were shown to produce spatial error patterns related to the flight configuration of the survey, as well as terrain conditions. The σ_{DEM} and σ_S tends to be highest on the edge of scan lines and in areas with high terrain slope, due to the existence of high incidence angles between the laser pulse and the terrain slope. The dominant factor in controlling the σ_{DEM} and σ_S was θ_i, which is a combined factor of the scan angle, aircraft attitude and terrain slope. This is contrary to uncertainty analysis on DEMs obtained from other sources, which identified terrain slope as a predictor of σ_{DEM} (Holmes et al., 2000), and σ_S (Oksanen and Sarjakoski, 2005).

Aspect showed a high sensitivity to LIDAR measurement errors with the maximum uncertainty reaching nearly 50°, confirming previous theoretical models provided in Oksanen and Sarjakoski (2005). The cell by cell based Gyasi-Ageyi et al., (1995) ratio provides a visualization of the areas which may be unsuitable for reliable hydrological analysis, and require enhanced observations to meet acceptable standards. This improves upon previous global estimates of the Gyasi-Ageyi et al., (1995) ratio, which predicted the suitability of an entire DEM for stream network extraction.

The variability in aspect causes uncertainty in stream network position, the location of stream network initiation, and stream length. The effects are pronounced in low order stream channels and in smaller field plots, however, the influence of LiDAR measurement errors decreases as the considered area increases. Therefore, careful consideration should be given to watersheds divided into smaller spatial units for modeling purposes, as errors at this scale could potentially propagate unacceptable uncertainty to watershed model outputs. Areas with low relief, characterized by low values of the Gyasi-Ageyi et al., (1995) ratio, should be identified as the areas with high probability for variable stream lengths.

In general, the results showed that the flight survey parameters selected during the survey acquisition can be an important driver for defining patterns of uncertainty in both the DEM and slope estimates. Typical DEM error analysis, which implements random fields of DEM error determined through global RMSE estimates and spatial autocorrelation parameters (e.g. Hunter and Goodchild, 1997; Holmes, 2000; Oksanen and Sarjakoski, 2005; Wechsler and Kroll, 2006; Raaflaub and Collins, 2006; Erksine and Green, 2007) would be unable to replicate similar error patterns. This analysis

demonstrates how to translate prior knowledge of the terrain shape and survey acquisition parameters into predictive capabilities of expected uncertainty in derived products. This facilitates the application of appropriate due diligence for assessing uncertainty of LiDAR DEMs for specific hydrological project requirements. If deemed necessary, flight plans can then be modified to further reduce the uncertainty in derived products. Future research will include the propagation of LiDAR primary observation measurement errors to the determination of hydrological model outputs such as flow rate and sediment yield.

CHAPTER 4 SENSITIVITY OF HYDROLOGICAL OUTPUTS FROM SWAT TO DEM SPATIAL RESOLUTION

4.1 Introduction

Watershed models capable of simulating hydrological processes are an essential tool for effective management of water resources. Simulated hydrologic outputs are often required for planning and assessing sustainable environmental strategies in response to ecosystem impacts, such as agricultural practices, land use development or climate change. An accurate virtual landscape representation is a fundamental requirement for hydrologic simulations because it controls the transfer of water, sediment, nutrients and pollutants within the modeled environment (Moore et al., 1991).

Virtual information on landscape shape and structure is typically provided by a DEM (Digital Elevation Model), as regularly spaced horizontal grid of elevation values (Collins and Moon, 1981; Moore, 1991). The horizontal spacing between grid nodes defines the spatial resolution and can be considered representative of map scale. Simulated hydrological outputs are known to exhibit scale dependent relationships associated with DEM grid cell size (Zhang and Montgomery, 1994), which will affect the parameterisations of distributed models (Lin et al., 2010). Scale driven investigations conducted under the assumptions and constraints of a particular model structure can guide users in selecting an optimum DEM resolutions, where the optimum resolution is defined as the resolution which enables accurate simulated outputs, and allow for an associated realistic model parameteristation. The model obtained through implementation of the optimum DEM resolution will be capable of generating sound and defensible evidence to develop environmental policy and implement future water resource planning strategies.

Previous evidence has shown that DEM resolution will affect hydrologic outputs as well as watershed and topographic attributes. Average terrain slope, for example, tends to increase as spatial resolution increases (Evans, 1979; Chang and Tsai, 1991; Zhang and Montgomery, 1994; Wilson et al, 2000; Kienzle, 2004; Hill and Neary, 2005; Deng et al, 2007; Hopkinson et al, 2010). Stream lengths have shown to increase as DEMs become increasingly fine (Wang and Yin, 1998; Thieken et al., 1999) while watershed

area has shown scale dependent irregularities (Cotter et al., 2003; Chaubey et al., 2005). Peak flow rates have been shown to decrease as DEM resolution increases (Quinn et al., 1991; Zhang and Montgomery, 1994) while the timing of peak flow tends to be delayed (Thieken et al., 1999). Simulated sediment loads have shown to both increase (Chaplot 2005; Cotter et al., 2003; Di Luzio et al, 2005) and decrease (Zhao et al, 2010) as DEM resolution increases. Despite the well-established sensitivity of topographic attributes, watershed attributes and hydrologic outputs with DEM resolution, no consistent guidelines are available for selecting an optimum DEM spatial resolution for simulated hydrological analysis.

Previous research into investigating the optimum DEM resolution to represent basin scale hydrologic outputs suggests that the DEM resolution should reflect the natural scale of the hillslope (Quinn et al., 1991; Zhang and Montegomery, 1994; Beven, 1997; Hutchinson and Gallant, 2000; McMaster, 2002). A DEM of lower resolution than the natural hillslope scale will lose important valley or hill structures. Landscape processes occurring within DEM grid elements, such as surface runoff or landscape sediment production, will be incorrectly aggregated across distinct spatial divisions and introduce model inaccuracy. Conversely, too fine a resolution may include topographic structure irrelevant to modeled processes, is expensive to acquire, and is a computational burden (Creed and Sass, 2011). Previous studies using Beven and Kirby's (1979) TOPMODEL have concluded that DEM resolutions of approximately 10 m are sufficient for modeling hillslope scale hydrological processes (Zhang and Montgomery, 1994; Thompson and Moore; 1996). While Quinn (1995) suggested coarse resolution DEMs (50 m) were sufficient for predicting macroscale hydrographs (50 m) in TOPMODEL, finer resolution DEMs (5 m) should be used for predicting internal state processes which initiate flow. Tarboton and Ames (2001) identify that an important distinction exists between processes on hillslopes and those in channels, which are both required for appropriate assessment of hydrology within a basin. Studies into optimum DEM spatial resolution for determination of channel attributes have suggested that resolutions finer than typical hillslope scales (up to 1 m) are the most accurate (Murphy et al., 2008; Remmel et al., 2008). This indicates an inconsistency exists between the ideal spatial resolution for modeling hillslope and

channel processes. Therefore, the choice of DEM resolution should reflect the individual modeling needs in both channels and hillslopes.

The SWAT (Soil and Water Assessment Tool; Arnold et al., 1998) is a popular semi-distributed hydrologic and water quality model, which requires a DEM as a primary data layer for parameterisation (Gassman, 2007). The SWAT considers hydrology within a single basin in two distinct phases: 1) a land phase, which models hillslope processes and 2) a routing phase, which considers channel processes (Arnold et al., 1995; Arnold et al., 1998; Neitsch et al., 2011). The DEM provides three fundamental functions in the parameterisation of a SWAT model including:

1) representation of the surface topography, which defines hillslope scale,
2) determination of stream channel attributes, and
3) delineation of watershed and sub-basin extent.

The necessary information for a SWAT model parameterisation is obtained from each DEM function during the watershed delineation process. This is typically executed as a single algorithmic process with a DEM of constant resolution. The process does not typically consider that the DEM functions could provide an improved parameterisation if implemented at unique resolutions.

The objective of this study is to determine the sensitivity of water quantity and sediment production of fine to medium scale (1 - 50 m) spatial resolution DEMs within the SWAT model framework. The study employs a scaling analysis to determine the relative effects of DEM resolutions at 1, 5, 10, 25 and 50 m, to hydrological outputs in a small agricultural watershed. The analysis separates the relative dependence of each DEM function to the variation in DEM resolution. Subsequently, the relative sensitivity of hydrological outputs of each DEM function and resolution are isolated, and the potential for implementing the DEM functions at unique resolutions assessed.

4.1.1 Previous studies on SWAT and DEM resolution

Previous studies have been conducted that analyze the effects of varying DEM spatial resolution on SWAT outputs and have found conflicting results to the sensitivity of simulated flow and sediment (Table 4.1). For example, Cho and Lee (2001) compared a USGS 1:24000 DEM and 1:250 000 DEM and found a respective decrease of 30% in

the volume of runoff predicted from a SWAT model with decreasing resolution. In a study of a mixed agricultural and forested landscape, Cotter et al. (2003) determined that SWAT outputs exhibited a higher sensitivity to DEM resolution than to the spatial resolution of soils and landuse information. The DEM was varied to several levels between 30 and 1000 m, and a 27% reduction in flow volume and 81% reduction in sediment mass loss were noted between the minimum and maximum tested spatial resolution DEMs respectively. It was concluded that to achieve less than 10% of error, relative to the 30 m DEM, simulated sediment production required a 30 m DEM and flow required a 300 m DEM. Using the same watershed as Cotter et al. (2003), but with a different set of calibrated parameters, Chaubey et al. (2005) similarly found that flow volume decreased as the spatial resolution was successively reduced from 30 m to 1000 m. Chaubey et al. (2005) determined that a minimum resolution of 200 m was required to achieve less than 10% of relative error in simulated flow in comparison to the 30 m DEM. Chaplot (2005) investigated resolutions that varied between 20 m and 500 m, in a 2183 ha agricultural watershed. He found minimal effects to runoff, and consistent sediment yields between 20 and 90 m resolutions, followed by a gradual reduction in sediment yield as resolution further decreased to 500 m. In a comparison of simulated hydrologic outputs generated from un-calibrated SWAT models to field observed flow and sediment data, Di Luzio et al. (2005) found that models generated from a 90 m DEM generally provided a better match than 30 m DEM models in a watershed with small alluvial valleys and hilly uplands. Dixon and Earles (2009) tested results from DEMs in SWAT that were re-sampled to spatial resolutions both higher and lower than the original datasets, in a watershed with moderate elevation change (~46 m) in central Florida. It was found that the 30 and 90 m DEMs produced similar monthly flow volumes while a 300 m DEM produced a relative increase in flow volume. No advantage was gained through resampling lower resolution DEMs to higher resolutions. Lin et al. (2013) analyzed three separate DEM sources, ASTER GDEM, SRTM and high resolution digital line graph (DLG) information in a primarily forested (96%) mountainous watershed. The ASTER GDEM and SRTM were created with spatial resolutions of 30 m and 90 m respectively, while the original resolution of the contour data is indicated to be ‘close to’ 5 m. Each data source was resampled to resolutions between 5 and 140 m to investigate the

Table 4.1 - Relevant research on DEM spatial resolution and SWAT water and sediment yield.

Study	DEM resolution	DEM source	Area (km^2)	Landscape type	Water yield (%) †	Sediment yield (%) †
Cho and Lee (2001)	30, 90	USGS NED	250	Mixed	77%	N/A
Cotter et al. (2003)	30 - 1000	USGS NED	18.90	Pasture (55%) and forested (39%)	73%	19%
Bosch et al. (2004)	30, 90	EPA, Georgia GIS Clearinghouse	22.1	Forested (67%), row crop (30%), pasture (2%)	60%	N/A
Chaubey et al. (2005)	30 - 1000	USGS NED	18.90	Pasture (55%), forested (39%)	79%	N/A
Chaplot (2005)	20- 500	USDA topographic survey	21.83	Farmland (90%), pasture (3%)	71%*	90%
Di Luzio et al. (2005)	30, 90	USGS NED	21.3	Rural agricultural land (100%)	88-89% **	44-60%
Dixon and Earles (2009)	30 - 300	USGS NED	855	Pasture (44%), tree crops (17%), shrub (7%), urban, wetland, forest (25%)	13%	N/A
Lin et al. (2013)	5 - 90	ASTER GDEM, SRTM, DLG	81.7	Mixed forest (96%)	~0%	95%
Beeson et al. (2013)	3 - 90	LiDAR, SRTM, USGS NED	788	Crop land (corn, soybean, 80%), pasture, forest, urban (20%)	0%	71%

†Reported as the percentage obtained from lowest resolution DEM to highest resolution, unless noted otherwise
*Results shown are between the 20 and 150 m DEM which contained the largest discrepancy
**Results are a range of several tested combinations of land use and soils information

contributions of data source and resolution on the SWAT outputs. Results showed that watershed area was not affected by DEM resolution, mean slopes showed a respective increase with finer resolution DEMs, and reach lengths showed no obvious trend with a decrease in resolution. It was reported that changes in flow seemed to correspond to changes in area based on data source, as larger areas also displayed an increase in flow. Beeson et al., (2013) investigated the sensitivity of sediment yield within the SWAT to DEM resolutions including 3, 10, 30 and 90 m resolutions. They noted an increase in mean slope of over 2.5 times between a 3 m and 90 m DEM, which resulted in an increase of simulated sediment yield of 130%. Contrary to results from other studies, Lin et al. (2013) found that a variation in DEM resolution resulted in only minor fluctuations in sediment output, as the maximum relative difference between the tested resolutions and the 5 m DEMs (used as control) was approximately 5%. The minor differences in sediment results due to the varied DEM resolutions noted by Lin et al. (2013) was likely a result of the primarily forested land cover in the watershed, which would produce minimal sediment regardless of DEM resolution.

With the exception of Lin et al., (2013) and Beeson et al., (2013), previous SWAT studies investigated DEM resolutions no finer than 30 m. The reason for the common termination at 30 m is typically the availability of public USGS NED (National Elevation Dataset) DEMs (Table 4.1). The NED provides seamless DEM coverage for all of the United States at a constant spatial resolution of at least 30 meters with some areas benefitting from access to 10 and 3 m DEMs where sufficiently dense source data is available (Gesch, 2007). NED DEMs are often used in hydrological studies, where the decision of spatial resolution is not prioritized on landscape complexity or local hillslope scale leaving the DEM resolution deficient at some locations while satisfactory at others. Consequently, unavoidable uncertainty of unknown quantity can be introduced into simulated hydrologic outputs that implement NED DEMs. Users are left without the ability to assess how processes will react to scale dependencies at finer resolutions. The recent availability of high resolution DEM data from contemporary remote sensing systems provides the ability to analyze the effects of fine resolution DEMs on models parameterised in the SWAT at previously unavailable map scales.

4.1.2 Background to the SWAT model framework

4.1.2.1 SWAT landscape processes

SWAT is a semi-distributed watershed model that partitions a catchment into spatially discrete sub-basins and further divides the sub-basin into Hydrological Response Units (HRUs). The HRU is a unique and homogeneous area of land use, soil type and topographic slope (Gassman, 2007). Each HRU is assumed to act in a hydrologically predictable manner, from which input meteorological information can be used to simulate hydrologic outputs. The simulated outputs from each HRU in a sub-basin are summed and routed into the channel network on a daily time step (Neitsch et al., 2011). The land phase of the SWAT framework includes surface runoff, evapotranspiration (ET), percolation, lateral flow, and groundwater flow as the major hydrological processes. For the parameterisations in this study, surface runoff is generated with the Soil Conservation Service (SCS) Curve Number (CN) method (USDA, 2004). Although the CN value can be adjusted for slope, a fundamental topographic attribute affected by DEM resolution, SWAT assumes a 5% grade of slope for calculation of slope values and does not perform an adjustment (Neitsch et al., 2011). ET is determined using the Hargreaves method, and does not consider topographic conditions for modeling incoming solar radiation. Percolation is calculated through a storage routing method and lateral flow is determined with a kinematic storage model developed by Sloan et al. (1983). Groundwater flow is divided between shallow aquifers and deep aquifers. Shallow aquifers can contribute flow to the main channel or reaches within each sub-basin, and deep aquifers are assumed to only affect hydrology outside of the watershed area (Neitsch et al., 2011).

Landscape erosion modeling in the SWAT is driven by the *MUSLE* (Modified Universal Soil Loss Equation) developed by (Williams, 1975), which is a modification of the *USLE* (Universal Soil Loss Equation) developed by (Wishmeier and Smith, 1978). The *USLE* is a combination of several empirical relationships of variables, which have been shown to significantly contribute to soil erosion. The formulation of the *USLE* is as follows:

$$sed = R_{USLE} \cdot K_{USLE} \cdot LS_{USLE} \cdot C_{USLE} \cdot P_{USLE} \quad (4.1)$$

where *sed* is the amount of soil loss (t/a), R_{USLE} is a rainfall and runoff factor, K_{USLE} is a soil erodibility factor, LS_{USLE} is a topographic factor, C_{USLE} is a cover management factor, and P_{USLE} is an erosion practice factor. The change to MUSLE from the original USLE includes substituting R_{USLE} for a rainfall-runoff factor (R_{runoff}) that includes the following terms:

$$R_{runoff} = 11.8 \cdot \left(Q_{surf} \cdot q_{peak} \cdot area_{HRU}\right)^{0.56} \tag{4.2}$$

where Q_{surf} (mm) is the surface runoff volume, q_{peak} (m^3/s) is the peak runoff rate, and $area_{HRU}$ (ha) is the area of the HRU. The *MUSLE* was introduced to better simulate sediment production for single precipitation events and provide sediment yields on a daily basis. Within the MUSLE, both the LS_{USLE} factor and q_{peak} are impacted directly by DEM spatial resolution due to their reliance on landscape slope. The LS_{USLE} factor is defined as

$$LS_{USLE} = (\lambda/72.6)^m(65.41sin^2\theta + 4.56\ sin\theta + 0.065) \tag{4.3}$$

where λ is the slope length (m), θ is the slope angle (rad), and *m* varies between 0.5 and 0.2 depending on the slope (Weisheimer and Smith, 1978). The value for q_{peak} is calculated in SWAT based on the modified rational method and given as

$$q_{peak} = \frac{\alpha_{tc} \cdot Q_{surf} \cdot Area}{3.6 \cdot t_{conc}} \tag{4.4}$$

where α_{tc} is the fraction of the daily rainfall that occurs during the time of concentration, Q_{surf} is the surface runoff (mm), *Area* is the sub-basin area (km^2), and t_{conc} (hr) is the time of concentration of the sub-basin. The time of concentration is defined as the length of time required for water to flow from the remotest area of the sub-basin to the outlet and can be found from

$$t_{conc} = t_{ov} + t_{ch} \tag{4.5}$$

where t_{ov} (hr) is the overland flow time of concentration and t_{ch} (hr) is the channel time of concentration. The overland flow time of concentration is found from

$$t_{ov} = \frac{L_{slp} \cdot n^{0.6}}{18slp^{0.3}} \tag{4.6}$$

where L_{slp} (m) is the sub-basin slope length, *n* is Manning's roughness coefficient and slp (m/m) is the average slope in the sub-basin. The channel time of concentration can be found as

$$t_{ch} = \frac{0.62 \cdot L \cdot n^{0.75}}{Area^{0.125} \cdot slp_{ch}^{0.375}} \tag{4.7}$$

where *L* (m) is the channel length, slp_{ch} is the channel slope (m/m) and *Area* is expressed in km^2.

4.1.2.2 SWAT channel processes

The SWAT routes water as a volume through the main channel of each sub-basin. The determination of the cross-sectional area of the channel, A_{ch} (m^2) is of significance here because it is dependent on the length of the channel, which is affected by the DEM spatial resolution. It is calculated as

$$A_{ch} = \frac{V_{ch}}{L_{ch}} \tag{4.8}$$

where V_{ch} is the volume of water in the channel (m^3) and L_{ch} is the length of the channel (m). The depth of water in the channel is a function of A_{ch} and the stream channel dimensions. From this information, the hydraulic radius (R_{ch}) of the channel (m) can be determined as

$$R_{ch} = \frac{A_{ch}}{P_{ch}} \tag{4.9}$$

where P_{ch} (m) is the wetted perimeter. Subsequently, the channel flow rate, q_{ch} (m^3/s), and flow velocity, v_c (m/s) are based on Manning's Equation can be calculated as;

$$q_{ch} = \frac{A_{ch} \cdot R_{ch}^{2/3} \cdot slp_{ch}^{1/2}}{n} \tag{4.10}$$

$$v_c = \frac{R_{ch}^{2/3} \cdot slp_{ch}^{1/2}}{n} \tag{4.11}$$

The flow rate is then utilized to determine the routing of water through channels. The variable storage routing method (Williams, 1969) and the Muskingum method are available, and the variable storage routing method was selected for this study.

Several methods exist for determining channel sediment transport processes in the SWAT 2005; however, the default method is based on Bagnold's stream power equations (Neitsch et al., 2011). The Bagnold method determines sediment transport by first estimating the maximum concentration *(conc$_{max}$)* of sediment that can be transported (kg/L) as

$$\mathrm{conc}_{\mathrm{max}} = \mathrm{c}_{\mathrm{sp}} \cdot \mathrm{v}_{\mathrm{ch,pk}}^{\mathrm{spexp}} \tag{4.12}$$

where *spexp* and c_{sp} are user defined parameters and $\mathrm{v}_{\mathrm{ch,pk}}$ is the peak channel velocity (m/s) determined as

$$v_{ch,pk} = \frac{prf \cdot q_{ch}}{A_{ch}} \tag{4.13}$$

where *prf* is a user defined peak rate adjustment factor. Combining equation 10, 11 and 13, $\mathrm{v}_{\mathrm{ch,pk}}$ can be expressed as follows

$$v_{ch,pk} = \frac{prf \cdot q_{ch} \cdot {V_{ch}}^{2/3} \cdot slp^{1/2}}{100 \cdot {L_{ch}}^{2/3} {P_{ch}}^{2/3} n}. \tag{4.14}$$

The result of *conc$_{max}$* is compared with the initial sediment concentration in the reach (*conc$_{sed}$*), based on landscape and upstream inputs. At each time step, if *conc$_{sed}$* is less than *conc$_{max}$* then the dominant process in the stream reach is erosion, and previously deposited material is eroded first. If *conc$_{sed}$* is greater than *conc$_{max}$*, deposition will be the dominant process. If deposition is the dominant process, the amount of material deposited is based on of difference between *conc$_{sed}$* and *conc$_{max}$* and the volume of water in the channel segment. If erosion is the dominant process, the amount of eroded material is based on the product of the difference between *conc$_{sed}$* and *conc$_{max}$*, the volume of water in the channel segment, and two additional parameters termed the channel erodibility factor and the channel cover factor. (Neitsch et al., 2011)

4.1.3 Research questions and hypotheses

1) How does a change in hillslope scale defined by DEM resolution affect simulated flow and sediment? The redefinition of hillslope scale with a controlled stream network and sub-basin delineation in experiment one, is hypothesized to exert only minor sensitivity to flow outputs because the CN method for generating surface runoff is not

directly influenced by changes in slope introduced through variations in DEM resolution. Additionally, precipitation totals, ET and groundwater sources are not directly related to changes in DEM resolution. Subtle variations could exist in water yield due to subtle modifications of HRU size, and land-use/soil/slope distribution. Landscape erosion is expected to increase in fine resolution DEMs due to an expected increase in topographic slope, which will serve to increase the LS_{USLE} of the *MUSLE* factor while all other variables remain constant.

2) Do changes in stream length and slope introduced through a change in DEM resolution affect flow and sediment channel processes in the SWAT? Changes in L_{ch} due to DEM resolution in experiment two are hypothesized to have negligible effect to surface runoff because the CN method is not affected by stream attributes. Landscape erosion will show minor sensitivity to modifications in L_{ch} due to changes in t_{conc} and t_{ov} in (4.5) and (4.6) respectively. The flow rate will decrease with an increase in DEM resolution due to the relationships between A_{ch}, L_{ch}, slp_{ch} and q_{ch} given in equations (4.8) – (4.10). An increase in L_{ch}, due to an increase in DEM resolution, will tend to decrease slp_{ch}, A_{ch} and $v_{ch,pk}$ and decrease the maximum carrying capacity of the stream as shown in equation (4.13). Therefore, increase in channel length will increase channel deposition if $conc_{sed}$ is greater than $conc_{max}$, or decrease the channel erosion if $conc_{sed}$ is less than $conc_{max}$.

3) Does the variation in DEM resolution affect the watershed delineations and subsequently simulated flow and sediment? The redefinition of the watershed boundary and sub-basin extents are hypothesized to affect both the landscape and channel phases through a reorganization of sub-basin boundaries and stream network. A decrease in overall watershed area will cause a decrease in the overall water yields and flow rates as well as sediment yield. Similar to the hypothesis from experiment two, an increase in L_{ch} with an increase in DEM resolution, will decrease $v_{ch,pk}$, which will increase channel deposition if $conc_{sed}$ is greater than $conc_{max}$, or decrease the channel erosion if $conc_{sed}$ is less than $conc_{max}$. A re-organization of HRUs into different sub-basins and routed through different sections of the stream network could result in unpredictable behavior to both the flow rate and sediment yield.

4.2 Study site and methods

4.2.1 Thomas Brook watershed study site

The 689 ha Thomas Brook watershed is located in the Annapolis Valley near Berwick, Nova Scotia, Canada (Figure 4.1). The site is part of the Watershed Evaluation of Beneficial Management Practices (WEBs) program administered by Agriculture and Agri-Food Canada (Stuart et al. 2010), and has stream flow and sediment yield monitoring between January 1st 2004 and December 31st 2008.

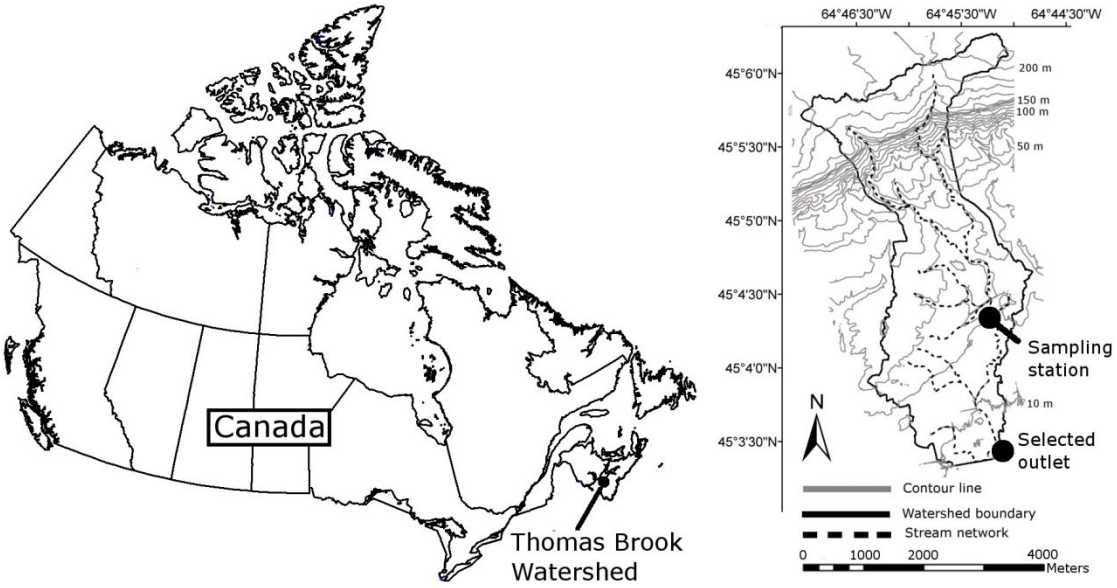

Figure 4.1 Thomas Brook watershed location, topography and boundaries.

The headwaters of Thomas Brook begin on the North side of the Annapolis Valley, termed the North Mountain, and flow southerly into the Annapolis Valley. The selected outlet point for the watershed is located at a culvert that passes under a road in the southern portion of the watershed (Figure 4.1). Two main tributary branches begin at separate locations in the headwaters and join at approximately one third of the distance from the selected outlet (Jamieson et al., 2003). The majority of the landscape slope is between 0 and 6° with 95% of slopes existing below 18° as determined from a 1 m DEM. The slope of the stream network averages 3.5% across the entire watershed; however, it can be as high as 30% on the North Mountain and as low as 0.5% on the valley floor (Sinclair et al., 2009). The stream width generally ranges from 2-3 m throughout the

network. Based on field observations, streams are generally degrading and incised within the valley floor and stable as they descend into the valley. The soils within the watershed are varied but consist predominately of fine grained sandy loams (Cann et al., 1965). Land use within the watershed consists of a mix of agricultural (~70%), residential (4%) and forested areas (~26%) according to a GIS layer collected by Agriculture and Agri-food Canada. The primary agricultural products of the watershed include corn, strawberries and grains (Sinclair et al., 2009).

4.2.2 DEM generation

Raw elevation information required for DEM generation was obtained from a LiDAR survey of Thomas Brook watershed, executed in August of 2006 with an Optech ALTM 3100 sensor. The aircraft was flown at an average elevation of 900 m above ground level (a.g.l), which resulted in an average spacing between raw elevation observations and their closest neighbor of 1.08 m, and 95% of the points having a neighbor within 1.45 m. Raw LiDAR observations were combined with a differentially corrected GPS airborne trajectory that contained high accuracy aircraft position and orientation information in REALM (Optech, 2006), a proprietary software package produced by Optech, to produce real-world coordinated elevation observations in a UTM mapping frame.

Raw LiDAR elevation information contains echo returns from both the physical terrain and natural and man-made structures on the surface. For hydrological analysis, only the physical terrain surface is desired. Non-ground information, such as vegetation and buildings, was filtered in proprietary LiDAR post-processing software. Background information on raw LiDAR observation filtering routines can be found in Pfeifer and Mandlburger (2009). The raw filtered LIDAR observations exist in a pseudo-random pattern that is related to flight conditions and sensor acquisition criteria and required interpolation to generate the regular grid structure of the DEM. This was performed in Golden Software's Surfer (Golden Software, 2012) with a natural neighbor (NN) interpolation routine at spatial resolutions of 1, 5, 10, 25 and 50 m. The NN routine was selected because it is an averaging interpolator and is computationally efficient (Sibson, 1981). Averaging within the interpolating algorithm is advantageous because it exploits

the redundancy of multiple observations to reduce the influence of random errors present in individual raw observations (Pfeifer and Mandlburger, 2009); these errors have been shown to reach decimetre levels in ideal conditions (Goulden and Hopkinson, 2010a) and can be higher in the presence of slopes or vegetation (Hodgson and Bresnehan, 2004; Hopkinson et al., 2005).

4.2.3 Parameterisation of SWAT models

SWAT models were formed in ArcSWAT (Di Luzio et al., 2002), a third party addition to the ESRI ArcMap (ESRI, 2003) GIS software package. Land use information was classified from aerial photographs and field validated, and publically available soils data was available from Holstrom and Thompson (1985). The digital GIS layers for land use and soils were generated in house at Agriculture and Agri-food Canada (Figure 4.2). A slope map was determined from each DEM resolution and classified into five discrete slope classes, the maximum number of discrete classes allowed by the SWAT. The limits of the slope classes were set between 0 and 2°, 2 and 4°, 4 and 8°, 8 and 15° and greater than 15° (Figure 4.2). The area for HRU creation was limited to 1 ha because it is the minimum area of an agricultural field plot within the watershed. In addition, the 1 ha limit eliminates HRUs with minor hydrological significance, maintaining efficiency during model execution. Within agricultural areas, thirteen separate detailed crop management rotation cycles were implemented based on reported farming practices in the area. The management cycles include tillage, planting, fertilizer application, grazing, harvesting, and harvest and kill operations, or some combination of these. Specific details of the crop rotation procedures implemented within the Thomas Brook watershed can be found in Ahmad et al. (2011). The SWAT will automatically generate channel widths and depths, however field observations identified that these quantities were incorrect along the main tributary channels and were manually modified to correspond with observed field data. Meteorological forcing data (temperature, precipitation) is supplied from a weather station operated by Environment Canada in Greenwood, Nova Scotia, which is in close proximity (<25 km) to the watershed in a similar topographic conditions.

The delineation of the watershed and stream networks is performed with algorithms existing in the ArcHydro (Maidment, 2002) software package, which follows

methods designed by Jenson and Dominigue (1988). This included pit filling, which raises the elevation of a pit to be equivalent with the lowest neighboring cell. During the delineation process the user must select an area threshold, which controls the initiation of stream networks. The choice of the threshold area remained consistent at 4 ha for all delineations of the stream network. The 4 ha value was chosen because it was the minimum value SWAT allowed and best correspond to *in-situ* field observations of the main tributary channels and headwater locations conducted in August 2011. The location of the initiation of streams was based on the appearance of flowing water at the highest elevation areas in the watershed from ground observations. Appropriate hydrological enforcement, which included filling sinks as well as stream-burning across road boundaries, was implemented in each DEM resolution to ensure appropriate flow paths were followed.

The SWAT is capable of simulating output for un-gauged basins; however, the outputs are typically inaccurate due to measurement limitations and spatial scaling approximations associated with parameter definition (Beven, 2001; Eckhardt and Arnold, 2001). To improve accuracy, a calibration procedure is implemented that involves a systematic modification of model parameters to match simulated outputs with observed historical field data (Gupta et al, 1999). The 1 m DEM was selected for calibration purposes because it represents the most accurate and precise resolution available for this study, providing a benchmark for relative comparison purposes. Chaubey et al., (2005), Cotter et al (2003) and Lin et al. (2013) also implemented a similar approach of calibrating with the highest resolution DEM when comparing the effects of varied DEM spatial resolution in the SWAT.

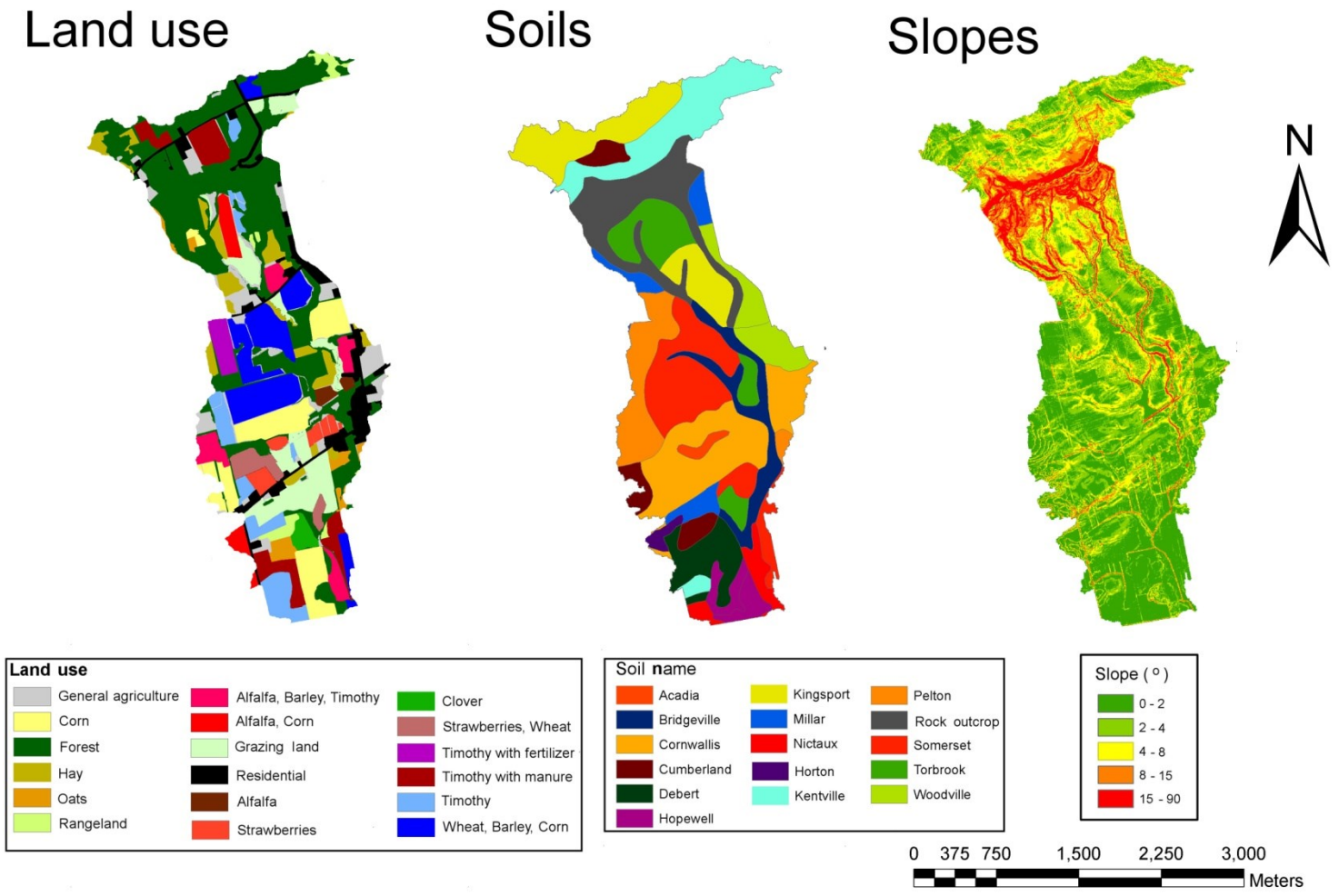

Figure 4.2 **Land use, soils and slope GIS information used to determine the HRUs. Slope information obtained from the 1m DEM.**

Field data collected for model calibration included both stream flow and suspended sediment transport at a monitoring station located approximately 1.5 km from the watershed outlet (Figure 4.1) for five years between January 2004 and December 2008. Stage measurements were acquired through pressure transducers, which monitored water depth on 60 second intervals. Several discharge measurements using the velocity area method (Canada General Standards Board, 1991) were made throughout each year and used to develop stage discharge relationships. Composite suspended sediment samples were collected over three-four day periods using auto-samplers with six hour sampling intervals during non-winter months (April - December), and discrete grab samples were gathered on a weekly basis during winter months (January – March). Sediment samples were analyzed using APHA method 2540 D (APHA, 2000) to determine TSS (total suspended solids) concentrations. Since sediment data was not available on a daily basis, both flow and suspended sediment data were aggregated to monthly totals for calibration purposes. Initially, the model was manually calibrated using parameter values obtained from a previous calibration detailed in Ahmad et al. (2011). Following the manual calibration, an auto calibration was implemented for flow and sediment simultaneously using the PARASOL method, outlined in van Grivenson and Meixner (2007). The PARASOL technique involves iteratively modifying selected model parameters to minimize a statistical assessment criterion between simulated outputs with observed field data.

A total of 20 years were executed during model simulations, including a 15 year spin-up period followed by a five year assessment period used to simulate results. Therefore, presented results were obtained from the same final five years as used for the calibration period. Model success was determined using statistical tools and qualitative ratings outlined in Moriasi et al. (2007) that included the RMSE-observations standard deviation ratio (RSR), Nash-Sutcliffe coefficient (NSE), and percent bias (PBIAS) between the simulated outputs of flow rate and sediment yield and field observed data. Differences between DEM resolutions were quantified on a monthly basis and, in some cases, quantified using a relative difference (RD) metric as:

$$RD_{test} = (x_{test}-x_{ref}) / x_{ref} \quad (4.15)$$

where *x* is the simulated variable (flow, sediment) *ref* is the 1 m DEM and *test* is either the 5, 10, 25 or 50 m DEM.

4.2.4 Experimental design

Three separate experiments were conducted to assess the sensitivity of hydrological outputs of the three DEM functions to changes in DEM spatial resolution (Table 4.2). Experiment one tested the sensitivity of hydrological outputs to a modification of hillslope scale. This was accomplished by maintaining a consistent watershed boundary, stream network delineation and calibrated parameter set from the 1 m DEM, and varying the spatial resolution of the underlying DEM. The controlled modification of only the hillslope scale was realized in the ArcSWAT watershed delineation tool by eliminating the delineation process of the stream network and sub-basin boundaries for the 5, 10, 25 and 50 m DEMs and imprinting the existing stream network and sub-basin boundaries obtained from the 1 m DEM. Experiment two tested the effects of spatial resolution on stream length and stream slope. One method of obtaining updated stream network lengths for each spatial resolution DEM would be to execute distinct delineations. However, a distinct delineation would introduce uncontrolled variability due to changes in the spatial location of the simulated stream and sub-basin boundaries. To control for the sub-basin boundaries and stream network location, a systematic scaling relationship between the stream length and DEM resolution was exploited. The relationship is mathematically described with the following power law:

$$g(x) = ax^{\alpha} \tag{4.15}$$

where *g(x)* is the stream length, *x* is the DEM spatial resolution, *a* is a constant equivalent to the stream length determined from the 1 m DEM, and α is a decay constant previously determined to be -0.059 in Goulden et al., (2012). Both the longest flow path and stream reach within the sub-basin were manually modified, which correspond to variables *CH_L(1)* and *CH_L(2)* in the SWAT theoretical documentation (Neitsch et al., 2011). The slope values associated with the longest flow path and stream reach, corresponding to *CH_S(1)* and *CH_S(2)* in the SWAT theoretical documentation respectively, were also modified. The values for *CH_S(1)* and *CH_S(2)* represent the overall slope from the

beginning to the end of the stream reach and do not consider variations of slope within the reach. Therefore, the modification of slope can be triangulated from the amended stream length and elevation change between the beginning and end of each stream reach. The elevation change was obtained from the 1 m DEM model and remained consistent as there was little variation in the elevation changes within the sub-basin for the remaining DEM resolutions.

The third experiment varied the landscape scale, the delineation of the stream network, and watershed boundary, sub-basin boundaries and HRU definitions with DEM resolution in order to analyze the effects of the three DEM functions simultaneously. This was achieved by executing a distinct delineation of the watershed from each spatial resolution DEM. The spatial location of each sub-basin outlet point determined in the delineation of the 1 m DEM model were generally maintained in the delineation of the other DEMs. However, due to differences in the watershed boundaries and spatial locations of the stream network, some outlet locations could not be located at repeatable positions. This introduced variation in the resulting sub-basin boundaries and stream length.

Table 4.2 Control of DEM function variables in each experiment

	Variables held constant	Variables allowed to vary
Experiment 1	Stream length, stream slope, sub-basin boundaries	Hillslope scale
Experiment 2	Sub-basin boundaries	Hillslope scale, stream length, stream slope
Experiment 3	None	Hillslope scale, stream length, stream slope, sub-basin boundaries

4.3 Results and discussion

The results are organized into sub-sections, which describe the sensitivity of slope classes, watershed attributes and hydrological outputs, including flow rate and sediment production. A sub-section is devoted to changes to the distribution of slope classes because it is a fundamental topographic parameter, which affects HRU creation, and will

subsequently affect results from each experiment. The section reporting on the sensitivity to watershed attributes is only relevant to the third experiment, since the sub-basin boundaries and stream network were allowed to vary in this case. Sections describing flow rate and sediment output include the results from each experiment, and are separated into results from the landscape and channel phases of the SWAT. The parameter calibration obtained from the 1 m DEM, and applied to all of the SWAT simulations resulted in acceptable performance metrics for both simulated flow and sediment results (Table 4.3).

Table 4.3 Performance metrics, based on Moriasi (2007), of the SWAT model calibration for Thomas Brook watershed using the 1 m DEM

Variable	RSR	NSE	PBIAS
Flow	0.57 (Good)	0.76 (Very Good)	4.8 (Very Good)
Sediment	0.64 (Satisfactory)	0.71 (Good)	4.8 (Very Good)

4.3.1 Slope classes

The increase in DEM resolution resulted in an increase in the proportion of area represented by high slope classes (Figure 4.3). The largest change occurs between the 1 m and 50 m DEMs in the lowest slope class (0-2°), where the area distribution is 34% and 55% respectively. The 1 m DEM also had the largest proportion of the highest slope class, due to the resolution enabling representation of fine-scale topographic details of the landscape, while low resolution DEMs tend to smooth the landscape and cannot characterize minor topographic variations. When implementing DEMs at the 1 m level, the effects of random vertical errors caused by sensor measurement errors must also be considered. Random elevation error will increase the incidence of high slope in fine resolution DEMs due to the introduction of noise into DEM grid node elevations. In DEM cell sizes which are small, elevation error will propagate into the calculation of slope resulting in a higher proportion of area in the highest slope class. As seen in Section

3.4.3, it is not unusual for noise in a DEM grid node to reach 0.05 m of elevation deviation. Subsequently, slopes typically varied up to ~1.5°, which could shift a cell to a higher slope classes. The effect of noise is not as prevalent in low resolution DEMs because the level of vertical error is low relative to DEM cell size. Therefore, the slope calculation will experience a reduced sensitivity to elevation errors as DEM resolution decreases. An effect of the pit filling algorithm in ArcHydro could also be to increase the absolute proportion of the low slope class in each DEM resolution, as filled pits will be flat surfaces.

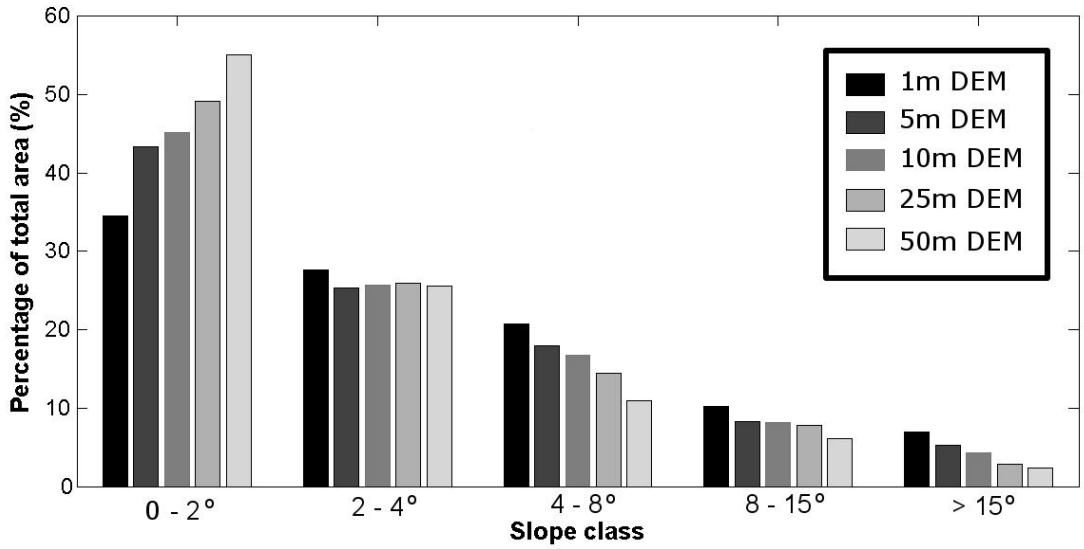

Figure 4.3 Percentage area of the respective slope classes obtained from each spatial resolution DEM and used to develop HRUs in the SWAT model

4.3.2 Watershed attributes

The third experiment uniquely delineated the watershed from each tested DEM resolution, which resulted in changes to the area, stream length, number of sub-basins, and number of HRUs (Table 4.4). The largest change in watershed area is the reduction which occurs with 10, 25 and 50 m resolution DEMs which experience a reduced area of 7.7, 6.7 and 7.0% respectively compared to the 1 m DEM. This reduction in area is due to a section of the watershed in the southwest corner incorrectly draining across a road and diverting from the true watershed outlet also identified in Section 2.4.1.1. The erroneous flow path is due to a scale related dependency of the DEM to the road width. The road is

8 m in width, allowing the 10, 25, 50 m DEMs to smooth the road feature and incorrectly permit drainage across to an adjoining field, diverting flow from the true outlet.

Table 4.4 Summary of watershed attributes for each DEM spatial resolution

DEM spatial resolution (m)	Area (km^2)	Stream length (m)	Number of Sub-basins	Number of HRUs
1	6.899	19,515	28	275
5	7.015	19,470	28	281
10	6.367	17,190	26	252
25	6.434	15,400	26	262
50	6.412	14,750	25	274

The observed reduction in stream length as the DEM resolution decreases is a result of a continuous loss of fine resolution details of the stream network. The largest decrease occurs between the 5 m and 10 m DEM, as this decrease is also supplemented by the reduction in watershed area that also occurs between these two resolutions. The reduction in the total number of sub-basins in the 10, 25 and 50 m DEMs is also a result of the reduction in the overall area because the missing sub-basins no longer existed within the watershed. A substantial decrease in the number of HRUs occurs with the decrease in area, which experiences a minimum at the 10 m resolution, and increased for the 25 and 50 m resolutions. The rise in the number of HRUs at the 25 and 50 m resolutions is a result of a more even distribution of slope classes in these DEMs (Figure 4.3). The more even distribution of slope classes results in a greater likelihood that HRU combinations with multiple slope classes will exist with sufficient area to form an HRU.

4.3.3 Flow

The modification of hillslope scale in experiment one produced negligible variability in the simulated flow on a monthly time scale (Figure 4.4). Table 4.5 shows that the average relative difference maximized at 2.5% for RD_{50}. A small number of months resulted in high values of RD (>5%) in each of the tested resolutions; however, these were always associated with a low monthly flow. In these months, such as September of 2004 (Figure 4.4), only very minor standard deviations result in high values of *RD*. The insensitivity of flow to DEM resolution result has similarly been observed by

Di Luzio et al. (2005) and Li et al. (2012). The minor variability which did exist, was due to slight changes in HRU distribution and size, which subtly altered CN values, the amount of ET, and ground water recharge contributions.

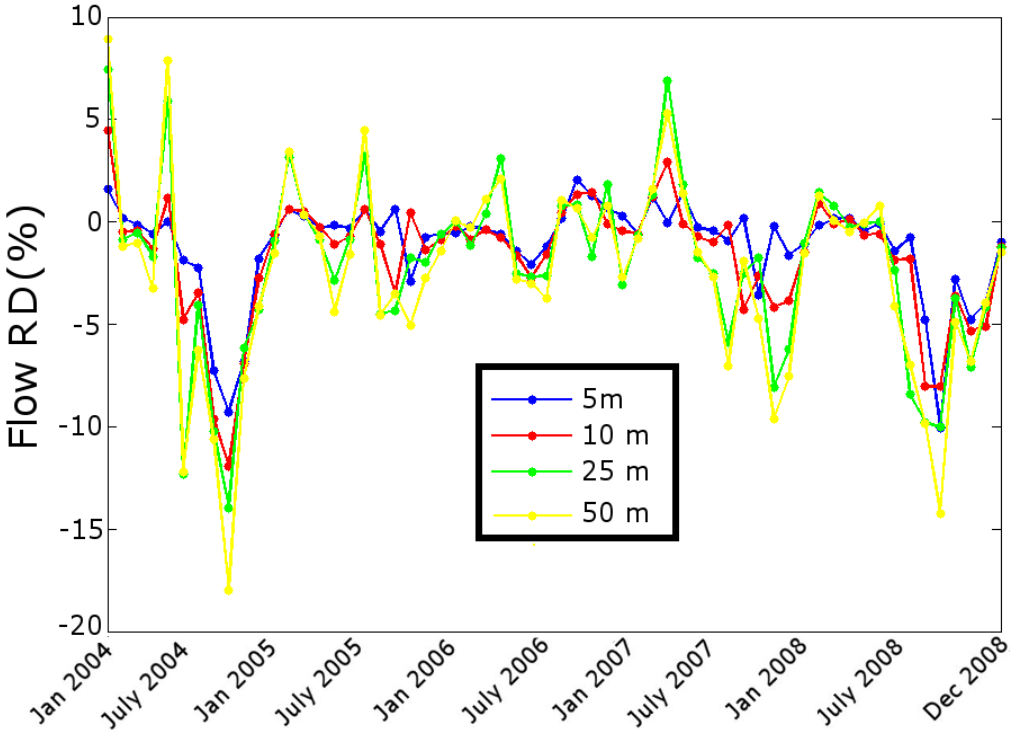

Figure 4.4 Flow relative difference for the sixty month simulation period for all DEM resolutions, compared to the 1 m DEM, for experiment 1

Kienzle (2010) identified in the Agricultural Catchments' Research Unit (ACRU) model, that an underestimation in true surface area in sloped regions, could have influence over ET and runoff predictions. This result infers that as DEM resolution decreases, the associated decrease in mean slope would create an underestimation of the true surface area and influence total water yield. A similar result was also observed in high relief glacierised catchments by Hopkinson et al. (2010). The SWAT considers only planimetric area, therefore, the slope-area relationship had no influence over flow results. This result confirms the hypothesis that surface runoff predictions based on the SCS Curve Number Method in the SWAT will show negligible variability to a change in hillslope scale initiated through a change to DEM resolution.

Table 4.5 Experiment 1 and experiment 2 mean relative differences for flow of all DEMs compared to the 1 m DEM over the 60 month simulation period

DEM resolution	Experiment 1 mean flow RD (%)	Experiment 2 mean flow RD (%)
5 m	1.1	1.4
10 m	1.7	1.9
25 m	2.1	2.4
50 m	2.5	2.8

The modification of the channel lengths and their respective slopes in experiment two also produced negligible change to simulated flow on a monthly time scale. Results from Table 4.5 show that the maximum mean RD occurred with the 50 m DEM reaching only 2.8%. The existing variability was due to slight changes in HRU distribution and size, which subtly altered CN values, levels of ET and ground water recharge contributions. The modification of the channel lengths and their respective slopes in experiment two also produced negligible change to simulated flow on a monthly time scale. The resulting insensitivity can be attributed to the small scale of the Thomas Brook watershed, which is characterized by travel times within the sub-basin reaches of less than a day, the minimum time step in SWAT. For example, the 1 m DEM experiences the longest flow paths, and of the sub-basins along the main tributary channels the longest travel time during the five year period is 27 hours. A travel time of 27 hours, just over one day, is rare for a subbasin within the Thomas Brook model, as the average travel time for this sub-basin is 13.9 hours. Since the SWAT calculates flow on a daily time step, water yield will not be sensitive to stream length if the travel times are less than a single day, regardless of resolution effects to stream length. Since flow results are output as a monthly average to correspond with available calibration data, a rare anomalous incidence of travel time over the daily threshold will have little effect to the monthly average. Drainage basins containing larger sub-basins, which commonly experience

travel times longer than a day, and analyzed on a daily time step, may show a sensitivity to simulated flow due to DEM induced changes in stream length.

Experiment three, where full delineations of the watershed were produced from each DEM, was the only experiment to show variability in simulated flow on a monthly time step. The 1 m and 5 m DEMs simulated similar, and higher, flow volumes than the 10, 25 and 50 m models. The difference in simulated flow can be attributed to the scale dependent planimetric area reduction that occurred in the 10, 25 and 50 m delineations, which excluded an area of the watershed because of an inability to represent the 8 m wide roadbed. The largest discrepancy in flow existed between the 1 and 50 m DEMs (Figures 4.5A and 4.5B). The largest RD of flow between the 1 m and 50 m DEM occurred in month 55, which reached approximately 20%. The majority of monthly flow rates resulted in differences of flow between 10 and 15% with the minimum occurring at month 12 at approximately 6%. Cotter et al. (2003), Chaubey et al. (2005) and Di Luzio et al. (2005) similarly observed a decrease in flow as DEM resolution decreased. Cotter et al. (2003) attributed the decrease in flow with coarse resolution DEMs to smaller stream slopes, longer slope lengths and a reduced watershed area. The reduction in flow observed in the Thomas Brook watershed appears to be exclusively related to the change in planimetric watershed area, as the smaller stream slopes and lengths had negligible effect in experiment two.

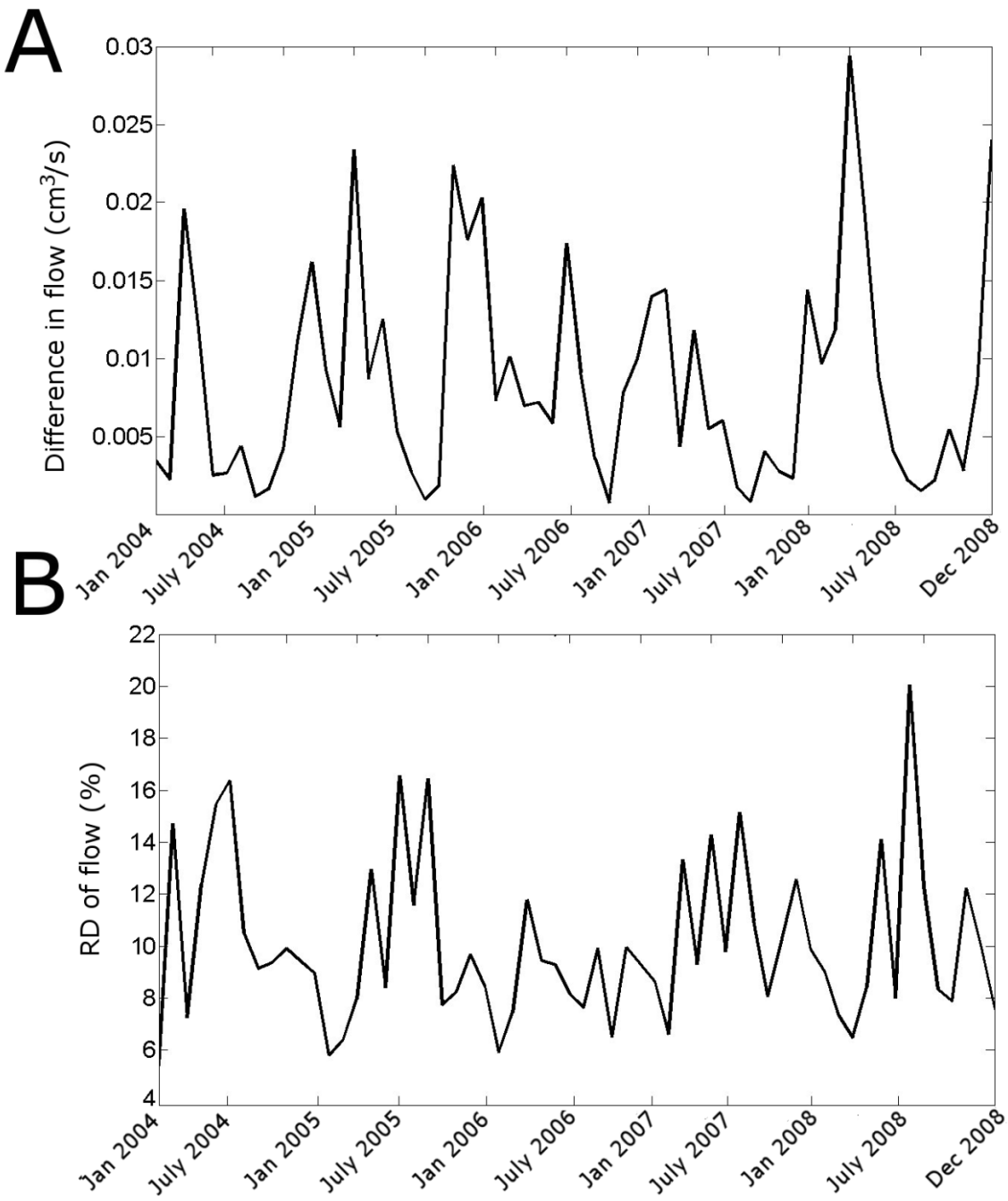

Figure 4.5 **A) Absolute difference between observed flow rate of the 1 m and 50 m DEMs and, B) the relative difference of flow between the 1 m and 50 m DEM models for the third experiment**

4.3.4 Sediment yield

4.3.4.1 Landscape sediment yield

The 1 m DEM resulted in the largest simulated cumulative sediment yield, which reached approximately 850 t over the simulated 60 months. As hypothesized, total suspended sediment yield decreased with a decrease in resolution (Figure 4.6A). The 50 m DEM resulted in the least amount of simulated sediment at approximately 650 metric tons over the 60 month time period; 76% of the total yield generated by the 1 m DEM. The reduction in the landscape sediment yield is caused by the shift in distribution of the slope classes within the HRUs. The 1 m DEM resulted in the largest number of HRUs with the highest slope class and an increase in landscape erosion followed. This is theoretically justified in equations (1) through (6), that relate the increase in sediment predictions of the MUSLE due to increases in slope, specifically from LS_{USLE} and R_{runoff} through q_{peak}, t_{ov}, and t_{ch}.

A discrepancy in sediment production occurred in the hypothesized trend of decreasing sediment output with DEM resolution between the 10 m and 25 m DEM models. The simulated sediment yield in these models are nearly equivalent (Figure 4.6A). Investigation into these models reveals that a single anomalous HRU in a north east sub-basin of the 25 m DEM model is responsible. The HRU in question contains an erosive *'harvest and kill'* crop management procedure that reduces ground cover and produces a high level of simulated erosion. In addition, the HRU from the 25 m DEM resulted in a higher overall slope than the HRU from the 10 m DEM model. Obtaining a higher slope class from a lower resolution model is rare, and it is due to the grid nodes of the 10 m and 25 m DEMs not being spatially coincident. The non-overlapping grid nodes in the 25 m DEM identified a ridge or valley feature in the HRU, which was not identified in the 10 m DEM and caused a higher slope. The higher slope class, coupled with the erosive crop management procedure caused erosion levels that overcame the differences in sediment yield produced throughout the remaining areas of the watershed. To show the general trend of decreasing simulated sediment yield with decreasing resolution, the slope of the problematic HRU in the 25 m DEM model was modified to be equivalent of the identical HRU in the 10 m DEM model. The resulting output displayed

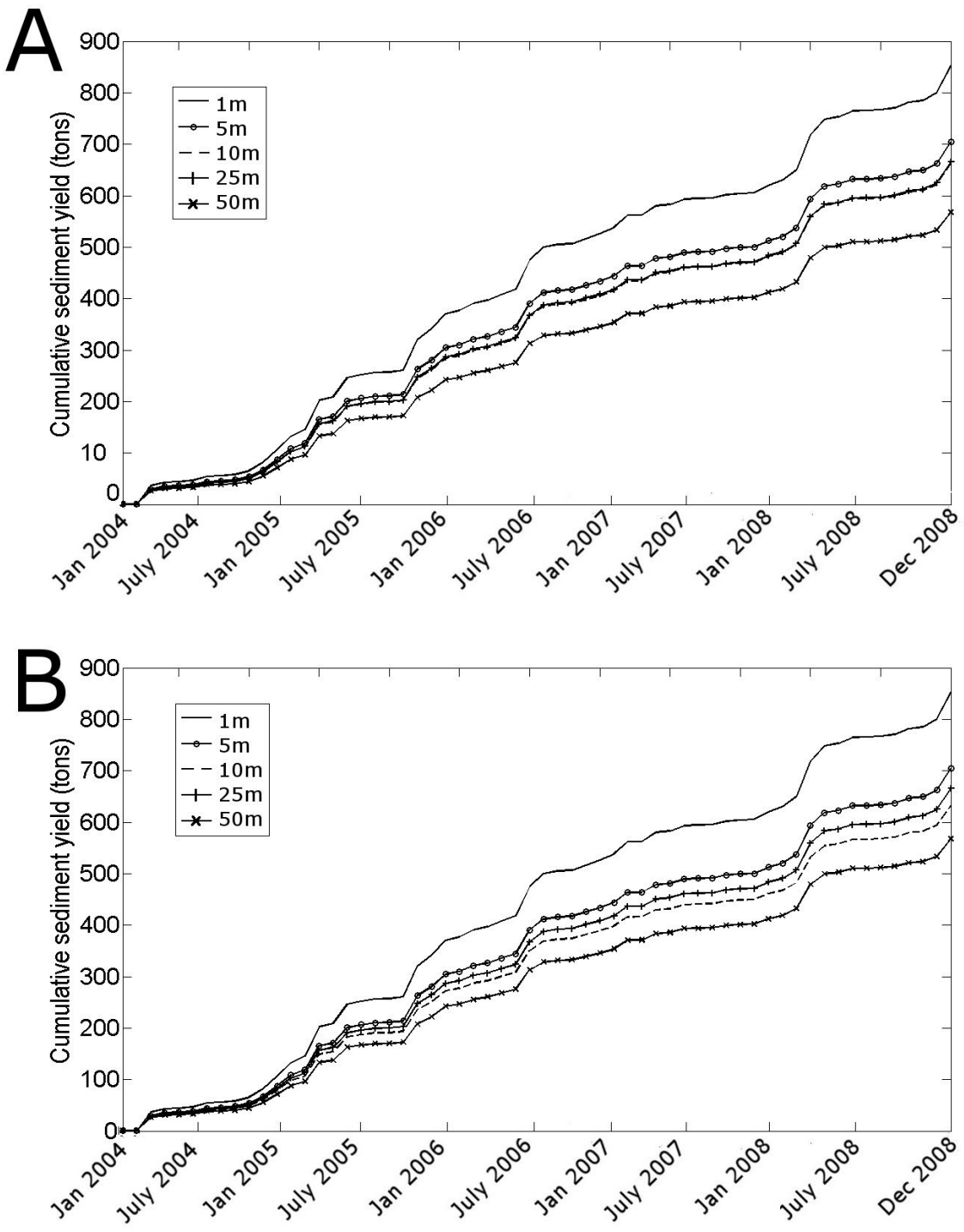

Figure 4.6 **A) Cumulative sediment totals at the watershed outlet for each of the spatial resolutions; note the 10 m and 25 m results are nearly coincident, B) cumulative sediment totals with an HRU from the 25 m resolution model modified to a level of slope equivalent to the identical HRU in the 10 m resolution model.**

the expected decrease of simulated sediment yield with DEM resolution (Figure 4.6B). This discrepancy in sediment production shows that the general trend of decreasing sediment yields with resolution may not exist under conditions of non-overlapping DEM grid nodes in areas with high propensity for erosion.

The modification of the stream lengths in experiment two did not affect simulated landscape erosion (Figure 4.7A). Theoretically, the *MUSLE* is dependent on *CH_S(1)*, which is used to determine the t_{conc}, a factor of q_{peak}. However, because t_{conc} is shorter than the minimum daily time step of SWAT under all the tested stream lengths, simulated landscape erosion was not sensitive to the changes in stream length. However, a decrease in landscape erosion was observed with the full delineations performed in experiment three (Figure 4.7A). The decrease observed in the 10, 25 and 50 m DEM models is a result of the reduced area of the watershed. Conversely, the 5 m DEM showed a decrease in landscape erosion despite an increase in total watershed area. This is attributed to the specific areas of the watershed that changed between the 1 m and 5 m DEM models. Although the overall area was larger in the 5 m model, areas that contained high erosion activities were reduced, while areas with a low propensity for erosion increased. For example, the *'Rock Outcrop'* class of soil type has very little potential for erosion and existed in higher quantities in the model delineated from the 5 m DEM. This highlights that a change in area doesn't necessarily result in an increase in sediment production. The nature of erosion potential of the land use and soils within areas that have been changed will be a factor in sediment uncertainty between DEM resolutions.

4.3.4.2 Sediment transport in channels

In each experiment the simulated sediment transport in all channels resulted in negligible levels of channel erosion and high levels of deposition. The exclusive existence of deposition is likely due to excessive simulated landscape erosion, which overwhelmed the stream channels. The 1 m DEM model resulted in the largest amount of channel deposition with a cumulative total of 171 metric tons for the 60 month simulation

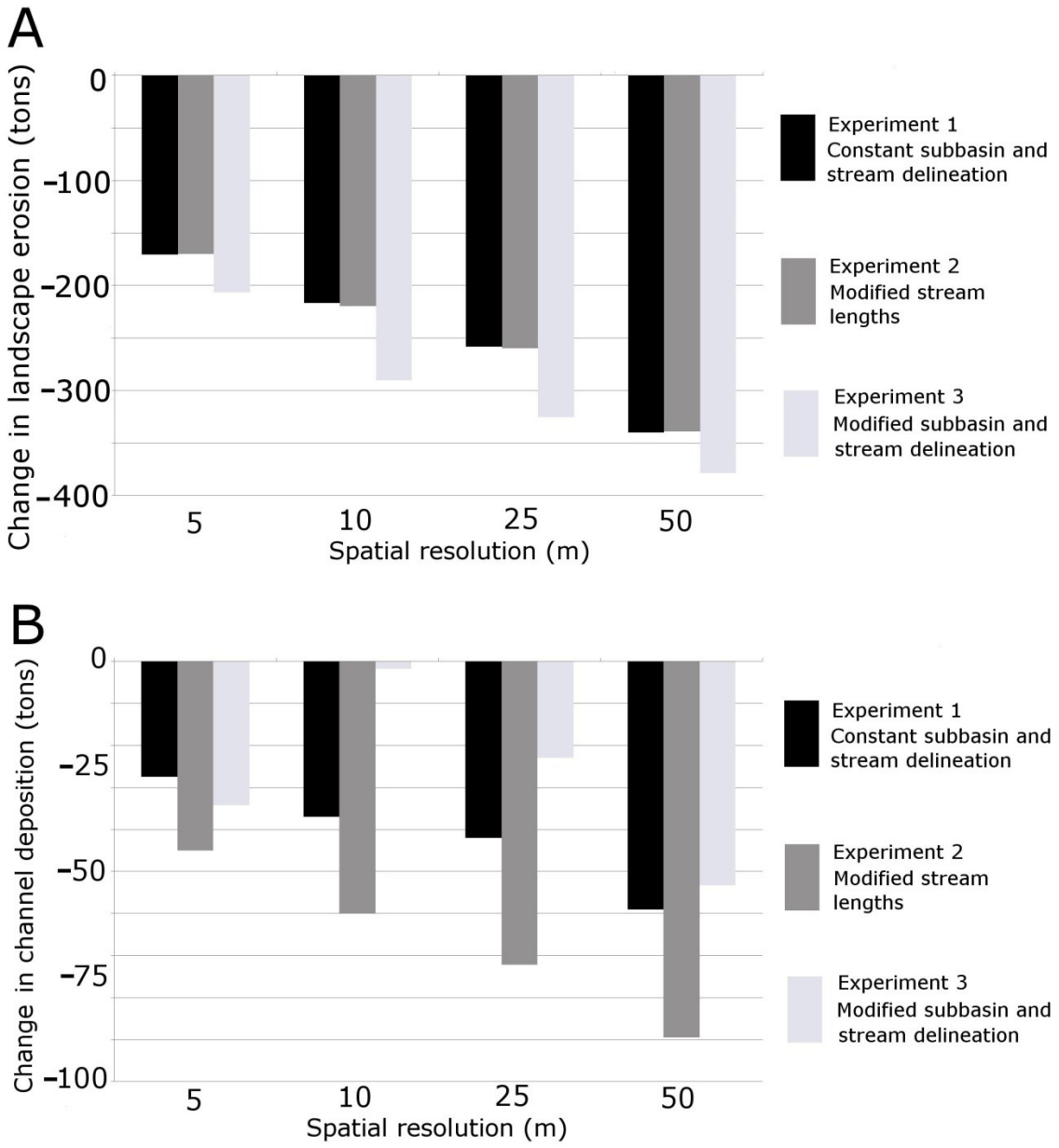

Figure 4.7 **A) Differences in landscape soil erosion and, B) channel deposition for each spatial resolution DEM of each experiment compared to their respective results from the 1 m DEM**

period. Models generated in experiment one showed a decrease in channel deposition with decreasing DEM spatial resolution (Figure 4.7B). The decrease is related to the previously discussed reduction in overall available sediment entering the streams from the landscape erosion simulated through the *MUSLE*.

Results from experiment two showed the hypothesized decrease in channel deposition as the spatial resolution decreased. The 50 m DEM from experiment two resulted in the largest decrease, totaling 90.0 t over the five year simulation period. The largest discrepancy in channel deposition between experiment one and experiment two with identical resolution DEMS occurred with the 50 m DEMs simulations, which showed a decrease of 33 t in experiment two. The decrease in channel deposition with decreasing stream length is caused by the increase in $v_{ch,pk}$ (equation 14), which serves to increase the sediment transport capacity of the stream channels.

The results from experiment three show the 10, 25 and 50 m delineations exhibiting a trend of decreasing channel deposition with a decrease in spatial resolution; however, a relative increase was experienced at these resolutions compared to the respective results from experiment one and experiment two. The observed relative increase in deposition for the 10, 25 and 50 m DEMs, compared to results from experiment one and experiment two, is related to a decrease of the slope in several tributary channels, which reduced the sediment transport capacity of the streams. An additional small decrease can be attributed to the elimination of two headwater sub-basins, which reduced the total stream length where deposition could occur. It is also possible that a re-organization of HRUs into different sub-basins between the delineations was partially responsible for the increase in deposition. For example, if a particularly erosive HRU originally existed in a sub-basin with a short and steep tributary channel with low propensity for deposition, and then moved into a sub-basin with a longer, flat channel with high levels of deposition it could cause an overall increase in channel deposition. Such re-organization of HRUs are likely to exist; however, their effects are unpredictable and difficult to isolate and therefore cannot be conclusively associated with the changes.

4.3.4.3 Calibration of P_{USLE}

It should be identified that Quinn (1995) and Lin et al (2010), in a study of TOPMODEL, found that uniquely calibrated flow outputs from varied DEM resolutions exhibited equifinality. Equifinality conditions (Beven and Binley, 1992) occur when

parameter modifications determined in the calibration process compensate for the variations introduced by DEM resolution. A similar result of equifinality would likely be observed at Thomas Brook, where an optimum parameter set obtained from different resolutions DEMs would provide results similar to the 1 m DEM parameterisation. This suggests that the DEM resolution is not critical as long as a statistically acceptable parameterisation can be achieved. However, in terms of the observed sediment outputs, it is important to identify that the LS_{USLE} represents a ratio of soil loss relative to a standard plot of 72.6 ft in length and a uniform 9% slope (Wishmeier and Smith, 1978). Values for LS_{USLE} were empirically tested on plots ranging from 30 to 300 ft (9.1 to 91.4 m) in length, with uniform 3 to 18 percent of slope steepness (Wishmeier and Smith, 1978). Therefore, the slope length defined by a 1 m DEM is finer than the original field plots tested for the LS_{USLE}. It is likely that uncertainty is introduced to the *MUSLE* through the spatial scaling of the original test plots, resulting in an overestimation in the amount of simulated landscape erosion. To compensate for the spatial inconsistency, the final calibrated value of the P_{USLE} factor was reduced to 0.12. Acceptable calibrations with the 25 m or 50 m DEMs, which have spatial scale within the spatial limits of the field plots tested, are possible with P_{USLE} values of 0.20 and 0.23 respectively.

Although uncertainty boundaries are not available for the P_{USLE} factor, we must consider that the design intention of P_{USLE} factor is to account for sediment reduction through farming practices such as strip cropping or terracing (van Vliet, 2002). It is identified by van Vliet (2002) that terracing is the only practice, which can reduce the P_{USLE} factor as low as 0.1. Within Thomas Brook, no terracing is occurring. Therefore, a P_{USLE} factor of 0.1 should be considered an unrealistic modification, despite a statistically valid calibration. Values of 0.2-0.23 for P_{USLE} are an improvement, but are also low for the conditions at Thomas Brook. One of the conditions that allows P_{USLE} as low as 0.2 is cross-slope farming (van Vliet, 2002), which does occur in several areas of the watershed, although it is not ubiquitous. The consistently low calibrated values of P_{USLE} are likely due to existing practices designed to reduce sediment transport and are not included in the definition of P_{USLE}, such as riparian buffer strips.

The existence of unrealistic parameter values should be treated with caution as it undermines future planning efforts within the watershed to achieve management goals.

For example, if additional practices designed to reduce sediment transport were initiated, the artificially low P_{USLE} factor prevents their correct incorporation into the model. Since these changes cannot be adequately simulated, it inhibits an assessment of the future environmental or economic viability of the modifications. The ability to achieve an improved parameterisation of the Thomas Brook model with the low resolution DEMs indicates they are a more appropriate choice for defining the hillslope scale.

4.4 Conclusions

Prior to parameterizing a SWAT watershed model a decision must be made on the spatial resolution of the DEM to be included. The spatial resolution of the DEM will define the representative hillslope scale, and affect the watershed boundary and stream network position and length. Proper selection of the appropriate DEM resolution will contribute a meaningful and scientifically defensible model parameterisation, which will provide more effective water resource planning strategies. This study demonstrated the sensitivity of water and sediment yield produced in the SWAT to DEM resolution changes. The effects of DEM resolution changes to hillslope scale, stream network delineation and boundary delineation were isolated in three separate experiments.

A primary effect of variation in landscape scale through DEM resolution is a redistribution of watershed area to relevant slope classes within the SWAT. The highest slope class size tends to increase as DEMs increase in resolution. Simulated flow results were not sensitive to the changes in the slope; however, simulated sediment loads from the lowest resolution DEM were 76% of the loads obtained from the highest resolution DEMs. The change in simulated sediment loads were related to changes in slope through the MUSLE variables q_{peak} and LS_{USLE}. Similar to Beeson et al., (2013), the highest sediment loads were obtained with the highest resolution DEM tested. High sediment loads from the 1 m resolution DEM created difficulties in calibrating the SWAT model. Model parameters related to landscape erosion, such as the P_{USLE}, had to be reduced to unrealistic values. This indicates that the spatial scaling of the original USLE plot sizes to fine resolution DEMs is inappropriate as it tends to overestimate simulated erosion.

The second experiment exploited a scaling relationship relating a decrease in spatial resolution to a decrease in stream length. The most striking effect was a reduction

in sediment deposition as DEM resolution decreased. The changes in deposition are governed by the sediment transport processes as predicted by Bagnold's stream power equations whereby reduced stream lengths caused an increase in $v_{ch,pk}$. This increased the predicted sediment transport capacity of the stream, thus reducing the amount of sediment deposition. The 50 m DEM resulted in the largest overall decrease in deposition of 90 tons over the five year simulation period. Given the varied results with stream length, the 1 m DEMs are recommended for model parameterisation because they render the most accurate prediction of stream length (e.g. Murphy et al., 2008). Typically, fine resolution DEMs are the most difficult to obtain, and if a DEM of suitable resolution is not available, stream lengths can be modified using the scaling relation defined in equation (4.1) to determine stream attributes for a desired resolution. Although a 1 m DEM is ideal for Thomas Brook, different resolutions may be ideal for other watersheds.

In the third experiment, original watershed boundaries and stream networks were delineated from each resolution of DEMs. The coarsest resolution DEMs (10, 25 and 50 m) resulted in a 10% reduction of area due to a section in the southeast corner incorrectly draining to a separate outlet point. The delineations with reduced areas showed an overall decrease to simulated flow. Landscape erosion also decreased due to the reduction in watershed area in the 10, 25 and 50 m DEMs. Despite the reduction in area and total stream channel length, deposition increased in these models due to a decrease in the slope of the tributary channels in several sub-basins. This indicates that when using coarse resolution DEMs, barrier features such as roads, which are below the scale of the DEM resolution must be considered potential sources of errors in area. Any error in area determination will affect flow rates and sediment yield. If the watershed does not contain features, which are below identification capabilities set by the DEM resolution, errors related to area should not be a concern. Therefore, additional expense and computing burden should not be introduced with high resolution DEMs if water yield is the only variable of interest and there is no reason to suspect area discrepancies will occur.

Traditionally, the parameterisation of a hydrological model with a DEM involves using the same spatial resolution for each individual input required from the DEM. However, this research has shown that hydrologic outputs, especially those related to simulated sediment output, will have specific responses to a variation in spatial resolution

associated with each DEM function. The relative importance of each DEM function can be used to prioritize decision making of DEM resolution. With respect to the watershed models developed for Thomas Brook, the importance of the DEM functions in terms of their sensitivity to simulated sediment output can be ordered as follows:

1. definition of hillslope scale,
2. watershed and sub-basin boundary delineation, and
3. stream attributes.

Previous literature has suggested that resolutions that mimic the natural scale of the landscape are optimum for hydrologic modeling, with a general rule indicating that 10 m is the minimum resolution required for satisfactory results (Zhang and Montgomery, 1994; Creed and Sass, 2011). However, fine resolution DEMs tend to produce the most accurate delineations of the boundary and stream network (Murphy et al., 2008; Remmel et al., 2008). Given the varied responses of the individual DEM functions to simulated outputs it is recommended that a multi-scale approach is implemented for parameterizing SWAT watershed models. This follows a similar suggestion by Quinn (1995) for TOPMODEL, who proposed nested DEMs of differing resolution for separately modeling basin-wide hydrographs and finer scale internal processes. Nested DEMs may prove cumbersome within the SWAT framework, therefore a multi-scale approach is more readily achieved within SWAT by utilizing an underlying DEM with resolution similar to the natural scale of the landscape for the determination of topographic slope, and using the highest resolution DEM for the delineation of stream networks and sub-basin boundaries. Paramaterizing a SWAT model with multiple scales for each DEM function will aid in generating accurate outputs with a more realistic parameter set, thus facilitating conscientious implementation of watershed models. For example, the model of Thomas Brook Watershed tested here would benefit from a delineation of the stream network and sub-basin boundaries from the 1 m DEM, and a coarser DEM for defining the hillslope scale. Ideally, the choice of resolution for defining hillslope scale should be selected to produce a calibration, which does not require unrealistic changes to parameters.

Future work in this area involving the SWAT should include a similar analysis in a larger scale watershed, or with different topographical and hydrological settings. A

different site should be chosen to specifically investigate the effects of DEM resolution on flow and sediment in a basin with travel times greater than the minimum daily time step of the SWAT. Additionally, obtaining sufficient calibration information to allow for daily simulations could provide better information on the simulated response of specific storm events. It is hypothesized that under conditions of increased travel time, simulated flow and timing will show a higher sensitivity to the variation of DEM spatial resolution, especially when analyzed on a daily time step. For other modeling environments which heavily rely on topographic information, the DEM spatial resolution would show an increased impact. For example, flood inundation models require high resolution information on flow blockages, especially in urban areas (Haile and Rientjes, 2004), and for the parameterisation of surface roughness (Lane, 2005; Casas et al., 2010). Flood wave travel times have shown to be sensitive to DEM resolutions between 10 m and 1000 m (Horritt and Bates, 2001), indicating further sensitivity could exist at the finer DEM resolutions achievable with LiDAR.

The updated SWAT 2009 now includes physically based algorithms for routing sediment in channels. For example, the Yang sand and gravel method (Yang, 1996) algorithm for sediment deposition depends explicitly on the tributary stream length (equation 7:2.2.33, Neitsch et al., 2011). Therefore, future work will investigate the sensitivity of the other available sediment transport algorithms. It is hypothesized that algorithms, which are directly affected by an estimate of stream length will have a higher sensitivity to modifications of DEM resolution than the Bagnold algorithm. Future work is also planned for investigating the effects of DEM resolution to simulated water quality outputs of the SWAT, such as bacteria and nutrient loads.

CHAPTER 5 SENSITIVITY OF THE SWAT TO MEASUREMENT UNCERTAINTY IN LIDAR DERIVED DEMS

5.1 Introduction

Hydrologic simulation models are informative for planning and management of water resources due to their ability to predict basin response to simulated alterations. This knowledge allows informed design of environmental planning strategies to facilitate economic and environmental sustainability. Due to constraints of representing complicated natural systems virtually, hydrological models will contain several sources of uncertainty which cause model results to deviate from reality. The sources and consequences of uncertainty introduced to a hydrological model should be well understood to allow for conscientious use of model outputs, and in the development of reliable environmental planning initiatives. Inadequate understanding of the uncertainty associated with simulated hydrologic outputs will ultimately undermine planning strategies, and could serve to produce ineffective policy actions.

Topographic information, virtually represented as a DEM (Digital Elevation Model), is a common data source used for the parameterisation of distributed hydrological models. The most common form of a DEM is a regularly spaced horizontal grid of elevation values (Collins and Moon, 1984; Moore, 1991). As a measured input, the DEM is subject to various sources of uncertainty, which will propagate through a hydrological model to simulated outputs. Wu et al., (2008) identify two primary sources of DEM uncertainty, 1) the DEM grid cell size and, 2) the elevation uncertainty at DEM grid nodes. Studies describing the response of simulated hydrological outputs due to DEM grid cell size uncertainty are available (see Chapter 4), however, few studies have reported on uncertainty estimates of simulated hydrological outputs due to elevation uncertainty of DEM grid nodes (Wu et al., 2008).

Kenward et al., (2000) tested the sensitivity of the DHSVM (distributed hydrology soil vegetation model) to three DEMs with unique error characteristics of the 7.2 km^2 USDA-ARS WE-38 experimental watershed. The DEMs included a USGS 30 m DEM, a reference 5 m DEM derived from aerial photography, and a 30 m DEM derived

from space-borne interferometric SAR (InSAR). Empirically derived estimates of the mean and standard deviation of vertical error at each DEM resulted in 1.8 m and 4.4 m for the 5 m photogrammetric DEM, 6.7 m and 6.8 m for the 30 m USGS DEM, and 4.0 and 13.5 m for the 30 m InSAR DEM. They found DEM accuracy did influence hydrologic predictions as mean annual predicted runoff volume from the USGS and InSAR DEMs showed relative respective increases of 0.3% and 7.0%, compared to the 5 m reference DEM. The change of simulated annual flow from the InSAR DEM was attributed to an increase in basin area of 3.6%. Hydrographs of the InSAR DEM also showed lower peak runoff, and delayed timing in peak runoff, compared to the reference DEM. The discrepancy in hydrographs was attributed to differences in the topographic index and longer channel lengths across the watershed in the InSAR DEM, caused by a rougher landscape. The increase in landscape roughness and channel lengths was likely caused by the high incidence of noise observed in the InSAR DEM. It was concluded that a DEM with error characteristics similar to the InSAR DEM was not appropriate for simulating hydrographs of individual storm events, but could be used for runoff predictions over longer time periods. Although this analysis demonstrated the influence of hydrologic models to DEMs with different accuracy levels, from different acquisition sources, it does not provide an indication of the level of internal variability expected from a single DEM source.

In a study of a single DEM source, Wu et al., (2008) analyzed the variability in hydrological simulations of TOPMODEL (Beven and Kirkby, 1979) to systematically varied DEM errors in a USGS 30 m DEM. The DEM was perturbed according to elevation errors of four selected RMSE values, including 2.0, 5.0, 10 and 15 m. An auto-correlation model was applied, however, details of the algorithm and parameters were not provided. Model executions without a unique parameter calibration showed that the mean simulated flow at the watershed outlet decreased, and uncertainty in flow increased, as the elevation RMSE increased. When TOPMODEL parameters were uniquely calibrated for each execution, equifinality conditions were observed yielding negligible variation in simulated outputs. The results from Wu et al. (2008) provide only preliminary information on the sensitivity of simulated hydrology to uncertainty in a DEM, given several deficiencies exist; 1) the tested RMSE values were only a general approximation

of the true magnitudes of DEM error, 2) the RMSE values were assumed constant throughout the DEM, whereas the RMSE is likely to vary spatially and be correlated to acquisition or terrain conditions, 3) the analysis was performed with a medium resolution DEM (30 m), 4) the analysis only considered flow .

The objective of this study is to determine the sensitivity of SWAT simulated flow and sediment outputs to a fine scale (1 m) LiDAR derived DEM. The analysis is unique within available literature because the DEM elevation uncertainty is obtained through a rigorous deterministic error propagation algorithm of the LiDAR sensor measurement errors. This provides a realistic and spatially variable model of DEM uncertainty and a more accurate approximation of the uncertainty in simulated hydrologic outputs. Additionally, the analysis considers the sensitivity of both flow and sediment yield, in the presence of detailed agricultural inputs.

The uncertainty results of SWAT model outputs are intended to provide enhanced decision making capabilities when selecting an appropriate source of DEM information for parameterisation of a SWAT model. Knowledge of the magnitude of uncertainty of simulated hydrologic outputs allows for robust risk assessments of management decisions. Consequently, if the uncertainty in simulated flow and sediment outputs from SWAT introduced through LIDAR DEMs is found to be too large, accommodations can be made to reduce measurement errors prior to data acquisition. If a LIDAR DEM shows a level of accuracy higher than required, a lower accuracy, more cost-effective DEM can be obtained without consequence.

5.2 Study site and methods

5.2.1 Thomas Brook watershed

The analysis was conducted at the Thomas Brook watershed (Figure 4.1). Details of the site description relevant to SWAT model parameterisation can be found in Section 4.2.1.

5.2.2 The SWAT

The required background information on the algorithmic processes of the SWAT model can be found in Section 4.1.2.

5.2.3 Generation of DEM realizations

Multiple DEM realizations were determined through the error propagation techniques of LiDAR measurement errors outlined in Section 3.2.2. DEMs were created from raw LiDAR coordinates using the TIN interpolation method, described in Section 2.3.2.1. A limit of 25 DEM realizations were created because additional simulations did not introduce a change to uncertainty estimates of more than 5%, rendering further simulations unnecessary.

5.2.3 Generation of SWAT model realizations

A unique SWAT model was determined from each of the 25 DEM realizations. The parameterisation of the SWAT models followed the same procedure outlined in Section 4.2.3. Consequently, the same calibrated parameters used in the SWAT models of Chapter 4 were also used in all SWAT models developed for this analysis. It should be noted that variability in channel paths between DEM realizations caused minor deviations in the spatial location of sub-basin outlets. The location of subbasin outlets between DEM realizations were maintained as near as possible to the outlets selected in the first simulated DEM realization to eliminate the introduction of additional variability in the subbasin boundaries and channel characteristics (channel slope and channel length).

5.2.4 Assessment of simulated flow and sediment uncertainty

The mean ($\bar{x}_t$), standard deviation (s_t) and coefficient of variation (CV) for all SWAT simulations (N) were determined for each month (t), for variables of interest (x) as follows:

$$\bar{x}_t = \frac{1}{N}\sum_{1}^{N} x_{tN} \tag{5.1}$$

$$s_t = \frac{1}{N}\sum_{1}^{N} (\bar{x}_t - x_{tN})^2 \tag{5.2}$$

$$CV_t = \frac{s_t}{\bar{x}_t} \tag{5.3}$$

Final values of *CV* were used as the descriptor of uncertainty, and were multiplied by 100 for reporting as a percentage. Results were generated at five locations throughout the Thomas Brook watershed (Figure 5.1) to demonstrate the relationship between the drainage area and uncertainty. The locations selected for analysis were coincident with several pre-existing sampling station sites, and station 5 is located at the selected watershed outlet.

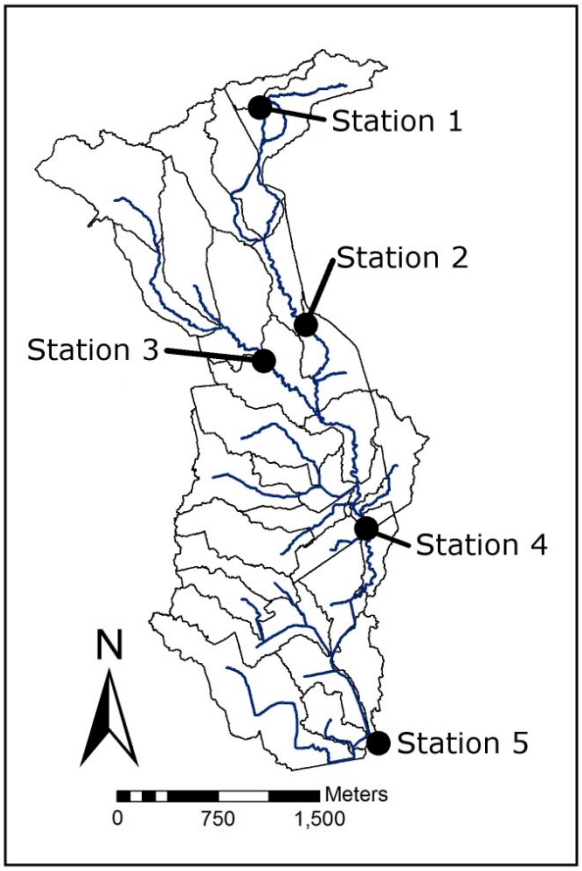

Figure 5.1 Thomas Brook watershed showing the location of stations where results were generated

5.3 Hypothesis

It is hypothesized that the flow rate simulated from the SWAT will show negligible variability across SWAT model realizations. This result is inferred because flow has shown a previous insensitivity to changes in terrain slope or to stream characteristics at Thomas Brook, following results given in section 4.3.3. An exception is expected if a DEM realization leads to variability in drainage area, which will result in an increase in the variability in flow results. Sediment outputs are expected to show higher variability compared to flow outputs due to a greater reliance on topographic conditions and their associated variation, as detailed in equations 4.1 through 4.7. The topographic variability will also modify HRU distributions creating higher variability in sediment results.

5.4 Results

The results for flow are presented first, followed by sediment. Results in the flow and sediment sections are initially focused at station 5, since it is the location with the greatest implication to management decisions. Results are then expanded to include intermediate stations throughout the watershed.

5.4.1 Flow

At station 5, monthly flow $\bar{x}_t$ values ranged between 0.006 m^3/s and 0.46 m^3/s during the five year simulation period. The associated s_t lead to flow *CV*s that were less than 5% in 46 of the 60 simulated months (Figure 5.2A). The months which resulted in *CV*s above 5% commonly showed low $\bar{x}_t$ values, where even minor s_t lead to high *CV*s (Figure 5.2B). The existence of high *CV*s in only low flow months indicates an overall insensitivity of simulated flow results to LiDAR measurement errors during high flow periods. The overall low sensitivity to flow was expected, as it has been shown in Section 4.3.3 that sensitivity to flow within the SWAT to grid cell based DEM uncertainty is

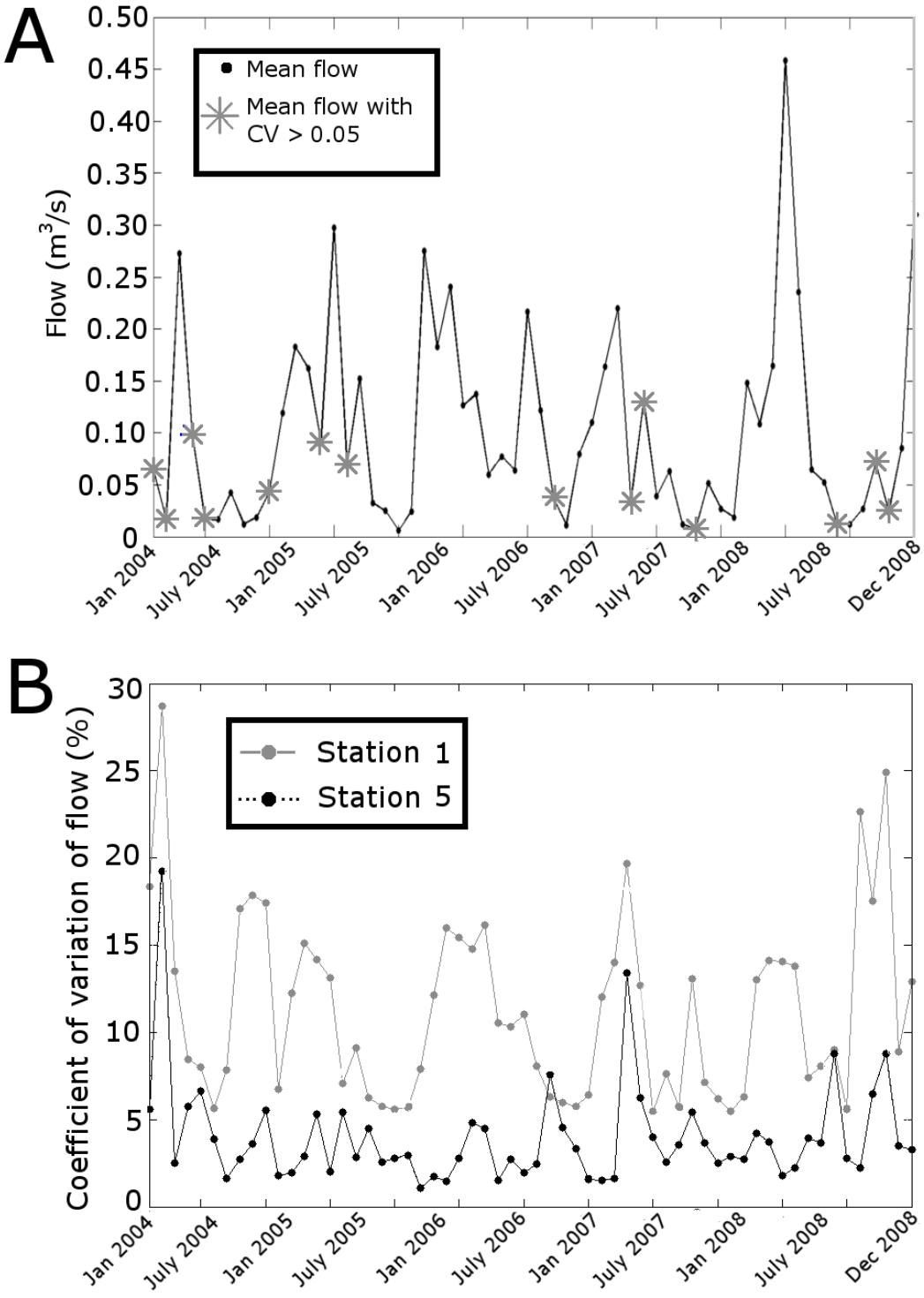

Figure 5.2 **A) Mean flow at station 5, highlighting months resulting in CV < 0.05 B) Monthly CVs at station 1 and station 5.**

largely associated with changes in area. The variability in drainage area, shown in Table 5.1, indicates a minor sensitivity to LiDAR measurement errors at the selected outlet, similar to results in Section 3.4.5.

Flow variability results at station 1 show *CVs* at the selected watershed outlet (Table 5.1) which are all above the 5% level, a maximum monthly *CV* of nearly 29%, and a mean of all monthly *CV*s of 14.5% (Figure 5.2B, Table 5.1). Station 2, which represents a drained area nearly 24 times larger than station 1, shows a reduction in the mean *CV* of flow to 4.4% (Table 5.1). The reduction in the mean monthly flow *CV* at station 2, relative to station 1, follows an increase in the total drained area and reduction in area *CV* (Table 5.1). Station 3 drains an area 15% larger than the area drained by station 2, and resulted in the smallest observed area *CV* and the lowest mean monthly flow *CV*. The lowest area *CV* occurred at station 3 because the drainage area consists primarily of high slope terrain. This follows results in Section 3.4.5, which demonstrated low variability exists in LiDAR DEM derived drainage areas in high slope regions. This suggests a variation in SWAT simulated flow will exist due to LiDAR measurement error if there is a corresponding uncertainty in the drainage area, which typically occurs in low slope regions.

To place the sensitivity of flow and sediment uncertainty due to a LiDAR derived DEM in a broader context, comparisons against previous analyses of hydrological model uncertainty can be investigated. Previous uncertainty analyses in SWAT has typically focused on the uncertainty of model parameters, for example, Sexton et al., (2011) found a mean flow *CV* of 15.2% through a deterministic error propagation approach of parameter uncertainty. Using Monte Carlo simulations, with a latin hypercube sampling routine, Sohrabi et al., (2003) determined a flow *CV* of 28.6% due to parameter uncertainty. These results indicate that parameter uncertainty is potentially a higher source of variability in simulated flow than the DEM. Cho et al., (2009) analyzed the sensitivity of SWAT flow due to raingauge distribution, another spatial input layer. In a 334 km^2 watershed, they found different scenarios of spatial raingauge distribution and subbasin size lead to average *CVs* of 5.2%, 4.5%, and 2.3% at three different stations. The lowest flow *CV* resulted from the delineation with the largest number of subasins. In an analysis of the uncertainty in the landuse classification, another spatial input, using the

Kinematic Runoff and Erosion Model (KINEROS2) (Smith et al., 1995; Goodrich et al., 2002), Miller et al., (2007) found near negligible variability (< 1%) in runoff predictions during five and ten year storm events. Comparison of the sensitivity of SWAT hydrological results due to LiDAR measurement errors with those of Cho et al., (2009) and Miller et al., (2007), indicate that the DEM uncertainty may be one of the largest contributors to flow variability of spatial inputs.

Table 5.1 Area statistics and simulated flow and sediment CV

	Mean drained area (ha)	Area drained *CV* (%)	Flow *CV* (%)	Sediment *CV* (%)
Station 1	5.3	14.5	11.3	11.3
Station 2	117.5	4.4	6.5	13.5
Station 3	135.2	0.32	4.0	16.8
Station 4	491.2	0.70	4.1	9.6
Station 5	692.5	0.73	4.0	5.8

5.4.2 Sediment

At station 5, the resulting sediment $\bar{x}_t$ ranged between 0 and 70 tons over the five year simulation period (Figure 5.3A). The sediment s_t ranged between 0 and 2.5 tons, and 29 of 60 months resulted in sediment *CV*s below 5%. Overall, the resulting sediment *CV*s ranged between 2.5% and 28% (Figure 5.2B), with the highest monthly sediment *CV* of 28% occurring in April 2007. Similar to the flow results, the highest monthly sediment *CV*s occurred during months which also had low values of sediment $\bar{x}_t$. Overall, average sediment *CV*s were higher than the average flow *CV*s at each station, indicating a higher sensitivity of sediment to LiDAR measurement errors than flow. The largest range of sediment results at station 5 from all DEM simulations was 8.7 t, occurring in November of 2005. November 2005 resulted in a relatively high sediment $\bar{x}$ of 63.2 t, yielding a ratio of the range in sediment output to mean sediment output of 0.14.

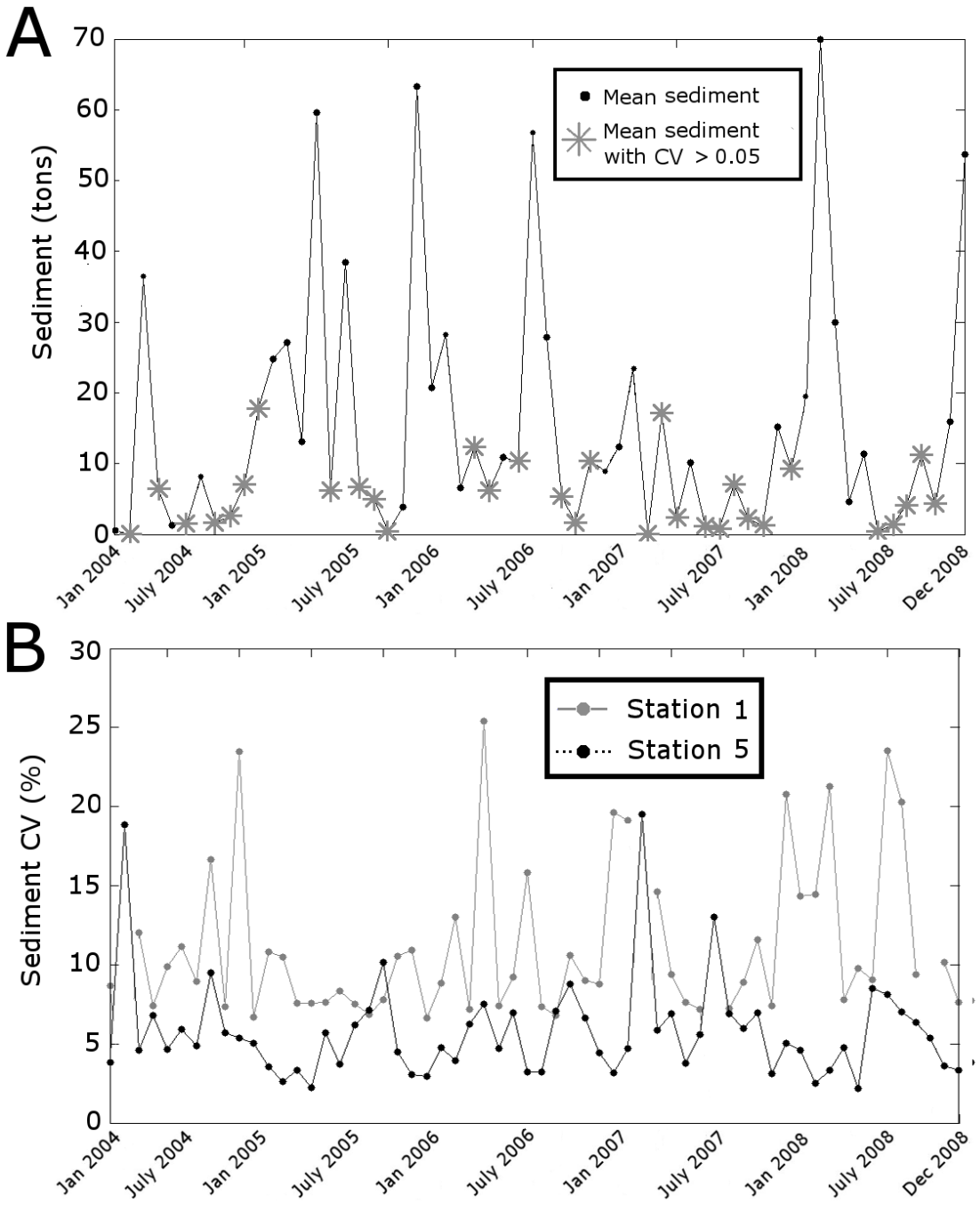

Figure 5.3 **A) Mean sediment at station 5 with months resulting in *CV*< 0.05 identified, B) Monthly *CV*s at station 1 and station 5. Discontinuities in the results for station 1 represent months in which all simulations showed zero sediment output.**

Previously documented variability in simulated sediment results due to parameter uncertainty has shown a higher sensitivity than DEM uncertainty. For example, Sexton et al. (2011) found a mean sediment *CV* of 28.3% in a 340 ha watershed through a deterministic error propagation approach. Sohrabi et al., (2003) implemented Monte Carlo error propagation with latin hypercube sampling of model parameters, which resulted in a sediment *CV* of 35.8%. This indicates that in order to improve simulated sediment accuracy, greater effort should be placed on reducing parameter uncertainty than LiDAR derived DEM uncertainty. However, if parameter accuracy is successfully maximised through well-known statistical calibration routines, DEM uncertainty may play a larger role in the overall uncertainty of model outputs.

Contrary to the *CV*s of the flow results, the sediment *CV*s did not show a relationship with area variability, as shown in the results of Table 5.2. The largest mean sediment *CV* occurred at station 3, which also resulted in the lowest variability in drainage area. The high level of variability in simulated sediment at station 3 can be sourced to the creation process of HRUs, and the development of the slope classes. The given hypothesis (Section 5.3) infers that the variability in simulated sediment export results from variability of the slope class areas, which would change the area of HRUs, and subsequently their associated landscape sediment production. However, analysis of the total area for each slope class within the watershed reveals only minor variability in the area of each slope class. The area *CV*s for the 0-2°, 2-4°, 4-8°, 8-15°, and 15-90° classes were only 0.09%, 0.07%, 0.05%, 0.08% and 0.05% respectively. The low *CV*s of the individual slope class areas indicate an associated low variability in landscape sediment production. However, due to the algorithmic process of HRU creation, variability in the area of HRUs cannot be directly related to the variability of slope class area. The low variability in the area of slope class distributions retains potential for introducing variability through the HRU creation algorithm which aggregates HRUs during model pre-processing.

Recall from Section 4.2.3 that the assignment of a unique land use, soil and slope required to form an HRU was constrained to a minimum threshold area of 1 ha. If an HRU does not meet the 1 ha limit, it is amalgamated with an existing HRU of the same land use. All HRUs below the 1 ha limit with common land use will be aggregated into a

final, representative HRU. The resulting representative HRU will be defined with a land use, soil and slope definition of the HRU with the largest area. Under the correct conditions, a minor variability in the area of a slope class can shift the representative HRU definition between different land use, soil and slope configurations. If there are several HRUs with common landuse below the 1 ha threshold, the shift in HRU distribution could involve a sizeable proportion of the subbasin area. If the competing HRUs have different soil, and slope conditions, a large difference in simulated sediment export will occur. A representative example of this phenomenon is provided for simulation 3 and simulation 9, of subbasin 9 in Table 5.2, which identifies all HRUs for the timothy grass with manure fertilization (TMAN) agricultural rotation landuse.

Table 5.2 HRU distribution for subbasin 9 in simulation 3 and simulation 9. LU designates HRU landuse, Cbld represents Cumberland soils, Kent represents Kentville soils.

Simulation 3		Simulation 9	
HRUs in Sub-basin 9 LU / Soil / Slope	HRU Area	HRUs in Sub-basin 9 LU / Soil / Slope	HRU Area
TMAN/Cbld/0-2	0.0406	TMAN/Cbld/0-2	0.1912
TMAN/Cbld/2-4	0.1246	TMAN/Cbld/2-4	0.1537
TMAN/Cbld/4-8	0.4281	TMAN/Cbld/4-8	**0.4681 / 1.82**†
TMAN/Cbld/8-15	0.1764	TMAN/Cbld/8-15	0.0443
TMAN/Cbld/15-90	0.0019	TMAN/Cbld/15-90	0.0013
TMAN/Kent/0-2	0.0042	TMAN/Kent/0-2	0.0055
TMAN/Kent/2-4	0.0251	TMAN/Kent/2-4	0.0274
TMAN/Kent/4-8	0.2451	TMAN/Kent/4-8	0.2484
TMAN/Kent/8-15	**0.4695 / 1.71**†	TMAN/Kent/8-15	0.4659
TMAN/Kent/15-90	0.0839	TMAN/Kent/15-90	0.0832

†Indicates both the area of the representative HRU before HRU amalgamation and after HRU amalgamation

The representative HRU with the largest area in simulation 3 was the TMAN landuse, Kentville soil group and slope class of 8-15° (TMAN/Kent/8-15° in Table 5.2). The reaming HRUs in simulation 3, which contained the TMAN landuse class, and were below 1 ha, were aggregated into the representative HRU, resulting in a total area of 1.71 ha. The variations to the DEM implemented in simulation 9 caused a slight increase in TMAN landuse, Cumberland soil and 4-8° slope class (TMAN/Cbld/4-8° in Table 5.2). Subsequently, in simulation 9 the TMAN/Cbld/4-8° HRU became the representative HRU with a total area of 1.82 ha. The Kentville and Cumberland soil types have different soil parameters, which serve to generate different estimates of simulated erosion, as Kentville soils have a higher propensity for erosion. The different slope classes also introduce variation to the estimates of simulated erosion, as the higher slope class results in an increase in simulated erosion through the *MUSLE* equation (4.1).

As the example in Table 5.2 displays, the thresholding behavior of representative HRU leads to a substantial impact on the simulated sediment outputs, despite only a minor variability in the area of the slope classes. Due to the resulting differences in the representative HRU of the TMAN landuse, and several other landuses within Subbasin 9, the range of sediment yield across all DEM simulations within the subbasin reached 0.75 tons. The mean sediment output of subbasin 9 is 1.70 tons, leading to a range that is 44% of the mean total. SWAT users should be aware of this thresholding behavior and the potential impacts introduced by the DEM uncertainty. The magnitude of the simulated sediment differences will be related to the area threshold selected during HRU creation, as well as the area distribution of the different landuses and soil classes within the subbasin. Minimal uncertainty will be introduced if all HRU combinations are well above the HRU creation area limit. Uncertainty introduced by changes in the representative HRU will be more prevalent in watersheds with a large diversity of land uses. Investigation into the potential for uncertainty introduced through amalgamation into a single representative HRU can be performed by creating HRUs with no area limit and analyzing the associated distribution of HRUs areas. If multiple HRUs with common land use have similar area, the potential exists for changes to the representative HRU.

5.5 Conclusion

Uncertainty in watershed simulation models is a critical consideration for developing sound and defensible environmental management decisions. A DEM plays a crucial role in parameterising semi-distributed hydrological models, however the impacts of uncertainty in the elevation of individual LiDAR derived DEM grid nodes are not well understood in terms of simulated hydrological outputs. This analysis characterizes the sensitivity of the SWAT watershed model to DEM grid node elevation uncertainty due to LiDAR measurement errors. This allows users of watershed simulation models to gauge whether the impact of the uncertainty introduced by a LiDAR derived DEM is acceptable for their modeling needs. If necessary, appropriate accommodations to generate a DEM with increased accuracy can be made, or the selection of a lower accuracy, more cost-effective DEM can be investigated.

Total watershed area showed minor variability to LiDAR measurement errors, which also lead to a negligible sensitivity in water yield predicted from the SWAT. However, small, predominately flat areas could generate unacceptable levels of flow uncertainty if they are associated with variability in drainage area. Sediment uncertainty was related to alterations in the configuration of HRUs due to changes invoked in the slope class distribution and representative HRU definitions. Sediment results showed high levels of uncertainty, which could warrant consideration when interpreting results from the SWAT. Maximum observed ranges in simulated monthly sediment export between all simulations reached 14% of the mean monthly sediment results. This indicates that planning strategies developed from SWAT simulation results, parameterized from LiDAR DEMs, must consider this level of potential variation.

Previous work by Wu et al., (2008), using TOPMODEL, has identified that unique hydrologic model calibrations using individual DEMs in error simulations will show equifinality conditions. Therefore, a unique parameterisation for each DEM realization could potentially absorb any uncertainty introduced by the DEM. In this analysis, flow showed only minor sensitivity to the DEM uncertainty at the selected outlet, indicating the parameter calibration would not be largely affected by the DEM uncertainty. However, if flow parameters are calibrated at stations which are draining primarily low relief areas, such as station 1, more considerable uncertainty could be

introduced to model parameters. Therefore, attempting a multi-site calibration (such as in Zhang et al., 2008) for the SWAT Thomas Brook model could be problematic if station 1, located in a low relief subbasin, is included. The increase of uncertainty at this station may cause inter-station inconsistencies between calibrated parameters, causing difficulties in convergence of statistical assessment criteria. It is currently unknown whether the sediment parameters in SWAT would also display equifinality conditions if each DEM realization was uniquely calibrated. If equifinality conditions are reached, the level of introduced uncertainty to sediment parameters would be important to characterize for comparison with previously documented uncertainties in parameter uncertainty. If the uncertainty introduced to sediment parameters allowed an unrealistic range of a parameter values, the DEM uncertainty should be a concern. This is similarly identified in Section 4.3.4.3, which showed that the uncertainty introduced by grid cell size of a 1 m LIDAR DEM reduced the $USLE_p$ to an unrealistically low value for the conditions in Thomas Brook. Therefore, investigation of the uncertainty introduced to sediment parameter calibration is a valuable direction for a continuation of this analysis.

Further work should also be considered in DEMs with different grid cell sizes and terrain conditions. It is possible that the topographic derivatives in coarser resolution DEMs will be less influenced by elevation errors, as shown in Erksine and Green (2007). Therefore, it is hypothesized a similar reduction of simulated sediment uncertainty may be observed in models parameterised from coarse resolution DEMs. It has also been shown in Section 3.4.3 that high resolution DEMs are not an appropriate choice for defining the hillslope scale within a SWAT model due to spatial scaling of the *MUSLE* relationships. The potential reduction in sensitivity of SWAT results to LiDAR measurement uncertainty in a coarse resolution DEM could also provide evidence that high resolution DEMs are not the optimum choice for SWAT parameterisation. Therefore, comparison of multiple resolution DEMs also presents an avenue for future research, which would provide additional guidance for the optimum selection of a DEM resolution for SWAT model parameterisation. Additional case study sites with different topographic conditions could also serve as a valuable future research direction. Watersheds with predominately low slope conditions are hypothesized to show a high sensitivity of flow to DEM uncertainty, and minor sensitivity to sediment, contrasting

results at Thomas Brook. This result is inferred because the low relief area would tend to produce higher variability in drained area, which is the key variable that affects the variability in flow results. Since slopes would be predominately low, only minor levels of landscape erosion and associate variability would likely be observed.

CHAPTER 6 CONCLUSION

6.1 Main findings and novel contributions

The main findings of this work, and their novel contribution to the geomatics, terrain analysis and hydrological communities can be summarized as follows:

- The influence of fine to medium (1 - 50 m) DEM resolutions to watershed attributes in distinct topographic landscapes had not been previously assessed in a controlled manner. Fine spatial resolution DEMs displayed scale dependent behavior at Thomas Brook, related to the scale of local anthropogenic modifications. Scale dependent relationships also existed in a predominately alpine environment, although their effects to delineated watershed area were minor. This contrasted results at Scotty Creek, a primarily flat landscape, where the effects caused by elevation uncertainty overcame scale dependent behavior. Therefore, uncertainty in DEM grid nodes due to spatial resolution or interpolation method should be considered in the context of local changes in elevation. If uncertainty levels are higher than changes in local DEM grid node elevations, uncertainty in watershed area, and subsequently modeled flow, can be introduced.
- Scaling laws, which permit the transfer of stream length between DEM resolutions, have not been previously established. Due to the complications of implementing a constant area threshold within the ArcHydro framework, it was determined that entire drainage networks cannot be scaled between DEM resolutions. However, it was shown that if the spatial location of a single stream channel is consistent, a fractal based scaling law allows the transfer of stream channel lengths between DEM resolutions.
- Accuracy assessments of stream lengths derived from LiDAR DEMs within the literature have been rare, leaving modelers without guidance for selecting a DEM resolution for modeling stream length. An accuracy assessment using high accuracy differential GPS measurements at Thomas Brook watershed, containing a 3 m wide stream, showed the best available tested DEM resolution was 1 m.

- Previous studies analyzing the sensitivity of watershed attributes to LiDAR DEMs have not considered a broad cross-section of interpolation routines. It was found that the interpolation method of raw LiDAR observations to DEM grid nodes has little effect on the delineation of watershed boundaries or stream networks; however, the MA method was an exception, which tended to under-predict stream lengths at high resolutions.
- The spatial pattern of LiDAR derived DEM, slope, and aspect uncertainty due to LiDAR measurement errors has not been previously documented. It was found that LiDAR-derived DEM uncertainty and slope uncertainty will increase with an increase in the incidence angle of the laser pulse, with high slope regions initiating a more rapid increase. LiDAR-derived aspect uncertainty will decrease with an increase in terrain slope according to a power function.
- The sensitivity of the delineation of watershed boundaries and stream network to LiDAR measurement uncertainty has not been previously reported. It was found that watershed area experienced minor variability due to LIDAR measurement errors, unless the terrain slope was predominately low. Stream network length experiences minor variability to LIDAR measurement errors on the spatial scale of the Thomas Brook watershed, however, the variability of stream network length to LiDAR measurement errors will increase as the drainage area decreases.
- Changes in simulated SWAT outputs due to DEM spatial resolution have been previously obtained with watershed parameters obtained from a single DEM resolution. Experiments here were conducted to separate individual DEM functions and it was determined that

    i. Flow derived from SWAT in a small scale watershed does not exhibit sensitivity to a modification of DEM resolution from 1 to 50 m unless the change in resolution initiates a change in area.
    ii. Landscape sediment yield derived from SWAT in a small (689 ha), primarily agricultural watershed, will increase as DEM resolution increases. Due to this, the calibrated sediment parameters of a SWAT watershed model may become unrealistic at fine DEM resolutions.

iii. Channel processes in SWAT are sensitive to changes in DEM resolution due to changes in stream length and stream slope. Peak flow rates tend to decrease in fine resolution DEMs due to an associate increase in stream length and decrease of stream slope, causing an increase in channel deposition, or reduction of channel erosion.

iv. A SWAT model of the Thomas Brook watershed benefits from a multi-scale DEM parameterisation, in which the stream network and watershed boundaries are determined from a high resolution DEM, and the hill slope scale is determined from a lower resolution DEM.

- The sensitivity of SWAT flow and sediment outputs to LiDAR measurement errors has not been previously quantified. Flow derived from SWAT shows minor sensitivity to LiDAR measurement uncertainty. However, the flow sensitivity will increase in regions where the DEM uncertainty causes variability in the drainage area. Sediment derived from SWAT shows a higher sensitivity to LiDAR measurement errors than flow. The sediment uncertainty can be traced to the creation of different representative HRU combinations. Different representative HRUs are caused by the varied slope class areas and the high density of agricultural landuses, which are near the limit of minimum HRU areas in the Thomas Brook watershed.

6.2 Directions for future work

- The fractal dimension of stream networks should be researched in relation to DEM resolution and stream geomorphology. Theoretically, a stream will increase its fractal dimension with an increase in complexity. An increase in stream complexity can be introduced through an increase in stream sinuosity. Therefore, as stream sinuosity increases due to geo-morphological constraints, an increase in the fractal dimension is hypothesized to follow. This indicates that a single global value of fractal dimension may not be appropriate for scaling stream lengths in different landscapes.

- Although the stream length of entire drainage networks could not be scaled due to complications associated with stream initiation threshold, each site did appear to show some unique systematic behavior between stream length and DEM resolution. Investigation into a relationship between landscape complexity, which can be described with a fractal dimension between 2 and 3, and changes in the total length of the drainage network could be an avenue to better understand this relationship. Knowledge of a more robust scaling law would enable modification of stream network lengths that is not restricted to single stream channels, and may provide additional insight into the selection of an optimum DEM resolution.

- Additional research is required on methods or procedures that enable consistent area and stream length results in environments with subtle changes in relief, such as Scotty Creek. This could involve improvements to LiDAR raw point filtering routines, which would increase the fidelity of observations in these environments.

- Investigation into the sensitivity of additional hydrological models to LiDAR measurement errors is required. The results obtained in Chapter 3 provide a valuable basis for developing hypotheses of the sensitivity of hydrological models with terrain inputs to LiDAR measurement error. Analysis should focus on distributed or semi-distributed models with a high reliance on topographic information. As uncertainty appears to have the largest effect in regions with minor changes in relief, flood inundation models would serve as an ideal candidate for additional testing. The current predictions of sea level rise due to climate change indicate there is an urgent need to study this application area due to immediate economic and environmental interests. Additionally, LiDAR is a data source used in FEMA's federal flood insurance risk mapping program. A vast amount of public LiDAR information has been collected for this purpose in the continental United States making existing data sets readily available for testing.

- Research on the implications of DEM resolution in the domain of 1 to 50 m is required with the SWAT model on larger scale watersheds. In particular, watersheds with travel times longer than the minimum daily time step are required. It is hypothesized that flow magnitude and timing would experience a greater sensitivity in a larger watershed system due to DEM grid cell size induced changes in stream length. Testing of this nature should ensure that all DEM resolutions result in stream lengths with modeled travel times greater than a single day. Therefore, during experimental design, the travel time of the lowest resolution DEM should be verified first.

- Access to daily calibration information would allow for analysis of the sensitivity of SWAT outputs to DEM uncertainty on a daily time step. The reduction from a monthly to daily time step would enable better analysis of the response of the system to DEM resolution during individual storm events.

- The uncertainty introduced to SWAT outputs from the DEM needs to be considered in terms of equifinality conditions and parameter uncertainty. A quantification of the uncertainty introduced by the DEM to model parameters would aid in placing the DEM influence into a broader context of hydrological uncertainty introduced from other sources. The newly developed automated calibration routine for SWAT, SWAT-CUP, produces parameter uncertainty estimates during the calibration process. Uncertainty introduced by the DEM could be determined though unique calibrations of DEMs, with systematically varied grid cell sizes and randomly varied elevations according to LiDAR measurement errors. Uncertainty introduced by the DEM could be compared against the typical levels of uncertainty obtained during calibration to assess the overall relevance of the DEM uncertainty. If minor significance is observed, it is an indication that model improvement should focus elsewhere. If uncertainty introduced by the DEM is significant, it suggests efforts would be placed on eliminating or reducing the uncertainty introduced by the DEM.

REFERENCES

Aguilar, F.J., Agũera, F., Aguilar, M.A., & Carvajal, F. (2005). Effects of terrain morphology, sampling density, and interpolation methods on grid DEM accuracy. *Photogrammetric Engineering and Remote Sensing,* 71(7): 805-816.

Aguilar, F.J., Mills, J.P., Delgado, J., Aguilar, M.A., Negreiros, J.G., & Perez, J.L. (2010). Modelling vertical error in LiDAR derived digital elevation models. *ISPRS Journal of Photogrammetry and Remote Sensing,* 65 (1): 103-110. DOI: 10.1016/j.isprsjprs.2009.09.003.

Ahmad, H.M., Sinclair, A., Jamieson, R., Madani, A., Hebb, D., Havard, P., & Yiridoe, E.K., (2011). Modeling sediment and nitrogen export from a rural watershed in Eastern Canada using the Soil and Water Assessment Tool. *Journal of Environmental Quality*, 40(4):1182-1194.

APHA, (2000). Standard Methods for Examination of Water and Wastewater, 21st ed., APHA, Washington, DC.

Applanix, (2013). POSPac Mobile Mapping Suite. Accessed on-line Feb. 2013 at http://www.applanix.com/products/land/pospac-mms.html, Applanix Corp.

Arnold, J.G., Williams, J.R., & Maidment, D.R., (1995). Continuous time water and sediment routing model for large basins. *Journal of Hydraulic Engineering*, 121(2):171-183.

Arnold, J.G., Srinivasan, R., Muttiah, R.S., & Williams, J.R. (1998). Large-area hydrologic modeling and assessment: Part I. Model development. *Journal of American Water Resources Association,* 34(1):73-89.

Atkinson, P.M. & Tate, N.J. (2000). Spatial scale problems and geostatistical solutions: a review. *Professional Geographer*, 52(4): 607-623.

Ayesworth, J.M., & Kettles, I.M. (2000). Distribution of fen and bog in the Mackenzie Valley, 60° N-60° N. Natural Resources Canada. *Geological Survey of Canada Bulletin*, Government of Canada publication, 547.

Band, L.E. (1986). Topographic partition of watersheds with digital elevation models. *Water Resources Research,* 22 (1) :15-24. DOI:10.1029/WR022i001p00015.

Barber, C.P., & Shortridge, A. (2005). LiDAR Elevation Data for Surface Hydrologic Modeling: Resolution and Representation Issues. *Cartography and Geographic Information Science,* 32 (4): 401 – 410. DOI: 10.1559/152304005775194692.

Bartier, P.M., & Keller, C.P. (1996). Multivariate interpolation to incorporate thematic surface data using inverse distance weighting (IDW). *Computers and Geosciences,* 22(7): 795-799. DOI:10.1016/0098-3004(96)00021-0.

Bater, C.W., & Coops, N.C. (2009). Evaluating error associated with LiDAR derived DEM interpolation. *Computers and Geosciences,* 35(2):289-300. DOI: 10.1016/j.cageo.2008.09.001.

Beeson, P.C., Sadeghi, A.M., Lang, W.M., & Tomer, M.D. (2013). Sediment Delivery Estimates in Water Quality Models Altered by Resolution and Source of Topographic Data. *Journal of Environmental Quality*, (in press).

Beven, K.J. (1997). TOPMODEL: a critique, *Hydrological Processes*, 11(9):1069-1085.

Beven, K.J. (2001). Down to Basics: Runoff processes and the modeling process, *Rainfall-runoff modeling : The primer*, John Wiley & Sons Ltd, West Sussex, England.

Beven, K.J., & Binley, A. (1992). The future of distributed models, model calibration and uncertainty prediction, *Hydrological Processes*, 6 (3): 279–298.

Beven, K J & Kirkby, M.J. (1979). A physically based variable contributing area model of basin hydrology, *Hydrological Sciences Journal*, 24(1):43-69.

Bosch, D. D., Sheridan, J. M., Batten, H. L., & Arnold, J. G. (2004). Evaluation of the SWAT model on a coastal plain agricultural watershed. *Transactions of the ASAE*, 47(5), 1493-1506.

Bowen, Z.H. & Waltermire, R.G. (2002). Evaluation of light detection and ranging (LiDAR) for measuring river corridor topography. *Journal of the American Water Resources Association,* 38(1): 33-41. DOI: 10.1111/j.1752-1688.2002.tb01532.x.

Brisbois, M.C., Jamieson, R., Gordon, R., Stratton, G., & Madani, A. (2008). Stream ecosystem health in rural mixed land-use watersheds. *Journal of Environmental Engineering Science,*7(5): 439-452. DOI: 10.1139/S08-016.

Canadian General Standards Board (1991). Liquid Flow Measurements in Open Channels – Velocity area Methods, CAN/CGSB-157.6-M/ISO 1088, National Standard of Canada, Ottawa, ON.

Cann, D., MacDougall, J., & Hilchey, J. (1965). Soil survey of Kings County, Nova Scotia, Report No. 15. Nova Scotia Soil Survey.

Carey and Associates, (2009). The Global Market for Airborne LiDAR Systems and Services, URL: http://caryandassociates.com/about/releases/pr16.html, Carey and Associates, Longmont, Colorado(last date accessed: 19 November 2012).

Casas, A., Lane, S.N., Yu, D., & Benito, G. (2010). A method for parameterising roughness and topographic sub-grid scale effects in hydraulic modelling from LiDAR data. *Hydrology and Earth System Sciences*, 14(8): 1567-1579.

Chang, K. & Tsai, B. (1991). The effect of DEM resolution on slope and aspect mapping. *Cartography and Geographic Information Science,* 18(1): 69-77. DOI: 10.1559/152304091783805626.

Chaplot, V. (2005). Impact of DEM mesh size and soil map scale on SWAT runoff, sediment and NO_3-N loads predictions, *Journal of Hydrology*, 312:207-222.

Chaplot, V., Darboux, F., Bourennane, H., Leguédois, S., Silvera, N., & Phachomphon, K.(2006). Accuracy of interpolation techniques for the derivation of digital elevation models in relation to landform types and data density. *Geomorphology,* 77 (1-2): 126-141. DOI: 10.1016/j.geomorph.2005.12.010.

Chaubey, I., Cotter, A.S., Costello, T.A., & Soerens, T.S. (2005). Effect of data resolution on SWAT output uncertainty. *Hydrological Processes,* 19 (3):621- 628. DOI: 10.1002/hyp.5607.

Chilès, J. & Delfiner, P. (1999). Geostatistics Modeling Spatial Uncertainty. John Wiley and Sons, Inc. ISBN 0-471-08315-1.

Cho, J., D. Bosch, R. Lowrance, T. Strickland & G. Vellidis. (2009). Effect of spatial distribution of rainfall on temporal and spatial uncertainty of SWAT output. *Transactions of the ASABE*, 52(5): 1545-1555

Cho, S.M., & Lee, M.W. (2001). Sensitivity considerations when modeling hydrologic processes with digital elevation models. *Journal of the American Water Resources Association*, 37(4):931-934.

Collins, S.H., & Moon, G.C. (1981). Algorithms for dense digital terrain models. *Photogrammetric Engineering and Remote Sensing,* 47(1): 71-76.

Costa-Cabral, M.C., & Burges, S.J. (1994). Digital elevation model networks (DEMON): A model of flow over hillslopes for computation of contributing and dispersal areas. *Water Resources Research,* 30(6): 1681-1692. DOI:10.1029/93WR03512.

Cotter, A.S., Chaubey, I., Costello, T.A., Soerens, T.S., & Nelson, M.A. (2003). Water Quality Model Output Uncertainty as Affected by Spatial Resolution of Input Data. *Journal of the American Water Resources Association (JAWRA)*, 39(4):977-986, DOI: 10.1111/j.1752-1688.2003.tb04420.x.

Collins, S.H. & Moon, G.C. (1981). Algorithms for dense digital terrain models. *Photogrammetric Engineering and Remote Sensing,* 47(1): 71-76.

Creed, I.F. & Sass, G.Z. (2011). Digital terrain analysis approaches for tracking hydrological and biogeochemical pathways and processes in forested landscapes, in *Forest Hydrology and Biogeochemistry: Synthesis of Past Research and Future Directions* edited by Levia, D.F., pp. 69-98, Springer Science.

Cressie, N. (1993). Statistics for Spatial Data Revised Edition. John Wiley and Sons Inc. ISBN 0-471-00255-0.

Csayni, N., & Toth, C.K. (2007). Improvement of LiDAR data accuracy using LiDAR specific ground targets. *Photogrammetric Engineering and Remote Sensing*, 73(4):385-396

Deng, Y., Wilson, J.P., & Bauer, B.O. (2007). DEM resolution dependencies on terrain attributes across a landscape. *International journal of Geographical Information Science*, 21 (2): 187-213 DOI:10.1080/13658810600894364.

Dietrich, W. E., Wilson, C. J., Montgomery, D. R., & McKean, J. (1993). Analysis of erosion thresholds, channel networks, and landscape morphology using a digital terrain model. *The Journal of Geology*, 259-278.

Di Luzio, M.D., Srinivasan, R., & Arnold, J.G. (2002). Integration of watershed tools and SWAT modeling into BASINS, *Journal of the American Water Resources Association*, 32(3): 499- 509.

Di Luzio, M., Arnold, J.G., & Srinivasan, R. (2005). Effect of GIS data quality on small watershed stream flow and sediment simulations. *Hydrological Processes,* 19(3): 629-650. DOI: 10.1002/hyp.5612.

Dixon, B., & Earls, J. (2009). Resample or not?! Effects of Resolution of DEMs in Watershed Modeling. *Hydrological Processes,* 23(12): 1714 – 1724. DOI: 10.1002/hyp.7306.

Eckhardt, K. & Arnold, J.G. (2001). Automatic calibration of a distributed catchment model, *Journal of Hydrology*, 251(1-2): 103-109.

Erskine, R.H. & Green, T.R. (2007). Digital elevation accuracy and grid cell size: Effects on Estimated Terrain Attributes. *Soil Science of America Journal,* 71 (4):1371-1380. DOI: 10.2136/sssaj2005.0142.

Environmental Systems Research Institute (ESRI) (2003). ArcGIS 9.3, Redlands CA, USA, ESRI.

Evans, I.S. (1979). An integrated system of terrain analysis and slope mapping, University of Durham, Durham, report number:DA-ERO-591-73-G0040.

Fairfield, J. & Leymarie, P. (1991). Drainage networks from grid digital elevation models. *WaterResources Research,* 27 (5): 709-717. DOI:10.1029/90WR02658.

Fisher, P.F. & Tate, N.J. (2006). Causes and consequences of error in Digital Elevation Models, *Process in Physical Geography*, 30(4):467-489.

Gallant, J.C., & Wilson, J.P. (2000). Primary terrain attributes, In Wilson, J.P. and Gallant, J.C., (eds.): Terrain Analysis: Principles and Applications, New York: John Wiley and Sons: 51-85.

Gassman, P.W., Reyes, M.R., Green, C.H., & Arnold, J.G. (2007). The Soil and Water Assessment Tool: Historical development, applications and future research directions. *Transactions of the ASABE*, 50(4): 1211-1250.

Garbrecht, J., & Martz, L. (1994). Grid size dependency of parameters extracted from digital elevation models. *Computers and Geosciences*, 20(1): 85-87.

Gesch, D.B. (2007). The national elevation dataset, in *Digital Elevation Model Technologies and Applications: The DEM user's manual 2nd edition*, edited by D.F. Maune, American Society of Photogrammery and Remote Sensing, Maryland

Glennie, C. (2007). Rigorous 3D error analysis of kinematic scanning LiDAR systems. *Journal of Applied Geodesy,* 1(3): 147-157.

Golden Software Inc. (2013). Surfer 11, Golden Software Inc., URL: http://www.goldensoftware.com/products/surfer, (last date accessed 1 May, 2013)

Gong, J., Li, Z., Zhu, Q., Sui, H. & Zhou, Y. (2000). Effects of various factors on the accuracy of DEMs: an intensive experimental investigation. *Photogrammetric Engineering and Remote Sensing,*66, 1113–17.

Goodrich, D.C., Unkrich, C.L., Smith, R.E., & Woolhiser, D.A., (2002). KINEROS2 – A Distributed Kinematic Runoff and Erosion Model. Proceedings of the Second Federal Interagency Conference on Hydrologic Modeling, Las Vegas, Nevada. CD-ROM, 12 pp.

Goulden, T. (2009). Prediction of LiDAR errors due to terrain slope, Masters Thesis submitted the department of Geodesy and Geomatics Engineering, University of New Brunswick, Fredericton, New Brunswick.

Goulden, T. & Hopkinson, C. (2010a). The forward propagation of integrated system component errors in airborne LiDAR data. *Photogrammetric Engineering and Remote Sensing,* 76(5):589-601.

Goulden, T. & Hopkinson, C. (2010b). Investigating the effects of the deflection of the vertical on LiDAR observations. *Canadian Journal of Remote Sensing,* 36(S2): S365-S375. DOI: 10.5589/m10-056.

Guo, Q., Li, W., Yu, H., & Alvarez, O. (2010). Effects of topographic variability and LiDAR sampling density on several DEM interpolation methods. *Photogrammetric Engineering and Remote Sensing,* 76(6):701-712.

Gupta, H.V., Sorooshian, S., & Yapo, P.O. (1999). Status of automatic calibration for hydrologic models: Comparison with multilevel expert calibration. *Journal of Hydrologic Engineering*, 4(2):135-143.

Gyasi-Agyei, Y., Willgoose, G., & Troch, F.P. (1995). Effects of vertical resolution and map scale of digital elevation models on geomorphological parameters used in hydrology. *Hydrological Processes*, 9 (3-4): 363-382. DOI: 10.1002/hyp.3360090310.

Haile, A. T., & Rientjes, T.H.M., (2005). Effects of LiDAR DEM resolution in flood modeling: a model sensitivity study for the city of Tegucigalpa, Honduras. *ISPRS WG III/3, III/4*, *3*, 12-14.

Helmlinger, K.R., Kumar, P., & Foufoula-Georgiou, E., (1993). On the use of digital elevation model data for hortonian and fractal analysis of channel networks. *Water Resources Research,* 29(8): 2599-2613. DOI:10.1029/93WR00545.

Hill, J.A. & Neary, V.S. (2005). Factors affecting estimates of average watershed slope. *Journal of Hydrologic Engineering,* 10 (2):133-139.DOI:10.1061/(ASCE)1084-0699(2005)10:2(133).

Hjelmfelt, A.T. (1988). Fractals and the river-length catchment-area ratio. *Water Resources Bulletin,* 24 (2): 455-459. DOI: 10.1111/j.1752-1688.1988.tb03005.x.

Hodgson, M. E. & Bresnahan, P. (2004). Accuracy of Airborne LiDAR-Derived Elevation: Empirical Assessment and Error Budget. *Photogrammetric Engineering and Remote Sensing,* 70 (3), 331-339.

Hodgson, M. E., Jensen, J., Raber, G., Tullis, J., Davis, B. A., Thompson, G., & Schuckman, K. (2005). An evaluation of LiDAR-derived elevation and terrain slope in leaf-off conditions. *Photogrammetric Engineering and Remote Sensing,*71, 817-823.

Hodgson, M.E., Jensen, J., Schmidt, L., Schill, S., & Davis, B. (2003). An evaluation of LiDAR and IFSAR derived digital elevation models in leaf on conditions with USGS Level 1 and Level 2 DEMs. *Remote Sensing of Environment*, 84: 295-308

Holmes, K. W., Chadwick, O. A., & Kyriakidis, P. C. (2000). Error in a USGS 30-meter digital elevation model and its impact on terrain modeling. *Journal of Hydrology*, 233(1), 154-173

Holmstrom, D.A., & Thompson, B.L. (1985). Soils of the Annapolis Valley are of Nova Scotia. Agriculture Development Branch, Agriculture Canada, Minister of Supply and Services Canada.

Horn, B.K.P. (1981). Hill shading and the slope reflectance map. *Proceedings of the IEEE*. 69 (1) : 14-47.

Horritt, M. S., & Bates, P. D. (2001). Effects of spatial resolution on a raster based model of flood flow. *Journal of Hydrology*, *253*(1), 239-249.

Horton, R.E. (1932). Drainage basin characteristics. *Transactions of the American Geophysical Union*, 13: 350-361.

Hopkinson, C. (2002). Investigating spatio-temporal variability of hydrological components in the Canadian Rockies. PhD thesis submitted to the Geography Department, Wilfred Laurier University.

Hopkinson, C., Chasmer, L.E., Sass, G., Creed, I.F., Sitar, M., Kalbfleisch, W., & Treitz, P.(2005). Vegetation class dependent errors in LiDAR ground elevation and canopy height estimates in a boreal wetland environment. *Canadian Journal of Remote Sensing,* 31 (2): 191-206. DOI: 10.5589/m05-007.

Hopkinson, C., Chasmer, L., Munro, S., & Demuth, M. (2010). The influence of DEM resolution on simulated solar radiation-induced glacier melt. *Hydrological Processes,* 24(6): 775-788.

Hopkinson, C., Crasto, N., Marsh, P., Forbes, D., & Lesack, L. (2011). Investigating the spatial distribution of water levels in the Mackenzie Delta using airborne LiDAR. *Hydrological Processes,* 25(19): 2995-3011. DOI: 10.1002/hyp.8167.

Hopkinson, C., Hayashi, M., & Peddle, D. (2009). Comparing alpine watershed attributes from LiDAR, photogrammetric, and contour based digital elevation models. *Hydrological Processes,* 23 (3):451-463. DOI: 10.1002/hyp.7155.

Hopkinson, C., Chasmer, L., Munro, S., & Demuth, M. (2010). The influence of DEM resolution on simulated solar radiation-induced glacier melt. *Hydrological Processes,* 24(6):775-788, DOI: 10.1002/hyp.7531.

Huising, E. J., & Gomes Pereira, L. M. (1998). Errors and accuracy estimates of laser data acquired by various laser scanning systems for topographic applications. *ISPRS Journal of Photogrammetry and Remote Sensing,* (53) 245-261.

Hunter, G. J., & Goodchild, M. F. (1997). Modeling the uncertainty of slope and aspect estimates derived from spatial databases. *Geographical Analysis*, 29(1), 35-49.

Hutchinson, M.F. & Gallant, J.C. (2000). Digital Elevation Models and representation of terrain shape, in: *Terrain Analysis*, edited by Wilson, J.P. and J.C. Gallant, J.C., John Wiley and Sons, New York, pg. 29.

Hyyppä, H., Yu, X., Hyyppä, J., Kaartinen, H., Kaasalainen, S., Honkavaara, E., & Rönnholm, P. (2005). Factors affecting the quality of DTM generation in forested areas. In ISPRS WG III/3, III/4, V/3 Workshop, Laser scanning 2005, Enschede, Netherlands, 12–14 September 2005. Remote Sens. and Spatial Info. Sci. (Part 3/W19). pp. 97–102. Available from www.helsinki.fi/~korpela/MINV12/DTM_accuracy.pdf [accessed 28 March 2013]

Jamieson, R., Gordon, R., Tattrie, S., & Stratton, G. (2003). Sources and persistence of fecal coliform bacteria in a rural watershed. *Water Quality Research Journal of Canada,* 38(1): 33-47.

Jensen, S.K. & Dominigue. J.O. (1988). Extracting topographic structure from digital elevation data for geographic information system analysis. *Photogrammetric Engineering and Remote Sensing*, Vol.54 (11):1593-1600.

Jha, M., Gassman, P.W., Secchi, S., Gu, R., & Arnold, J. (2004). Effect of watershed subdivision on SWAT flow, sediment, and nutrient predictions. *Journal of the American Water Resources Association*,40(3), 811-825

Jones, K.L., Poole, G.C., O'Daniel, S.J., Martes, L.A.K. & Stanford, J.A. (2008). Surface hydrology of low relief landscapes: Assessing surface water flow impedance using LiDAR-derived digital elevation models. *Remote Sensing of Environment,* 112 (11): 4148-5158. DOI : 10.1016/j.rse.2008.01.024.

Kenward, T., Lettenmaier, D. P., Wood, E. F., & Fielding, E. (2000). Effects of digital elevation model accuracy on hydrologic predictions. *Remote Sensing of Environment*, *74*(3), 432-444.

Kienzle, S. (2004). The effect of DEM raster resolution of first order, second order and compound terrain derivatives. *Transactions in GIS,* 8 (1):83-111. DOI: 10.1111/j.1467-9671.2004.00169.x.

Kienzle, S.W., (2010). Effects of area under-estimations of sloped mountain terrain on simulated hydrological behavior: a case study using the ACRU model, *Hydrological Processes,* (in press)

La Barbera, P. & Rosso, R. (1989). On the fractal dimension of stream networks. *Water Resources Research,* 25(4): 735-741. DOI:10.1029/WR025i004p00735.

Lane, S. N., (2005). Roughness–time for a re-evaluation?. *Earth Surface Processes and Landforms*, *30* (2): 251-253.

Li, J., & Wong, D. W. (2010). Effects of DEM sources on hydrologic applications. *Computers, Environment and urban systems*, *34*(3), 251-261.

Lin, K., Zhang, Q., & Chen, X., (2010). An evaluation of impacts of DEM resolution and parameter correlation on TOPMODEL modeling uncertainty. *Journal of Hydrology*, 394(3): 370-383.

Lin, S., Jing, C., Coles, N. A., Chaplot, V., Moore, N. J., & Wu, J. (2013). Evaluating DEM source and resolution uncertainties in the Soil and Water Assessment Tool. *Stochastic Environmental Research and Risk Assessment*, *27*(1), 209-221.

Lindsay, J. B. (2006). Sensitivity of channel mapping techniques to uncertainty in digital elevation data. *International Journal of Geographical Information Science*, 20(6), 669-692.

Lloyd, C.D., & Atkinson, P.M. (2002). Deriving DSMs from LiDAR data with Kriging. *International Journal of Remote Sensing,* 23(12): 2519-2524. DOI:10.1080/01431160110097998.

Lohani, B. & Mason, D.C. (2001). Application of airborne scanning laser altimetry to the study of tidal channel geomorphology. *ISPRS Journal of Photogrammetry and Remote Sensing,*56(21) 100-120. DOI: 10.1016/S0924-2716(01)00041-7

Maidment, D. R., (2002). *Arc Hydro: GIS for Water Resources*, ESRI Press, Redlands, Ca.

Martz, L.W., & Garbrecht, J. (1993). Automated extraction of drainage networks and watershed data from digital elevation models. *WaterResources Bulletin,* 26 (6):901-908. DOI: 10.1111/j.1752-1688.1993.tb03250.x.

Maidment, D.R. (2002). Arc-Hydro: GIS for water resources. Redlands, CA: ESRI Press. 203 pp.

McMaster, K.J. (2002). Effects of digital elevation model resolution on derived stream network positions. *Water Resources Research,* 38 (4): 1042-1050. DOI:10.1029/2000WR000150.

Miller, S. N., Phillip Guertin, D., & Goodrich, D. C. (2007). Hydrologic modeling uncertainty resulting from land cover misclassification, *JAWRA Journal of the American Water Resources Association*, *43*(4), 1065-1075.

Montgomery, D.R., & Dietrich, W.E. (1988). Where do channels begin? *Nature,* 336 (6196): 232-234.

Montgomery, D.R., & Dietrich, W.E. (1992). Channel initiation and the problem of landscape scale. *Science*, 255 (5046): 826-830.

Montgomery, D. R., & Foufoula-Georgiou, E. (1993). Channel network source representation using digital elevation models. *Water Resources Research*, *29*(12), 3925-3934.

Moore, I.D., Grayson, R.B., Ladson, A.R. (1991). Digital terrain modelling: a review of hydrological, geomorphological, and biological applications. *Hydrological Processes,* 5 (1): 3-30. DOI: 10.1002/hyp.3360050103.

Morton, B., & Young, J. (2012). Chapter 5: Guidelines for LiDAR data collection. In: Manual of Airborne Topographic LiDAR, edited by: Michael S. Renslow. American Society of Photogrammetry and Remote Sensing, Bethesda Maryland.

Moriasi, D.N., Arnold, J.G., Van Liew, M.W., Binger, R.L., Harmel, R.D., &Veith, T.L., (2007). Model evaluation guidelines for systematic quantification of accuracy in watershed simulations, *Transactions of ASABE*, 50(3):885-900.

Murphy, P.N.C., Ogilvie, J., Meng, F., & Arp, P. (2008). Stream network modelling using LiDAR and photogrammetric digital elevation models: a comparison and field verification. *Hydrological Processes,* 22 (12) : 1747-1754. DOI: 10.1002/hyp.6770.

Neitsch, S.L., Arnold, J.G., Kiniry, J.R., & Williams, J.R. (2011). Soil and water assessment tool: Theoretical documentation, version 2009. Texas Water Resources institute Report No. 406.

O'Callaghan, J.F. & Mark, D.M. (1984). The extraction of drainage networks from digital elevation data. *Computer Vision,Graphics and Image Processing*, 28: 323-344. DOI: 10.1016/S0734-189X(84)80011-0.

Oksanen, J., & Sarjakoski, T. (2005). Error propagation of DSM-based surface derivatives. *Computers and Geosciences,* 31(8), 1015-1027.

Optech, Inc. (2004). *ALTM Specifications*, Optech, Inc

Optech, Inc.(2006). REALM : Results of airborne laser mapping, Optech Incorporated, URL: http://www.optech.ca/pdf/Brochures/REALM.pdf (last data accessed 20 March 2013).

Passalacqua, P., P. Tarolli, and E. Foufoula-Georgiou, (2010), Testing space-scale methodologies for automatic geomorphic feature extraction from lidar in a complex mountainous landscape, *Water resources research*, *46* (W11535), doi:10.1029/2009WR008812

Pfeifer, N. & Mandlburger, G. (2009). LiDAR data filtering and DTM generation, in *Topographic laser ranging and scanning: Principles and processing*, edited by Shan, J. and C.K. Toth, CRC Press, Taylor and Francis Group, Boca Raton, FL. pp. 307-334.

Qin, C., Zhu, A-X., Pei, T., Li, B., Zhou, C., & Yang, L. (2007). An adaptive approach to selecting flow partition exponent for multiple flow direction algorithm. *International Journal of Geographical Information Science,* 21(4): 443-458. DOI:10.1080/13658810601073240.

Quinn, P., Beven, K., Chevallier, P., & Planchon, O. (1991). The prediction of hillslope flow paths for distributed hydrological modelling using digital terrain models. *Hydrological Processes,* 5(1): 59-79.DOI: 10.1002/hyp.3360050106.

Quinton, W.L., Hayashi, M., & Pietroniro, A. (2003). Connectivity and storage functions of channel fens and flat bogs in northern basins. *Hydrological Processes,* 17(18): 3665-3684. DOI: 10.1002/hyp.1369.

Quinton, W.L., Hayashi, M., & Carey, S.K. (2008). Peat hydraulic conductivity in cold regions and its relation to pore size and geometry.*Hydrological Processes,* 22(15): 2829-2837. DOI: 10.1002/hyp.7027.

Raaflaub, L. D., & Collins, M. J. (2006). The effect of error in gridded digital elevation models on the estimation of topographic parameters, *Environmental Modelling & Software*, 21(5), 710-732.

Remmel, T.K., Todd, K.W., & Buttle, J. (2008). A comparison of existing surficial hydrological data layers in a low relief forested Ontario landscape with those derived from a LiDAR DEM. *The Forestry Chronicle,*84(6): 850-865. DOI: 10.5558/tfc84850- 6.

Reutebuch, S.E., McGaughey, R.J., Andersen, H., & Carson, W.W. (2003). Accuracy of a high-resolution LiDAR terrain model under a conifer forest canopy. *Canadian Journal of Remote Sensing,*29(5): 527-535. DOI: 10.5589/m03-022.

Rodríguez-Iturbe, I., & Rinaldo, A. (2001). *Fractal river basins: chance and self-organization*. Cambridge University Press.

Schaer, P., Skaloud J., Landtwing S., & Legat, K. (2007). Accuracy Estimation for Laser Point Cloud Including Scanning Geometyr. ISPRS - The 5th International Symposium on Mobile Mapping Technology, Padua, Italy, May 29-31

Seibert, J. & McGlynn, B.L., (2007). A new triangular multiple flow direction algorithm for computing upslope areas from gridded digital elevation models. *Water Resources Research*, Vol. 43, W04501. DOI:10.1029/2006WR005128.

Sexton, A. M., Shirmohammadi, A., Sadeghi, A. M., & Montas, H. J. (2011). Impact of Parameter Uncertainty on Critical SWAT Output Simulations. Transactions of the ASABE, 54(2):461-471

Sibson, R. (1981). A brief description of natural neighbour interpolation, in *Interpreting Multivariate Data*, edited byV. Barnett, John Wiley and Sons, New York, pp. 21-36.

Sinclair, A., Hebb, D., Jamieson, R., Gordon, R., Benedict, K., Fuller, K., Stratton, G., & Madani, A. (2009). Growing season surface water loading of fecal indicator organisms within a rural watershed. *Water Research*, 43(5):1199-1206.

Sloan, P.G., Moore, I.D., Coltharp, G.B., & Eigel, J.D. (1983). Modeling surface and subsurface stormflow on steeply sloping forested watersheds. *Water Resources Inst. Report 142*, University of Kentucky, Lexington.

Smith, R.E., Goodrich, D.C., Woolhiser, D.A., & Unkrich, C.L. (1995). KINEROS – A Kinematic Runoff and Erosion Model. In:Computer Models of Watershed Hydrology, V.P. Singh (Editor).Water Resources Publications, Highlands Ranch, Colorado, pp. 697-732.

Sohrabi, T. M., Shirmohammadi, A., Chu, T. W., Montas, H., & Nejadhashemi, A. P. (2003). Uncertainty analysis of hydrologic and water quality predictions for a small watershed using SWAT2000. *Environmental Forensics*, *4*(4), 229-238.

Stoker, J., (2013). Special issue forward: Are we moving past the pixel? The third dimension in national landscape mapping. Photogrammetric Engineering and Remote Sensing, 79(2):133-134.

Strahler, A.N. (1952). Hypsometric (area-altitude) analysis of erosional topography. *Geologica Society America Bulletin*, 63(11): 1117-1142. DOI: 10.1130/0016-7606(1952) 63[1117:HAAOET]2.0.CO;2.

Stuart, V., Harker, D.B., Scott, T., & Clearwater, R.L.(2010). *Watershed evaluation for beneficial management practices (WEBs): towards enhanced agricultural landscape planning – four year review (2004/5-2007/8)*, Agriculture and Agri-Food Canada, Ottawa, Ont.

Tarboton, D.G., & Ames, D.P. (2001). Advances in the mapping of flow networks from digital elevation data, *Proceedings of World Water and Environmental Resources Congress*, 20-24, May, Orlando, Florida.

Tarboton, D.G., Bras, R.L., & Rodrìguez-Tturbe, I. (1988). The fractal nature of river networks. *Water Resources Research,* 24 (8): 1317-1322. DOI:10.1029/WR024i008p01317.

Tarboton, D.G. (1997). A new method for the determination of flow directions and upslope areas in grid digital elevation models. *Water Resources Research,* 33 (2): 309-319.

Thieken, A.H., Lucke, A., Diekkruger, B., & Richter, O. (1999). Scaling impact input data by GIS for hydrological modeling. *Hydrological Processes,* 13(4): 611-630. DOI: 10.1002/(SICI)1099-1085(199903)13:4<611::AID-HYP758>3.0.CO;2-6.

Thompson, J.C., & Moore, R.D.(1996). Relations between topography and water table depth in a shallow forest soil, *Hydrological Processes*, 10(11):1513-1525.

TMS International Ltd. (2005). The Global Market for Airborne LiDAR Systems and services. TMS International Ltd. Houston Texas. 158 pp.

Tribe, A. (1992). Automated recognition of valley lines and drainage networks from grid digital elevation models: a review and a new method. *Journal of Hydrology***,** 139 (1-4): 263-293, DOI:10.1016/0022-1694(92)90206-B.

USDA, (2004). Estimation of direct runoff from storm rainfall, *National Engineering Handbook Hydrology Chapters*, U.S. Department of Agriculture, pp. 10-1:10-22

van Grivenson, A., & Meixner, T.(2007). A global and efficient multi-objective auto-calibration and uncertainty estimation method for water quality catchment models, *Journal of Hydroinformatics*, 9(4): 277-291.

van Vliet, L.J.P., (2002). Chapter 6 : The support practice factor, in Wall, G.J., D.R. Coote, E.A. Pringle and I.J. Shelton (eds), RUSLEFAC — Revised Universal Soil Loss Equation for Application in Canada: A Handbook for Estimating Soil Loss from Water Erosion in Canada. Research Branch, Agriculture and Agri-Food Canada. Ottawa. Contribution No. AAFC/AAC2244E, 117 pp.

Vaughn, C., Bufton, J., Krabill, W., & Rabine, D. (1996). Georeferencing of airborne laser altimeter measurements. *International Journal of Remote Sensing*, 17(11), pp. 2185-2200.

Vieth, E. (1989). Fitting piecewise linear regression functions to biological responses. *Journal of Applied Physiology*, 67:390-396.

Wang, X. &Yin, Z. (1998). A comparison of drainage networks derived from digital elevation modelsat two scales. *Journal of Hydrology,* 210 (1-4):221-241. DOI: 10.1016/S0022-1694(98)00189-9.

Wechsler, S. P. (2003). Perceptions of Digital Elevation Model Uncertainty by DEM Users, *URISA Journal*, 15: 57-64.

Wechsler, S.P. (2007). Uncertainties associated with digital elevation models for hydrologic applications: a review. *Hydrological Earth Systems Science,*11(4): 1481-1500.

Wechsler, S. P., & Kroll, C. (2006). Quantifying DEM Uncertainty and its effect on Topographic Parameters. *Photogrammetric Engineering and Remote Sensing*, 72:1081–1090.

Williams, J.R. (1969). Flood routing with variable travel time or variable storage coefficients, *Transactions of the ASABE*, 12(1):100-103.

Williams, J.R. (1975). Sediment routing for agricultural watersheds, *Water Resources Bulletin*, 11(5):965-974.

Wilson, J.P., Repetto, P.L., & Snyder, R.D. (2000). Effect of data source, grid resolution, and flow-routingmethod on computed topographic attributes, in *Terrain Analysis: Principles and Applications,*edited by Wilson, J.P. and J.C. Gallant, New York: John Wiley and Sons: Chapter 5: 51-85.

Wishmeier, W.H., & Smith, D.D.(1978). Predicting rainfall erosion losses – a guide to conservation planning, *Agriculture Handbook No. 537*, U.S. Department of Agriculture.

Wolf, P., & Ghilani, C. (1997). Adjustment computations, statistics and least squares in surveying and GIS, Wiley Interscience.

Wu, S., Li, J., & Huang, G.H., (2008). Characterization and Evaluation of Elevation Data Uncertainty in Water Resources Modeling with GIS. *Water Resource Management*, 22:959-972

Yang, C.T., (1996). Sediment transport theory and practice, The McGraw-Hill Company, Inc., New York.

Zhao, Z., Benoy, G., Chow, T.L., Rees, H.W., Daigle, J., & Meng, F. (2010). Impacts of accuracy and resolution of conventional and LiDAR based DEMs on parameters used in hydrologic modeling. *Water Resources Management*, 24:1363-1380.

Zhang, W., & Montgomery, D.R. (1994). Digital elevation model grid size, landscape representation and hydrologic simulations. *Water Resources Research,* 30 (4): 1019-1028.

Zhang, X., Srinivasan, R., & Van Liew, M. (2008). Multi-Site Calibration of the SWAT Model for Hydrologic Modeling. *Transactions of the ASABE*, 51(6): 2039-2049.